MICROFAFBRICATED MULTI-ANALYSIS SYSTEM FOR ELECTROPHYSIOLOGICAL STUDIES OF SINGLE CELLS

A Thesis
Presented to
The Academic Faculty

by

Arum Han

In Partial Fulfillment
Of the Requirements for the Degree
Doctor of Philosophy in the
School of Electrical and Computer Engineering

Georgia Institute of Technology
August 2005

MICROFAFBRICATED MULTI-ANALYSIS SYSTEM FOR ELECTROPHYSIOLOGICAL STUDIES OF SINGLE CELLS

Approved by:

Dr. A. Bruno Frazier, Advisor
School of Electrical and
Computer Engineering
Georgia Institute of Technology

Dr. Kathrin L. Engisch
Department of Physiology
School of Medicine
Emory University

Dr. Oliver Brand
School of Electrical and
Computer Engineering
Georgia Institute of Technology

Dr. William D. Hunt
School of Electrical and
Computer Engineering
Georgia Institute of Technology

Dr. Robert J. Butera, Jr
School of Electrical and
Computer Engineering
Georgia Institute of Technology

Date Approved: July 5, 2005

ACKNOWLEDGEMENTS

First and foremost, I need to thank my parents and my sister for always encouraging me throughout my long study. I would like to thank my advisor, Dr. Bruno Frazier, for providing me the opportunity to study under his guidance and encouraging me with patience throughout the years. I would also like to thank Dr. Kathrin L. Engisch, Dr. Thiagarajan Ramachandran, and Teclemichael Tewolde from the Emory University for valuable discussion and help regarding patch clamping and providing bovine chromaffin cells. Appreciation is also given to Dr. Lily Yang from the Emory University for providing the breast cancer cell lines. Appreciation is given to all the members of the Micro Instrumentation Research Lab. at Georgia Institute of Technology. Many thanks also go to the staff of the Microelectronics Research Center at the Georgia Institute of Technology. Finally, I would like to thank my former advisors, Dr. Chong H. Ahn from the University of Cincinnati, and Dr. Dongil "Dan" Cho from the Seoul National University who always encouraged me and provided guidance and mentoring.

TABLE OF CONTENTS

LIST OF FIGURES

SUMMARY

This dissertation presents the development of a micro-electrophysiological analysis system (μ-EPAS) using various microfabrication techniques for single cell study. The design and fabrication of the system and the characterization of the system in the patch clamping mode and the whole cell electrical impedance spectroscopy (EIS) mode are presented. The ion channel activities of primary cultured bovine chromaffin cells were measured in both the patch clamping mode and the whole cell EIS mode. The dielectric properties of human breast cancer cell lines from different pathological stages were measured and compared in the whole cell EIS mode. The measured properties were correlated to the pathological stages of the breast cancer cells.

Conventional patch clamp recording and impedance spectroscopy are widely used for studying electrophysiological characteristics and events of biological samples. These conventional systems require labor-intensive operation and are limited in analyzing a single cell, have limits in integrating different analysis capabilities into a single system, and lack the capability to perform high-throughput parallel analysis.

The developed system is composed of four arrays of 16 analysis sites, each capable of analyzing a single cell. Each analysis site has a via to create giga-seal for patch clamping and to hold a single cell in position during the impedance analysis operation, a cavity around the via into which a single cell can be trapped, multiple

electrodes surrounding the analysis cavity to measure the electrical characteristics of a captured cell, and integrated fluid channels/interfaces to control the intracellular and extracellular fluid environment. Conventional microfabrication techniques combined with plastic and polymer microfabrication techniques have been used to realize the system.

The developed system eliminates the labor-intensive nature of conventional patch clamp recording, enables better control over intracellular and extracellular fluid environment, and can achieve high throughput utilizing the array format of the system. The capability to perform analysis on a single cell enables fast and accurate characterization through whole cell EIS.

Primary cultured bovine chromaffin cells were first tested in the patch clamping mode. Seal resistance in the giga ohm range was achieved and methods to improve seal resistance were investigated. The ion channel currents resulting from voltage stimuli were measured and compared to that obtained through conventional patch clamp recording. The result from the μ-EPAS was comparable to that from a conventional patch clamping system. The ion channel activities were also studied in the whole cell EIS mode over a frequency range of 100 Hz to 5.0 MHz. K and Ca channels of the chromaffin cells were blocked using toxins. These cells could be distinguished from cells with no ion channels blocked using the measured impedance. The membrane capacitance of normal cells at 100 kHz were 0.75 $\mu F/cm^2$ and increased by 21 % to 0.91 $\mu F/cm^2$ when the K channels were blocked, increased by 77 % to 1.33 $\mu F/cm^2$ when the Ca channels were blocked, and increased by 163 % to 1.97 $\mu F/cm^2$ when both K and Ca

channels were blocked at 100 KHz. The membrane resistance changed from 93.5 MOhm to 80.7 MOhm, 85.5 MOhm, and 90.7 MOhm respectively at 100 kHz.

The impedances of human breast cancer cell lines from different pathological stages were measured in the whole cell EIS mode and compared to a normal human breast tissue cell line. Normal human breast tissue cell line MCF-10A, early stage breast cancer cell line MCF-7, invasive human breast cancer cell line MDA-MB-231, and metastasized human breast cancer cell line MDA-MB-435 were used. The impedance measurements at a frequency range of 100 Hz to 3.0 MHz showed clear difference between each cell line in both magnitude and phase. Not only were the impedances of the cancer cell lines different from the normal cell line, but also cell lines from different cancer stages were different. The calculated capacitances of MCF-10A, MCF-7, MDA-MB-231, and MDA-MB-435 were 1.94, 1.86, 1.63, and 1.57 $\mu F/cm^2$ respectively at 100 kHz. The changes in capacitance of the cancer cell lines compared to the normal cell line MCF-10A was 4.1 %, 16.0 %, and 19.1 % respectively at 100 kHz.

CHAPTER 1

INTRODUCTION

1.1 Objective and Motivation

The objective of this work is to demonstrate a microfabricated multi-analysis system for electrophysiological analysis of single cells. The research focuses in particular on patch clamp recording and whole cell electrical impedance spectroscopy (EIS) of single cells, as well as methodologies developed to interface single cells with this microsystem.

Patch clamping technique is the most direct and accurate method for studying the ion channel behavior of a single cell. It is achieved by recording the current flowing across the cell membrane through the ion channels. This technique is widely used in the pharmaceutical industry for drug discovery. Currently available systems require labor-intensive, manual operation that limits the throughput of such systems. Also, these systems lack the capability to exchange intracellular solutions during patch clamp recording. Furthermore, integrating additional analysis methods such as amperometry is not trivial.

Impedance spectroscopy is a technique used to distinguish different types of tissues and different pathological statuses of tissues by measuring the dielectric properties of a tissue. Previous studies show that different types or pathological statuses of tissues can be distinguished using this technique, but the complex structure of a tissue that affects the impedance measurement is challenging for the analysis of the impedance data. Impedance studies have also been conducted on populations of cells to provide information about their dielectric properties. Although these studies provide valuable information about the dielectric properties of cells, it would be ideal to analyze a single cell to study its dielectric property.

A micro-electrophysiological analysis system (μ-EPAS) that can perform both patch clamp recording and whole cell EIS simultaneously on a single cell was designed and fabricated using MicroElectroMechanical Systems (MEMS) techniques combined with plastic and polymer microfabrication techniques. The developed system is expected to eliminate the labor-intensive nature of conventional patch clamp recording, enable control over the intracellular and extracellular fluid environment, enable fast and accurate characterization of single cells through whole cell EIS, and achieve high throughput utilizing the array format of the system. By realizing automated and miniaturized multi-functional patch clamp recording and single-cell EIS into a single system, the developed μ-EPAS is expected to provide an in-depth look at electrophysiological events occurring at the single-cell level and pathological status of single cells with high throughput. The system can be easily expanded to have additional functionalities such as amperometry or impedance tomography by creating additional integrated electrodes or different electrode configurations around the analysis sites. The result of this study is expected to be applied

for high-throughput drug screening and cancer diagnosis by providing an accurate and effective analysis instrument.

1.2 Patch Clamp Recording

Ion channels located in cell membranes have crucial roles in physiology and pathophysiology and are important targets for drug discovery. They allow particular ions to pass through them from one side of the membrane to the other. The ion channels show selectivity to the ions to which they are permeable. They can be switched on or off to control the movement of the ions. Gating of the ion channels can be controlled by chemicals, such as neurotransmitters or cytoplasmic messenger molecules, changes in the voltage across the cell membrane, or sensory stimuli of various kinds. The extracellular solution typically contains relatively high concentrations of sodium and chloride ions and much lower concentrations of potassium, calcium, and other ions. A plasma membrane in a cell acts as a barrier so that the ionic concentrations inside the cell can be maintained at a different level from those of the extracellular fluid.

Patch clamp recording is the most direct and accurate method for studying ion channel behavior by recording the current flowing across the cell membrane through the ion channels. This technique was first developed in 1976 by Neher and Sakmann [1]. The development of this technique caused a revolutionary advancement in both cellular and molecular biology, and the developers were awarded the Nobel Prize in physiology or medicine in 1991.

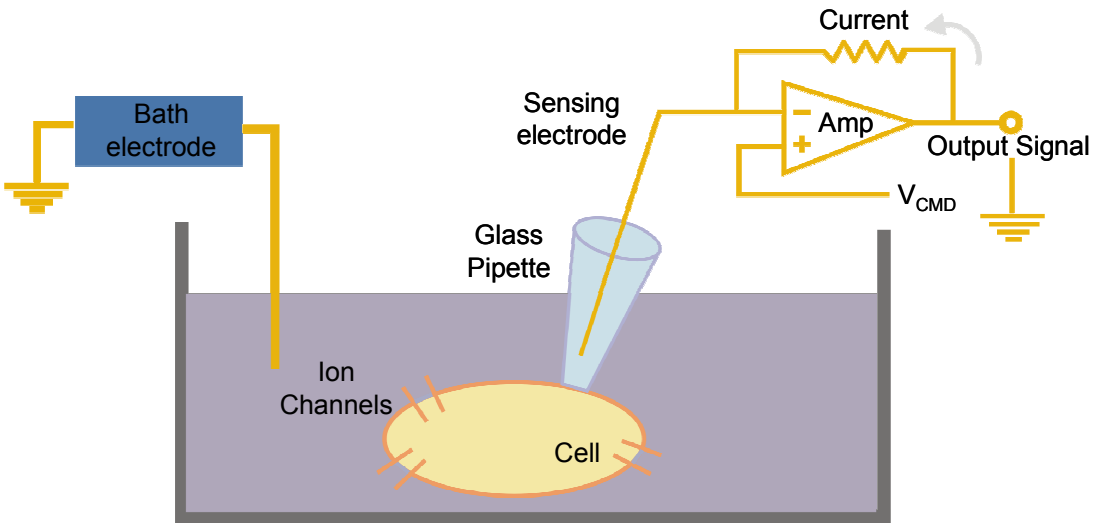

Figure 1.1 Illustration of the principle of conventional path clamp recording.

In a conventional patch clamping setup, a glass pipette is used to aspirate a cell membrane partially into the pipette to form a tight electrical seal, as shown in Figure 1.1 [2, 3]. The glass pipette is pulled from a glass capillary using heat and has a final inner diameter as small as 1 µm. Using a precision micromanipulator, the glass pipette is manipulated toward the cell and touches the cell gently. This is followed by a slight amount of suction to the pipette to achieve a tight electrical seal between the cell membrane and the glass pipette. This tight electrical seal enables the measuring of the current flowing through the ion channels located in the small patch of membrane isolated by the glass pipette. The voltage across this patch is held steady ("clamped") by a feedback amplifier so that the current through the ion channels can be measured. The

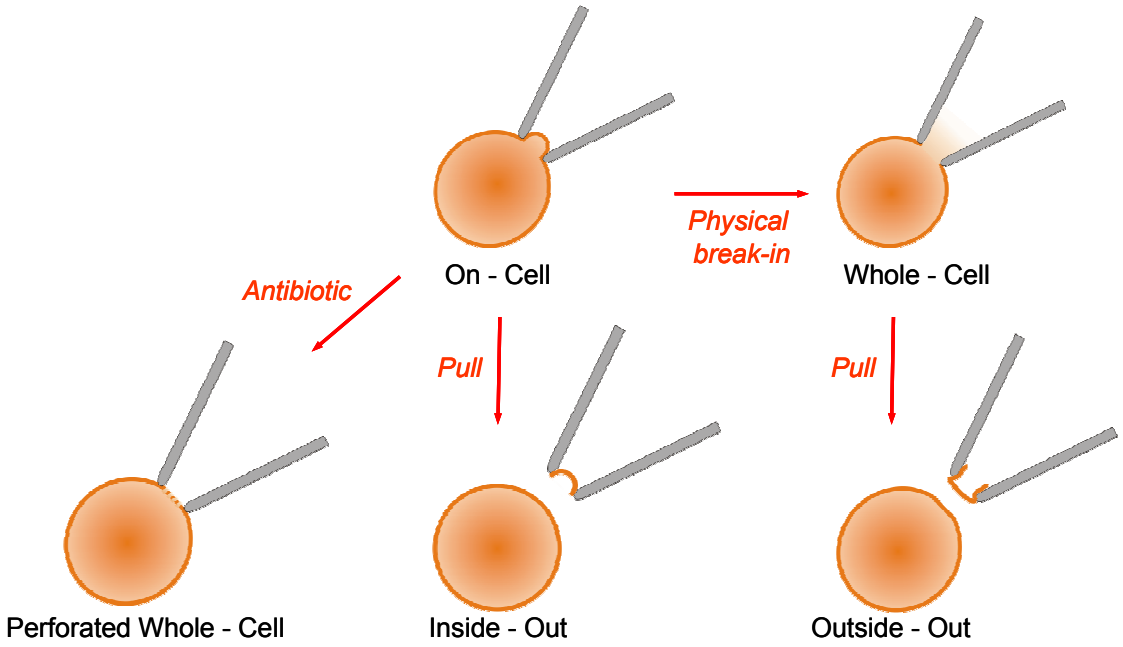

Figure 1.2 Illustration of the various patch clamping configurations.

seal resistance is typically in excess of $10^9\ \Omega$ and is thus called a "giga-seal." There are various patch clamping configurations, such as cell-attached, inside-out, perforated-patch, whole-cell, and outside-out, as shown in Figure 1.2 [4, 5]. In our study, whole-cell and perforated patch clamping was used. Using these configurations, the ion currents of an entire cell can be recorded with the advantage of recording an average response of all the channels in the cell membrane. This method is also used for characterizing the exocytotic activity of secretory cells by measuring the capacitance of a cell membrane. To access the inside of the cell, the membrane region in the glass pipette has to be broken and open. Hard suction, voltage pulse, and perforation with chemicals are typically used.

One of the major problems of whole-cell patch clamping using hard suction or voltage pulse is that the patched region of the membrane is physically open and the cytosolic constituents can be washed out during the recording process. Perforated patch clamping utilizes channel-forming substances to create pores through which ions can move in and out but not other larger molecules [2, 6]. This method is less damaging to the cell and long recording is possible without losing the functions of the cell. Some of the disadvantages of this method are that it does not allow for the exchange of intracellular solutions during recording and takes longer to access the inside of a cell through the formation of perforated pores. Nystatin is a polyene antibiotic that can create transmembrane channels 8 Å in diameter. These channels are permeable to all small monovalent cations and anions that enable control of K^+, Na^+, and Cl^- through the extracellular ionic concentrations and are not voltage dependent. Some of the drawbacks of nystatin are that it inhibits the formation of seals, has poor solubility in water and thus tends to aggregate, and is light sensitive. Amphotericin B is another polyene antibiotic that is widely used having similar characteristics as nystatin [7]. In this study, hard suction, voltage pulse, and perforation with amphotericin B will be used to access the interior of the cell.

The conventional patch clamping process is labor intensive, requiring precision micromanipulation of a glass pipette or electrode in a vibration-damped environment. Figure 1.3 shows an illustration of a conventional patch clamp recording setup. The glass pipettes are also mechanically weak and a mere touch can result in broken tips. Because of these drawbacks, there is great interest in improving the stability and throughput of this technique by using an automated system potentially capable of parallel analysis of

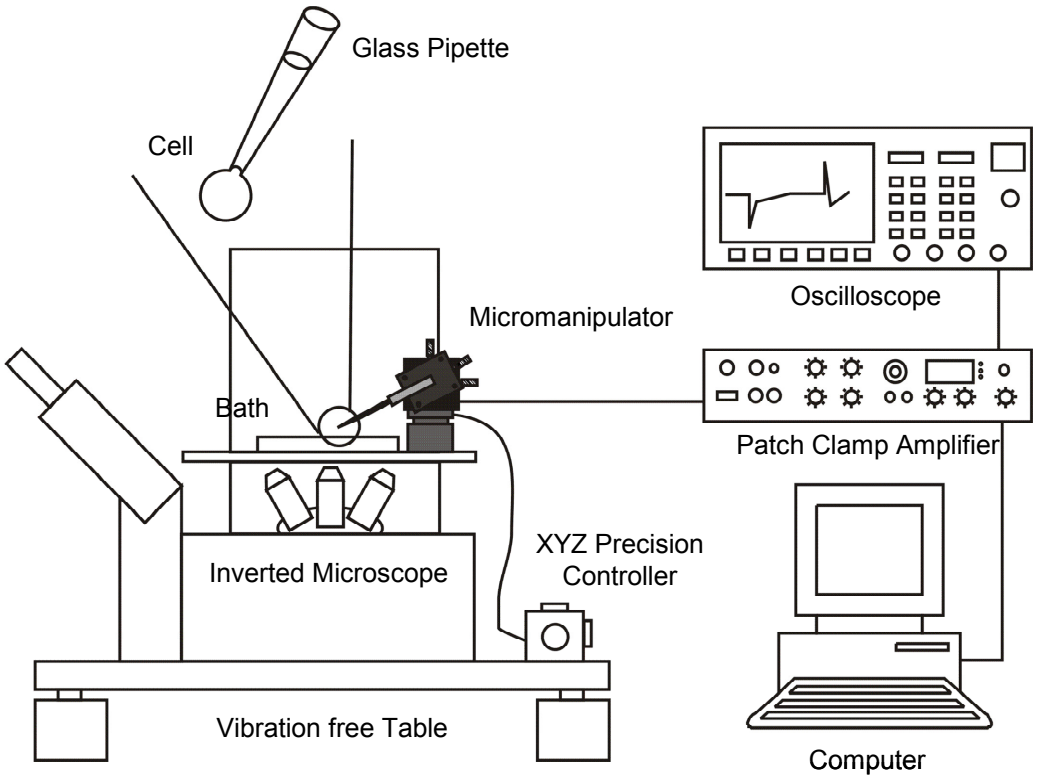

Figure 1.3 Illustration of a conventional patch clamp recording setup.

multiple cells, primarily to facilitate drug screening in the pharmaceutical industry [8]. From the top 100 best-selling drugs in 2000, only three of 43 different molecular targets were ion channels even though the sales was on the order of US $7 billion [9, 10]. For pharmaceutical companies, screening large numbers of compounds against the ion channels in a meaningful manner to maximize the potential of the targets and efficiently exploit new targets is becoming more and more important. Also, the recent discovery of the *h-erg* channel, which can interact with certain prescription drugs and possibly lead to sudden death, caused the preclinical testing of candidate compounds against cardiac ion channels, a very important part of the safety screening [9, 11, 12].

Because of to the low throughput of conventional patch clamping method in a time of high demand for such screening, many companies are compromising data quality to increase throughput by using methods such as radioligand binding, fluorescent detection, and ion flux measurements [13, 14]. These methods are limited in providing appropriate pharmacological values for many classes of ion channels and lack the sensitivity required. On top of this, cell membranes are not easily accessible by fluid when using the conventional patch clamping setup, making it hard to control and change the intracellular fluid environment. A system with a means to access the intracellular fluid environment easily during recording will greatly expand the applications of such a system.

Several microfabricated planar patch clamping systems have been introduced recently. Planar glass chips with a hole diameter as small as 1 μm have been created in glass using irradiation with a single heavy ion and subsequent wet track etching [15-17]. Both single-channel and whole-cell currents were measured, although the measured seal

resistance was a factor of 3 to 5 lower compared to that from conventional patch clamping. Another material, poly(dimethylsiloxane) (PDMS), has also been used for planar patch clamping systems [18-20]. Holes with diameters as small as 2 μm have been created by either cast molding followed by slicing or by multiple sequences of molding. A seal resistance as high as 10.2 GΩ was reported using this method. Also, several systems with parallel analysis capabilities have been designed and fabricated in different materials and with different fabrication methods [21-30]. Some of these technologies have been commercialized in the past couple years to an automated array-type planar patch clamping systems. PatchXpress® from Axon Instruments (Now part of Molecular Devices, http://www.axon.com), and QPatch from Sophion Biosciences A/S (http://www.sophion.dk) are some of the most successful and advanced systems currently available.

1.3 Impedance Spectroscopy

Impedance spectroscopy is a technique mainly used to characterize tissues based on the knowledge of their electrical properties in the frequency spectrum [31]. In biological tissues, electric current influences components that have a net electric charge and/or dipolar electrical moment, such as ions, polar molecules of tissue water, and protein/lipid structures of membranes or cell interfaces [32, 33]. The induced conduction and dielectric relaxation phenomena are used to study the electrical properties of tissues defined by conductivity and permittivity [34]. These electrical properties of tissues are

frequency dependent. In a conventional system, electrical parameters are usually obtained using reflectometry or capacitive methods. In reflectometry, the reflection coefficient in a coaxial line is measured to characterize the locally disturbed impedance by the presence of a tissue sample. In the capacitive method, tissues under study are placed between two flat electrodes through which current is injected and potential is measured. By measuring the impedance of a tissue over a frequency, the dielectric properties of the tissue can be calculated [35, 36].

From the various applications of impedance spectroscopy, distinguishing different types of tissues and studying pathological tissues are of great interest [37]. Among the studies relative to pathological tissues, one of the more promising areas seems to be the characterization of cancerous tissues. Several studies have been conducted to characterize cancer tissues using impedance spectroscopy [31, 38-43]. These studies show that the permittivity and conductivity of the tumor tissues are higher compared to that of normal tissues. The studies also show that the membrane capacitances of tumor cells are lower compared to those of normal cells. It has also been shown that the dielectric properties of cancer tissues at different tumor development stages are different [44].

Although measuring the impedance of tissues can provide valuable information, the measurement is inaccurate because of the complex composition and structure of tissues. It is expected that the measurement on cells instead of tissues can provide more accurate and in-depth information. The impedance measurement on cell suspensions has drawn wide interest, and varieties of single-particle measurement methods that exploit different force effects have been developed over the last two decades [45-49]. When

cells, healthy or not, are exposed to dynamic external fields, they exhibit complex fluid dynamic behaviors which include several sub-cellular dielectric responses. For biological cells, the main components for these differences are Maxwell-Wagner dispersions, i.e., the dispersions of structural polarizations of the cytoplasmic membrane or of internal membrane systems, as well as the polarization of the cytoplasm. The resulting spectra then serves as an analysis tool for the quantitative understanding of this inhomogeneous system.

Recent advances in microfabrication and the lab-on-a-chip concept enabled electrical impedance spectroscopy (EIS) devices to measure small sizes of samples quickly and accurately. There have been several studies to use microfabricated electrical impedance spectroscopy (μEIS) devices for interrogating biological or chemical samples. These devices have been used to sense variations in solution temperatures [50], ionic concentrations [51], and bacterial metabolism [52, 53]. These systems typically analyze target solutions using arrays of metal electrodes in a fluidic chamber or channel.

These systems have been expanded to detect and characterize a single cell, which is of great interest. The characterization of individual cells by μEIS has many experimental and simulation advantages over tissue and cell suspension measurements. Contrary to previous methods where a population of cells is used, the single-cell approach does not require a uniform population of cells and greatly simplifies the theoretical model needed. A μEIS provides a method for quantifying the physiological state of a whole cell based on the membrane and the cytosolic properties. This quantification allows for the detection of abnormal cells as well as classification of normal cell types.

The single-cell detection and analysis method using integrated probes in μEIS has the ability to track differences associated with cell plasma membrane and intracellular contents [52, 54]. Biological cells are placed into an electric field that leads to local distortion of the field, leading to the measurement of the characteristic impedance signature of the cells [55, 56]. Microsystems with impedance measurement probes directly in contact with a single cell have also been developed that can measure the impedance of a single cell without the effect from the surrounding media [57, 58]. Changes in the ion channel activities have also been measured using this method [59]. Electrical impedance measurements of human prostate carcinoma cell lines (DU-145) have also been reported [60].

These studies show that detecting different types of cells, cell viability, and cell reaction to toxins are possible using such systems. Most of these systems utilize fluidic channels through which samples can be delivered and opposing electrode pairs positioned inside these channels to measure the electrical impedances of a target sample. Figure 1.4 shows an illustration of a typical flow-through type μEIS system. Positioning a single cell between these electrodes can be accomplished by controlling the fluid pressure and the channel geometry. Although these systems show promising results in characterizing single cells, the inaccuracy in aligning a single cell between the opposing electrodes typically results in higher deviation. Because of the sensitivity of the measurement in response to the relative position of a cell between the impedance measurement probes, positioning the target cell precisely at a desired location is important. A system with accurate cell positioning capabilities will enhance the understanding of correlations between the electrical impedance and the physiological characteristics of a cell.

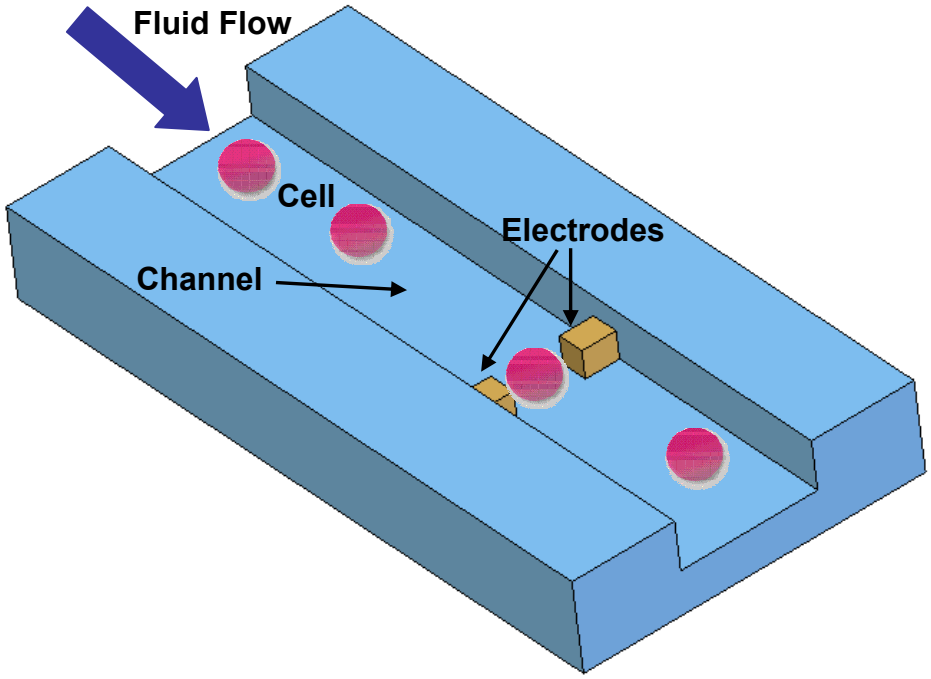

Figure 1.4 Illustration of a typical flow-through type electrical impedance spectroscopy system.

1.4 Chromaffin Cell

Chromaffin cells, found in the adrenal gland, serve as a valuable tool for neuroscientists interested in adrenergic functions. Often termed adrenal paraneurons, they share a number of features with postganglionic neurons of the autonomic nervous system [61]. These cells secrete catecholamines and are electrically excitable [62, 63]. The two principal catecholamines, adrenaline and noradrenaline, are stored within vesicles inside the cell, commonly referred to as chromaffin granules. The secretion of these vesicles occurs by a Ca^{2+} -dependent exocytotic mechanism. The intracellular Ca^{2+} concentration is much lower than that of outside the cell, and an increase in the concentration of extracellular calcium ions through the voltage-gated Ca channels triggers the exocytosis. Large numbers of chromaffin cells are present in the adrenal glands of cattle, providing an easy source of the cells at minimal cost. Chromaffin cells are obtained by perfusing the adrenal gland through its central blood vessel with a solution of collagenase, which breaks down the material that holds the chromaffin cells together in the intact adrenal medulla.

Ion channels in the cell membrane can be blocked by a variety of toxins to study a specific ion channel [64-67]. Typically, all other ion channels except for the ion channel of interest are being blocked by toxins to obtain recordings from the desired ion channel. Toxins such as tetrodotoxin (TTX), tetraethylammonium chloride (TEACl), and CdCl can be used to block the Na, K, and Ca channels, respectively.

Neurotransmitters secreted from chromaffin cells can be studied by amperometry in conjunction with patch clamp recording [68, 69]. Electrochemical detection, such as

cyclic voltammetry and amperometry, is a technique where a voltage is applied to an electrode to oxidize molecules that donate electrons to the electrode, followed by a current measurement with respect to time to observe changes in the molecular concentration that occur at the electrode surface. In amperometry, the potential at the electrode is held constant, whereas in cyclic voltammetry, the potential is periodically scanned in a triangular waveform. Amperometry can provide time resolution but cannot provide information on the chemical nature of the molecules detected [70]. Cyclic voltammetry has lower temporal resolution but can provide information on the electroactive chemicals being detected. These are direct methods used for measuring neurotransmitters such as catecholamines secreted from bovine chromaffin cells and are widely used to study exocytosis at a single cell level.

Typically, a carbon electrode is manipulated with a precision micromanipulator in a vibration-damped environment to measure the release of the secreted molecules. It has been known that these molecules secrete from specialized regions of the membrane, called active zones, where secretory vesicles accumulate and undergo exocytotic fusion [71-74]. With the current micromanipulation technology, there is a limit on the number of electrodes that can be manipulated in close proximity to a single cell to measure such release.

1.5 Breast Cancer Diagnosis

Breast cancer is the most common type of cancer affecting women these days, causing approximately 45,000 deaths per year [75-78]. Many breast cancer patients have already had long-distance metastases upon diagnosis and a large percentage of these patients develop metastatic diseases following surgical removal of the primary tumor [79]. The current diagnosis of breast cancer is achieved from a combination of radiological, surgical, and pathological assessments of tissue samples requiring the evaluation of tissues under a microscope for diagnosis and prognostic result generation. Any area of the breast that appears suspicious is typically tested using a biopsy-based technique such as fine-needle aspiration, core-needle biopsy, and excisional biopsy. The whole process is invasive and time consuming, and the risk of a false positive result is still in the range of 20-50 % [80]. At present, there is no widely accepted and reliable serum tumor marker for the diagnosis of breast cancer. It is well known that mover than 90% of the breast cancer cases arise in the epithelial cells lining the milk ductal system. The transition from normal mammary epithelial to invasive ductal carcinoma is a multistage process, that involves a series of histological changes in the breast tissues from hyperplasia, atypical hyperplasia to ductal carcinoma in situ (DCIS), to invasive ductal carcinoma and to metastatic breast cancer. Cells from each development stage also show different morphology.

Metastatic spread of breast cancer begins with the dissociation of cancer cells from the primary tumor into the blood circulation and bone marrow. The detection of circulating cancer cells constitutes an important aspect in staging, predicting prognosis,

and designing therapy for breast cancer patients [81-83]. It has been shown that breast cancer cells may be detected in the blood circulation of the majority of patients with metastatic breast cancer [84]. Current approaches for cancer cell detection in blood and/or bone marrow include immunocytochemistry, flow cytometry, reverse transcriptase polymerase chain reaction (PCR), fluorescent detection using antibody-coated magnetic beads, and DNA microarray analysis for tumor markers that are expressed in breast cancer cells [85-88]. However, most of the current tumor markers are not specific for breast cancer cells, and only 30 to 40% of the breast cancer cells can be expressed by the commonly used cancer markers. The lack of reliable cellular surface markers and the presence of a low percentage of tumor-marker positive tumor cells significantly reduce the specificity and sensitivity of the current methods for cancer detection. Recent studies also show that cancers begin shedding neoplastic cells into the circulation at an early stage [89]. It has also been shown that the level of circulating tumor cells can predict the prognosis of the disease [90].

1.6 Chapter Outlines

The design and modeling of the μ-EPAS are described in Chapter 2. Working principles of the system in the patch clamping mode and the whole-cell EIS mode are described. The design criteria for realizing the system are addressed. An equivalent circuit model for a single cell in the analysis system is developed.

Chapter 3 shows the microfabrication methods used and the resulting system. Fabrication results from the analysis site formation in the silicon wafer, plastic microfabrication for the backside fluidic channels/interfaces, and soft lithography for the frontside fluidic channels/interface are presented. Assembly and device preparation steps to prepare the system for characterization and biological testing are shown.

Chapter 4 shows studies conducted on bovine chromaffin cells and human breast cancer cells using the developed system. Bovine chromaffin cells were first tested in the patch clamping mode. Giga-ohm seal formation and methods to improve the seal resistance are presented. Results from patch clamp recording are compared to those from a conventional patch clamp recording. Next, the chromaffin cells are interrogated in the whole cell EIS mode to study the ion channel activities.

Human breast cancer cells are studied in the whole cell EIS mode. Breast cancer cells from different pathological stages are compared to normal breast tissue cells to demonstrate the feasibility of the μ-EPAS for cancer diagnosis.

The last chapter is the conclusion of this thesis. The work performed and the results are briefly summarized. Future work is also proposed and discussed.

CHAPTER 2

DESIGN AND MODELING

2.1 Designing the Analysis System

Patch clamp recording and impedance spectroscopy are widely used analysis tools for studying electrophysiological characteristics of biological samples. These systems require labor-intensive manipulation and are limited in the capability of analyzing a single cell, have limits in integrating different analysis capabilities into a single system, and lack the capability to perform high-throughput analysis. By miniaturizing such systems and integrating microfluidic functionalities into the systems, easy manipulation and analysis of a single target cell and easy control over the intracellular and extracellular fluid environments can be achieved. Compact microfabricated systems containing arrays of analysis sites can perform fast and parallel analysis in an automated fashion, increasing the overall throughput. Also, by integrating different analysis methods such as patch clamping and whole cell electrical impedance spectroscopy (EIS) into a single system, various analyses can be performed on a single target cell simultaneously.

To design a system capable of performing the analyses described above required the following components and design criteria.

- An analysis cavity into which a single cell can fit
- Means to trap a single cell inside this cavity
- Integrated pairs of opposing electrodes inside the analysis cavity that can be in direct contact with the trapped cell
- Integrated electrodes above to be positioned in the middle of a trapped cell for optimum impedance measurements
- Means to exchange the intracellular solution during patch clamp recording
- Means to constantly monitor the cell analyzing process under a microscope
- Arrays of such analysis sites that can be both electrically and fluidically accessible to enable high-throughput analysis

Microfabrication using conventional semiconductor fabrication techniques and non-conventional plastic/polymer microfabrication techniques were used to realize a system that can fulfill these design criteria. The developed μ-EPAS has the capabilities to perform both patch clamp recording and whole cell EIS simultaneously, has integrated microfluidic channels and interfaces for sample delivery and intracellular/extracellular fluid environment control, and contains arrays of such analysis sites for high throughput parallel analysis.

The μ-EPAS is composed of four arrays of 16 analysis sites on a three-inch diameter silicon wafer, each capable of analyzing a single cell. Each analysis site has a 10 or 16 μm diameter, 7-10 μm high analysis cavity created in polyimide, into which a single cell can be trapped. Most mammalian cells fall into this size category. Each cavity has a 2.0-3.0 μm diameter via at the center created in a 1.8 μm thick SiO_2

membrane. Fluidic channels covering each analysis cavity and fluidic interfaces are located on the backside of the system. When a negative pressure is applied through the via and the backside fluidic channel, a single cell can be manipulated toward the analysis site and trapped inside the cavity. This via is also being used to form a seal between the device and the captured cell when the system is used in the patch clamping mode. The backside fluidic channel can also be used to exchange the intracellular solution during patch clamp recording.

The main difference between this design and that of a conventional patch clamp recoding system is that instead of having to manipulate a glass pipette toward a single cell using a precision micromanipulator, a single cell can be manipulated toward the analysis site using a fluidic flow without the need for a precision micromanipulator. This eliminates the labor-intensive nature of the conventional system and enables patch clamp recording to be performed in the absence of a vibration-free table. The sizes of the cavities can be easily modified depending on the size of the cells being tested. To provide a means to select a specific target cell for analysis and to improve the failure rate associated with sample delivery, frontside microfluidic channels covering each analysis cavity were also incorporated. This channel is connected to a syringe, and cells can be selected and manipulated toward the analysis cavity using a fluidic flow.

Each analysis cavity has two or four opposing gold electrodes created inside the cavity and around the via. In the patch clamping mode, one of the electrodes is being used as a reference electrode. Silver/silver chloride (Ag/AgCl) detection electrodes for patch clamping are located on the backside of the wafer. In the patch clamping mode, the frontside and backside electrodes are used to apply stimulating voltage pulses and to

measure resulting ion channel currents. The other frontside electrode can be used as a detection electrode for amperometry. In conventional amperometry, especially in conjunction with patch clamp recording, a carbon electrode is positioned a couple of microns away from the target cell using a precision micromanipulator [68]. The distance between the target cell and the amperometry detection electrode is very important in measuring molecules secreting from the cell. Having an integrated microelectrode at a known distance from the cell eliminates the need for such manipulation and provides consistency and accuracy to the measurement. Amperometry can be performed either by itself or in conjunction with patch clamp recording.

In the whole cell EIS mode, the opposing electrodes are used to measure the electrical impedance of a trapped cell. The trapped cell inside the cavity will be in direct contact with the electrodes, increasing the accuracy of the impedance measurement by preventing current leakage through the surrounding media. Figure 2.1 shows an illustration of the μ-EPAS design.

2.2 Modeling a Cell

A trapped cell inside such an impedance analysis system can be modeled as a series of parallel RC components [47, 54, 58, 91-95]. The cell membrane and cell cytoplasm can each be modeled as a lumped impedance component. The measured impedance is affected by the device shunt impedance since the calibration is typically performed off-chip at the end of the probes of an impedance analyzer. When impedance

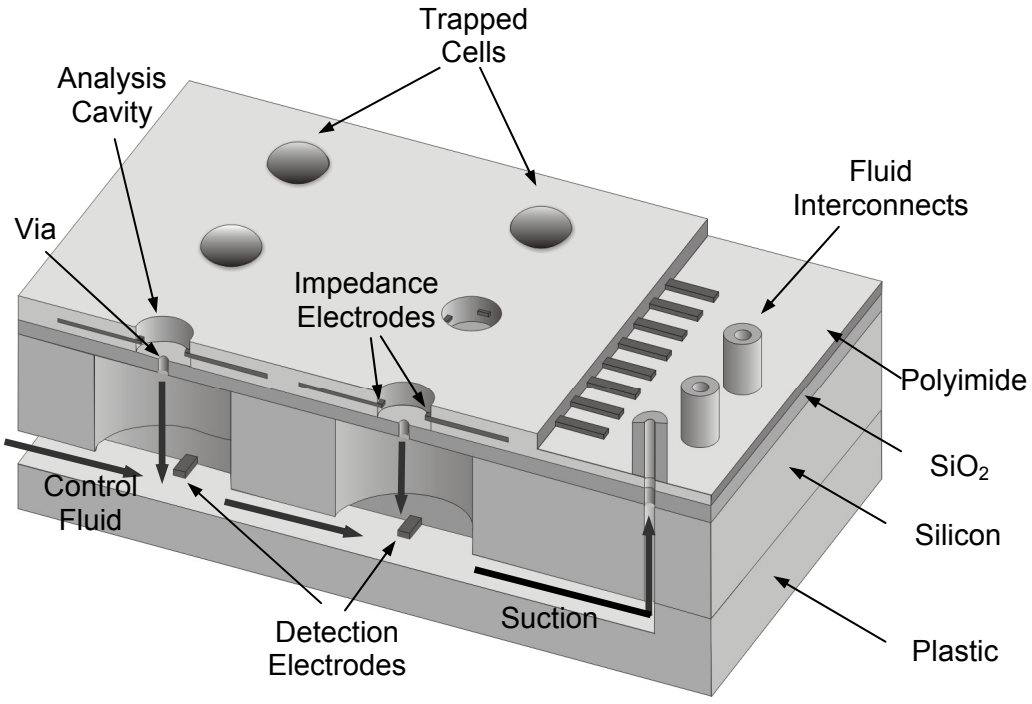

Figure 2.1 Illustration of the designed micro-electrophysiological analysis system (μ-EPAS).

measurements are conducted on solutions, electrode polarization at the liquid/solid interface has to be considered. This effect is minimal during impedance measurements on cells, since the electrodes are in direct contact with the cell. When impedance measurements are conducted on air, the impedance can be modeled as a capacitor. Figure 2.2 shows the schematic diagram of the impedance constituents of a measured cell and a measured solution. By using the impedance measurement of the air and solution as a reference and comparing that to the impedance measurement of a cell, most of the impedance affected by the device shunt can be subtracted. Each lumped impedance Z shown in Figure 2.2 can be replaced with a simple RC circuit model in order to calculate the capacitance of the cell membrane.

Figure 2.3 shows the equivalent circuit of a cell. Both the cell membrane impedance and cell cytoplasm impedance shown in Figure 2.2 are replaced with parallel RC circuits, where R_m is the membrane resistance, C_m is the membrane capacitance, R_c is the cell cytoplasm resistance, and C_c is the cell cytoplasm capacitance.

The membrane capacitance C_m and the membrane resistance R_m are the values that characterize the cell membrane, which is typically associated with the biophysical statuses of a cell and can also vary from cell to cell. To obtain the R and C value of the cell membrane, the measured impedance graph was fit to the model circuit. Cell cytoplasm capacitance was ignored to simplify the model and the R_c value was calculated using the previously reported cytoplasm conductivity of 0.5 S/m [54]. A frequency range of 100 Hz to 5.0 MHz was used since this is the frequency range of interest for most biological samples. The obtained values show the characteristic electrical signature of a target sample. This model was also used to study how ion channel activities affect

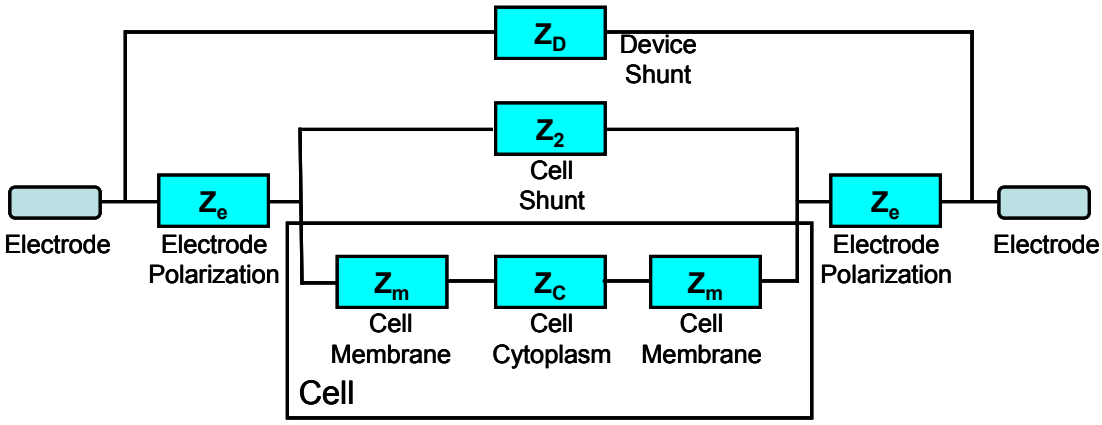

(a)

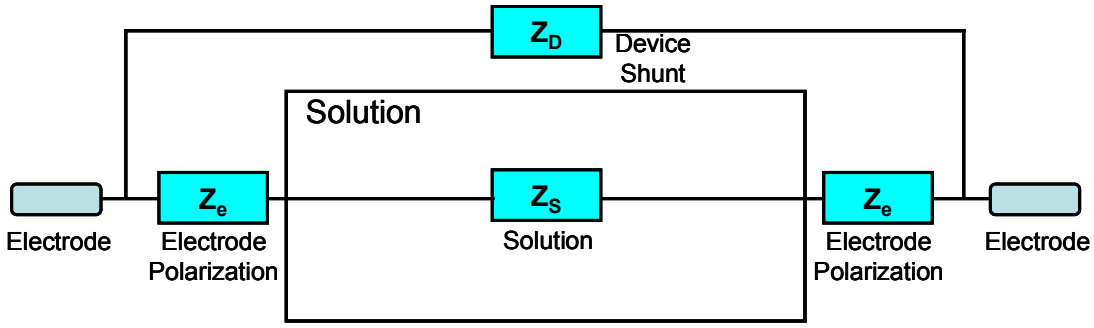

(b)

Figure 2.2 Schematic diagrams of overall impedance constituents of a (a) cell and (b) solution.

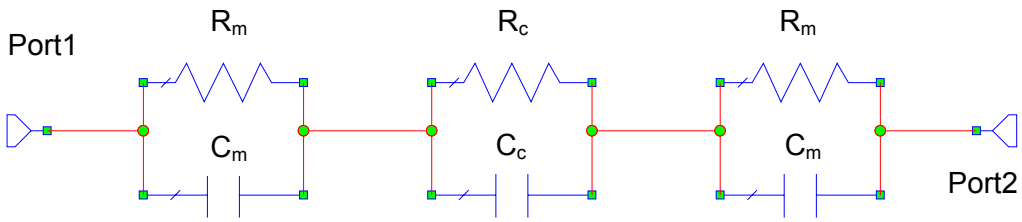

Figure 2.3 Schematic diagram of impedance constituents of a cell.

the cell impedance and how cancer cells from different pathological stages can be differentiated using their characteristic impedances.

CHAPTER 3

SYSTEM FABRICATION AND CHARACTERIZATION

In this chapter, the fabrication steps and the resulting micro-electrophysiological analysis system (μ-EPAS) will be described in detail. The fabricated μ-EPAS went through basic characterization to test its functionality. Fluid testing and electrical testing were performed.

3.1 Microfabricated Analysis System

The μ-EPAS is composed of two parts. The first part was fabricated in a 3-inch diameter silicon wafer. This silicon part contained arrays of analysis sites each composed of an analysis cavity, a via for cell capturing, and integrated electrodes for patch clamp recording and electrical impedance spectroscopy (EIS). The second part was fabricated in plastics and polymers and contained fluidic channels and fluidic interfaces. These two parts were assembled together and connected to fluidic tubing and electric wires.

3.1.1 Silicon Part

The silicon part was fabricated in a 3-inch diameter silicon wafer starting with a 1.8 μm thick SiO_2 film grown thermally in a furnace (Lindberg, USA). A 1.3 μm thick photoresist (Shipley 1813, Rohm and Haas Electronic Materials Corp., USA) was spin-coated at 5000 RPM, followed by baking on a 115 ^oC hotplate for 90 seconds, and patterned to create a 2.0 μm diameter via. The wafer was hard-baked in a 120 ^oC oven for 30 minutes, and the patterned SiO_2 layer was etched using an inductive coupled plasma etching system (ICP, Plasma-Therm, Inc., USA). Next, a 3.5 μm thick polyimide layer (PI 2611, HD Microsystems L.L.C., USA) that served as the bottom portion of the cavity was spin-coated, followed by baking in a 270 ^oC oven for 3 hours. To improve adhesion of the polyimide film to the substrate, an adhesion promoter (VM 652, HD Microsystems L.L.C., USA) was spin-coated at 2000 RPM and baked on a 110 ^oC hotplate for 1 minute. To minimize thermal stress induced during curing, the polyimide-coated substrate was first placed in a 100 ^oC oven for 30 minutes followed by ramping up the temperature to 270 ^oC at a rate of 4 ^oC/minute. The substrate was held at 270 ^oC for 2 hours and cooled down slowly to room temperature inside the oven by turning off the power.

A Ti/Au film was evaporated (CVC SC 5000 E-beam Evaporator, CVC, Inc., USA) to a thickness of 250 Å and 4000 Å respectively and patterned to create one or two pairs of opposing electrodes inside the analysis cavity and around the via. The titanium was etched in 2 % HF, and the gold layer was etched in KI:I_2:DI water = 4:1:40 solution. The width of the electrodes were 4-8 μm inside the analysis cavity, increasing to 200 μm

as the traces were routed toward the bonding pads located at the edge of the wafer. The bonding pads were 1 mm wide and 1.25 mm apart so that a surface-mount crimping connector such as DF13 (Hirose Electronic Co. LTD., Japan) with 1.25 mm pitch could be directly soldered on top of these bonding pads for convenient electrical interconnects. Figure 3.1 shows the mask layer of the electrodes and the traces connecting the electrodes to the bonding pads. After soldering, epoxy was applied between the bonding pads and wires to increase the mechanical stability.

A second layer of 3.5 μm thick polyimide was spin-coated that served as the top portion of the cavity and also as an insulating layer. Again, the adhesion promoter VM 652 was used before spin-coating the polyimide. To pattern the polyimide, aluminum was chosen as an etch mask. Aluminum induces less stress to the polyimide film with minimal over-etching of the patterns compared to other metals. For example, Cr induces high stress and cracks the underlying polyimide film. Copper does not induce large stress but over-etching of the patterns are significant when using copper etchant, such as HNO_3:H_2O_2:DI water = 1:1:10 or H_2SO_4:H_2O_2:DI water = 1:1:10. Aluminum was evaporated on the polyimide layer to a thickness of 1000 Å, and the 10.0-16.0 μm diameter analysis cavities were patterned using photoresist. The patterned aluminum layer was etched using aluminum etchant (Type A, Transene Company, Inc., USA) at 50 ^{o}C. Polyimide was etched using reactive ion etching (RIE) in a 90% oxygen and 10% CHF_3 environment with a two-step process. The polyimide was first etched in a 300 mTorr, 300 W environment for 10 minutes followed by a second etch step in a 100 mTorr, 100 W environment for 15 minutes. The two-step process was chosen to minimize polyimide residue left on the substrate. The first high-power etching step

(a)

(b)

Figure 3.1 Mask layer of the (a) overall electrode configuration and (b) enlarged view of the electrode configuration.

removed the bulk of the polyimide that minimizes residue whereas the second low-power etching step provided a more controlled etching. The photoresist was removed using photoresist remover (1112A, MicroChem Corp., USA). The remaining aluminum layer was removed using aluminum etchant at 50 ^{o}C.

Circles, 200 μm in diameter, were patterned on the backside of the Si wafer using a 33 μm thick negative photoresist layer (NR9-8000, Futurrex, Inc., USA) and a double-side mask aligner (MA6, Suss MicroTec AG, Germany). The negative photoresist was spin-coated at 700 RPM for 30 seconds, soft-baked in a 95 ^{o}C oven for 30 minutes, exposed at 1000 mJ, followed by a post-exposure bake on a 100 ^{o}C hotplate for 2.5 minutes. Futurrex photoresist provided excellent patterning capability and performed well as an etch mask in the subsequent silicon etching step. The Si wafer was etched all the way through from the backside using the ICP Bosch etching process (Plasma-Therm, Inc., USA). The SiO_2 film on the frontside of the wafer served as an etch stop. To insulate the exposed silicon, a 4000 Å thick SiO_2 was deposited using a plasma enhanced vapor deposition system (STS PECVD, Surface Technology Systems plc., UK).

Figure 3.2 shows a micrograph of the fabricated device. Arrays of analysis sites and electrodes connecting each analysis cavity on a 3-inch diameter silicon wafer can be seen. Bonding pads located toward the edge of the wafer can be also seen. Figure 3.3 (a) shows an array of eight cavities with two and four opposing electrode configurations interfacing with each analysis cavity. The analysis sites share a common electrical ground. Figure 3.3 (b) shows a 16.0 μm diameter polyimide cavity with a 3.0 μm via in SiO_2 at the center and four 4.0 μm wide electrodes. Figure 3.3 (c) shows a 10.0 μm diameter polyimide cavity with a 2.0 μm via in SiO_2 and two 4.0 μm wide electrodes.

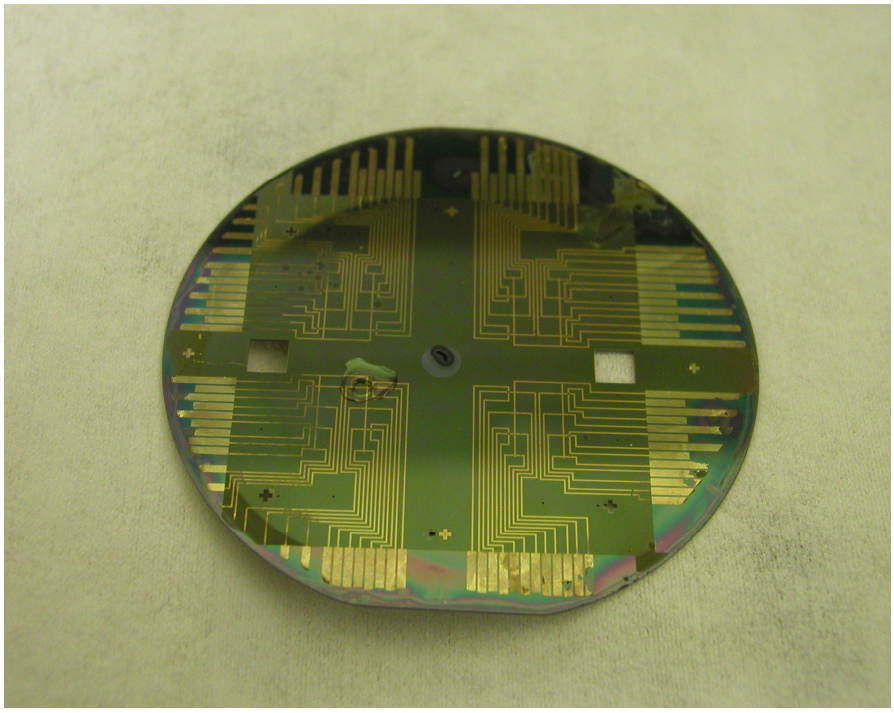

Figure 3.2 Picture of the fabricated silicon part. Each quarter of the 3-inch diameter silicon wafer has 16 analysis sites. All the electrodes are routed to the bonding pads located at the edge of the wafer for easy electrical connection.

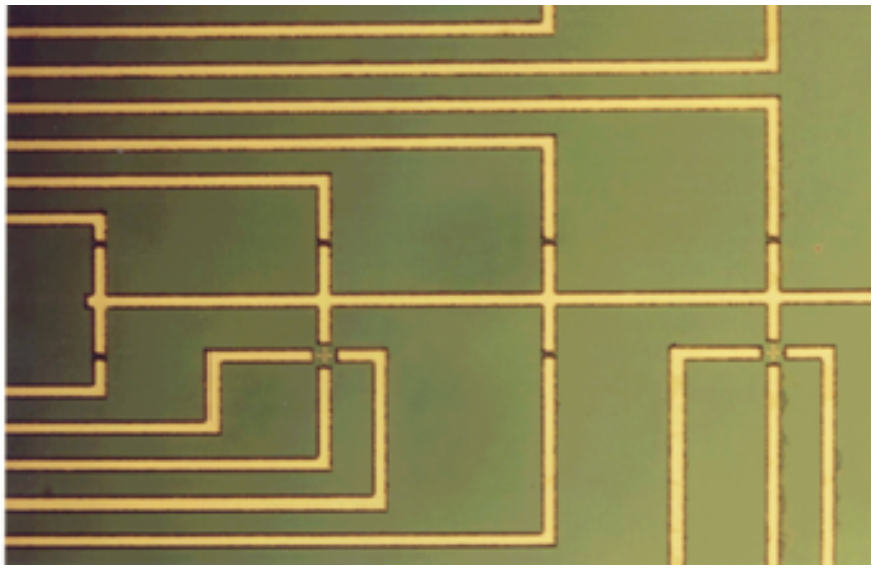

(a)

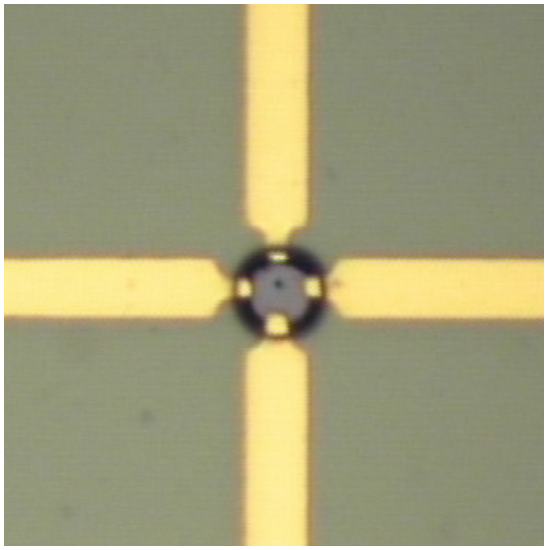

(b)

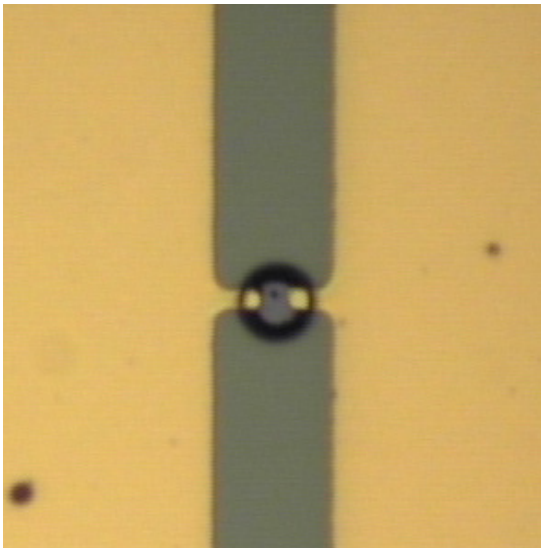

(c)

Figure 3.3 Picture of the enlarged views of the fabricated silicon part. (a) An array of 8 analysis sites with two and four electrode configurations. (b) Enlarged view of an analysis site with 16 µm diameter cavity, 3 µm diameter via, and four opposing electrodes. (c) Enlarged view of an analysis site with 10 µm diameter cavity, 2 µm diameter via, and two opposing electrodes.

Figure 3.4 shows a single analysis site in more detail. Figure 3.4 (a) shows a scanning electron micrograph of a 2.0 μm diameter via fabricated in SiO_2. The smooth edge of the via helps create a high seal resistance when the μ-EPAS is used in the patch clamping mode. Figure 3.4 (b) shows a scanning electron micrograph of an analysis site showing a via, analysis cavity, and two opposing electrodes. Figure 3.4 (c) shows a 3-D profilometer scan (Wyko NT 3300, Veeco Instruments, Inc., USA) of an analysis site.

One drawback of this configuration is that the thin SiO_2 film can be easily cracked when a negative pressure is applied through the backside fluidic channel to capture a single cell inside an analysis cavity. To improve the mechanical stability of the film, leaving a certain thickness of supporting silicon during the ICP Bosch process is desirable. To enable this, silicon was etched to a depth of 30 μm through the frontside via using the ICP Bosch process right after the 1.8 μm thick SiO_2 film was etched to create the via. The SiO_2 film was used as a masking layer. When the silicon was etched from the backside using the ICP Bosch process, instead of etching all the way through the wafer, a 20 μm thick silicon layer was left by time-controlled etching. To remove any clogging of the via caused by the spin-coated polyimide at the subsequent step, the device was placed in a RIE at a 90 % oxygen, 10 % CHF_3 environment for 10 minutes with the backside toward the plasma.

Silver/silver chloride (Ag/AgCl) detection electrodes used for patch clamp recording were patterned on the backside of the wafer using microstenciling [96, 97]. The conventional electrode fabrication method uses metal evaporation followed by photolithography and metal etching. These processing steps are not compatible with the processed silicon part due to the holes and thin membranes in the wafer. Evaporation or

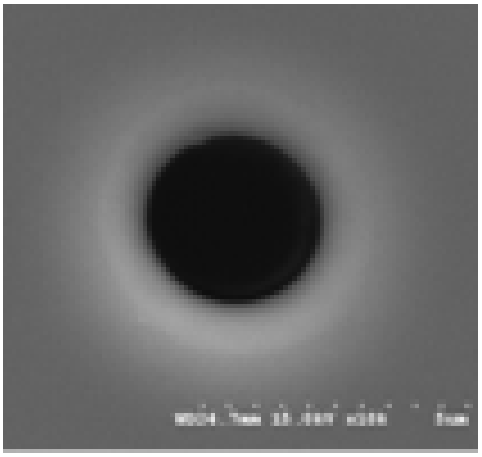

(a)

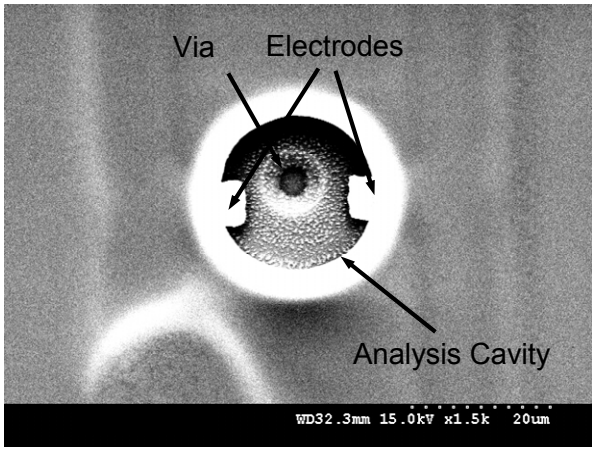

(b)

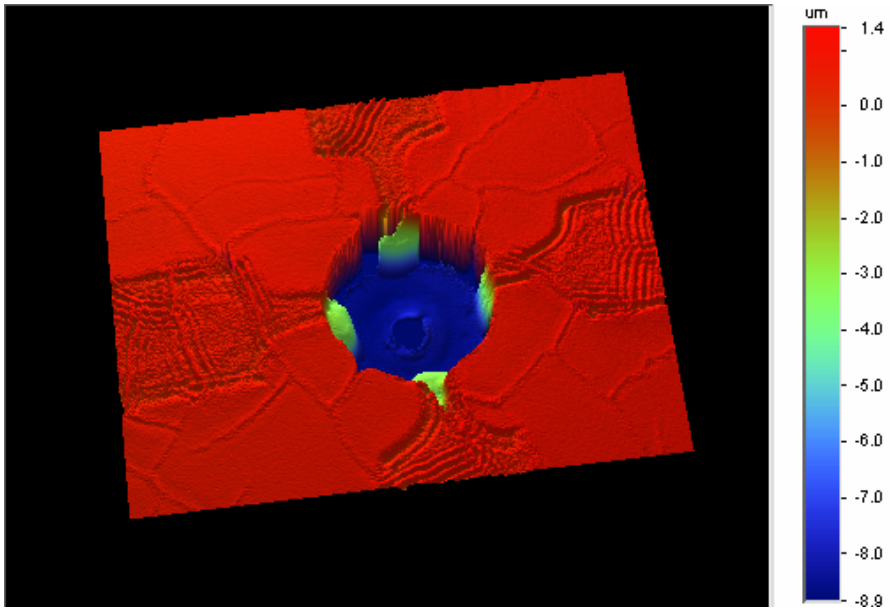

(c)

Figure 3.4 (a) Scanning electro micrograph of a 3.0 µm diameter via created in SiO_2. (b) Scanning electro micrograph of an analysis site. (c) 3-D optical profilometer scan of an analysis site.

sputtering of a metal layer on the entire backside of the wafer can possibly clog the via. The SiO_2 film on the frontside of the processed wafer can crack during the spin-coating process due to the vacuum applied from the vacuum chuck of a spin-coater. Also, the silver etchant ($KI:I_2$:DI water = 4:1:40) will etch the gold electrodes patterned on the frontside of the wafer. Removing the photoresist would also be problematic since the underlying negative photoresist dissolves in acetone. All of the problems listed above limit the use of the conventional electrode fabrication steps. Therefore, an alternative method was needed for creating metal electrodes onto the backside of the fabricated device.

The microstenciling technique, also called shadow mask technique, illustrated in Figure 3.5 was chosen to overcome these problems. A 3-inch diameter silicon wafer was patterned with NR9-8000 photoresist to a pattern shown in Figure 3.6. The wafer was etched through using the ICP Bosch process. The smooth photoresist-side of the fabricated microstencil was placed against the substrate, and silver was evaporated to a thickness of 4000 Å. To create the Ag/AgCl electrodes, the silver electrodes were dipped in chlorine solution for 15 seconds followed by rinsing.

Figure 3.7 (a) shows the microstencil fabricated in silicon. The smooth frontside was placed against the target wafer to enable good pattern replication. The microstencil and the substrate were visually aligned through the cross-shaped alignment marks. Figure 3.7 (b) shows the microstenciled silver electrodes on the backside of the silicon part. The electrodes were located next to the 200 μm diameter openings created on the backside of the fabricated device. The silver electrodes were 100 μm wide and 4000 Å

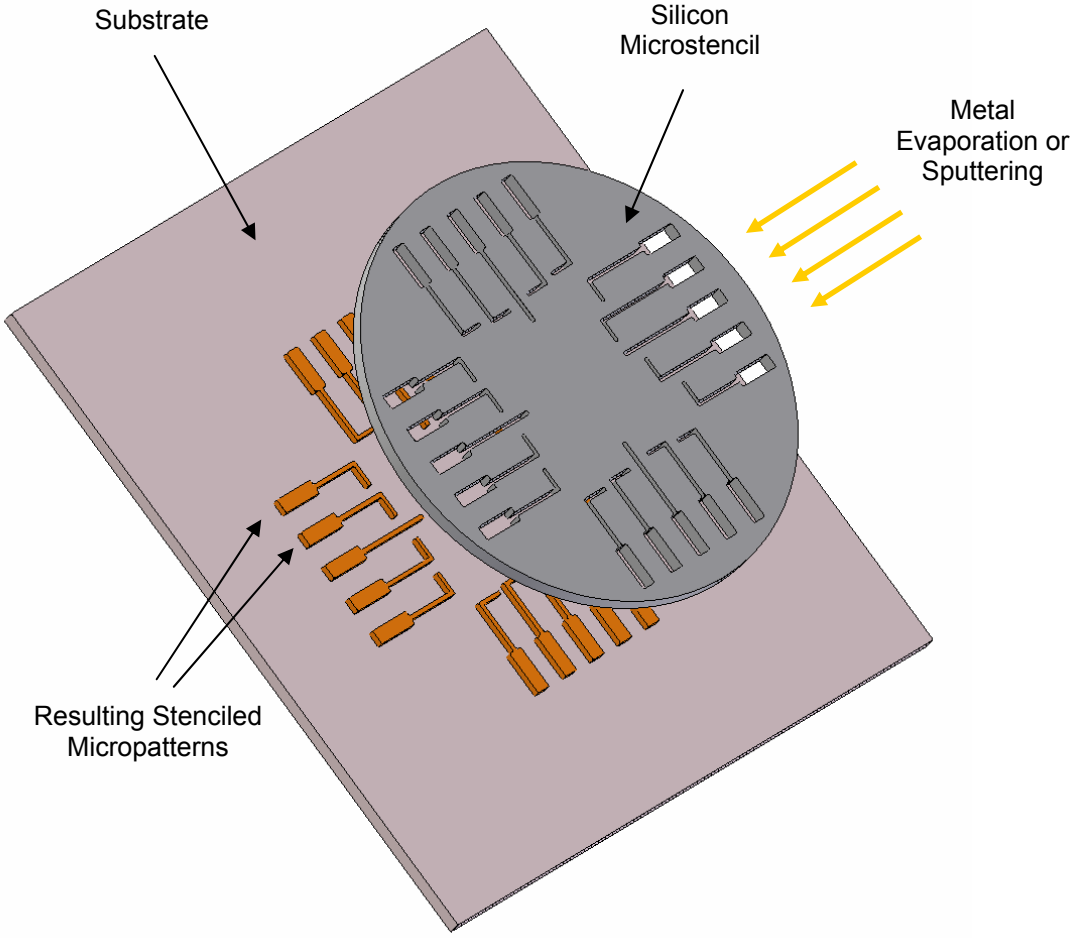

Figure 3.5 Illustration of the microstenciling process.

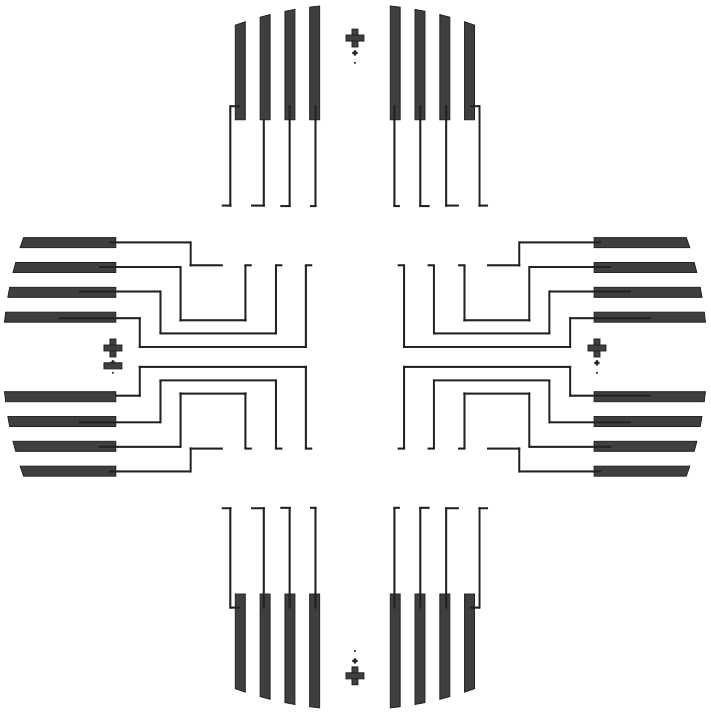

Figure 3.6 Mask design for the backside electrodes.

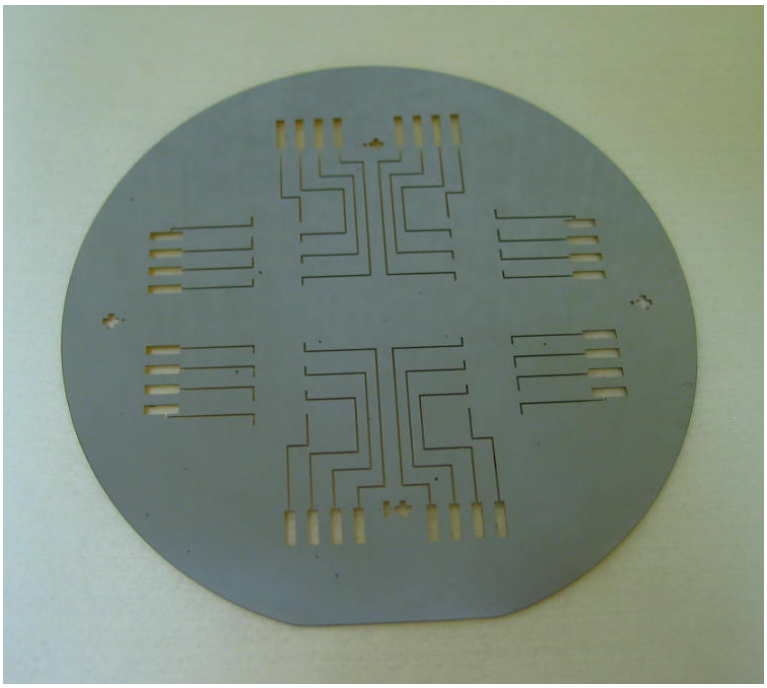

(a)

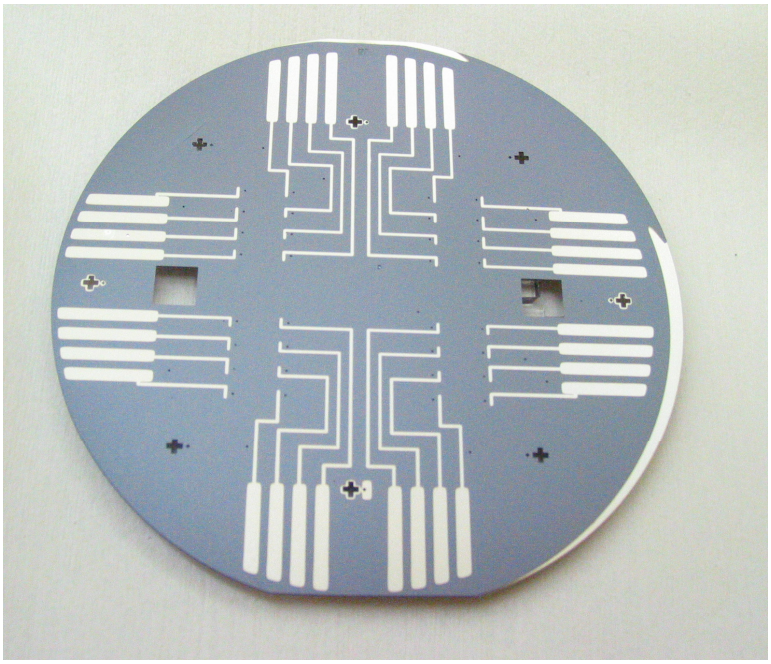

Figure 3.7 (a) Picture of the fabricated three-inch diameter silicon microstencil. (b) Silver electrodes stenciled on the backside of the silicon part of the fabricated analysis system.

thick, and the bonding pads were 1 mm wide. Good pattern replication and smooth pattern edges were observed.

On a 3-inch diameter silicon wafer, arrays of 16 analysis cavities were positioned on each quarter of the wafer, resulting in 64 analysis sites overall. Figure 3.8 shows the overall fabrication steps.

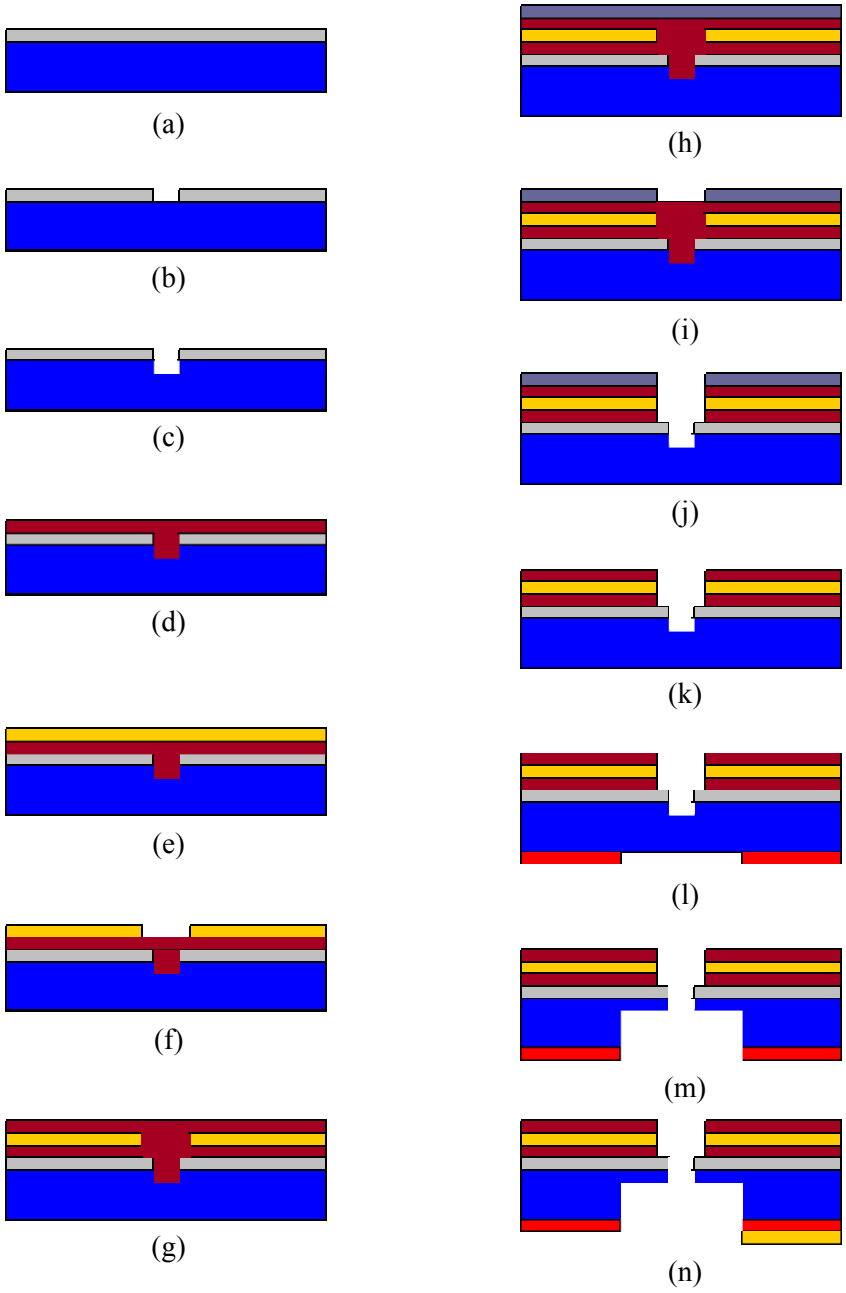

Figure 3.8 Fabrication steps for the silicon part. (a) SiO_2 deposition on Si (b) SiO_2 patterning in ICP (c) Si etching using ICP Bosch process (d) Spincoating polyimide (e) Ti/Au deposition (f) Electrode patterning (g) Spincoating polyimide (h) Aluminum deposition (i) Aluminum patterning (j) Polyimide etching in RIE (k) aluminum removal (l) Patterning backside (m) Etching Si using ICP Bosch process (n) Microstenciling silver electrode.

3.1.2 Microfluidic Channels & Interfaces

3.1.2.1 Backside Fluidic Channel/Interface Part using Stereolithography

Microfluidic channels and fluidic interfaces were created using stereolithography. Stereolithography is a technique where a laser is used to cure a photosensitive polymer structure layer by layer, as shown in Figure 3.9 [98]. By simply providing a 3-D design as an input to a stereolithography system (Viper SI2, 3D Systems Corp., USA), parts with minimum resolution of 75 μm can be easily created [97]. The first two fluidic channel/interface design shown in Figure 3.10 were created using the 3-D design software Solid Edge® (Electronic Data Systems Inc., USA). The first design contains four fluidic chambers, and the second design contains eight fluidic channels 800 μm in

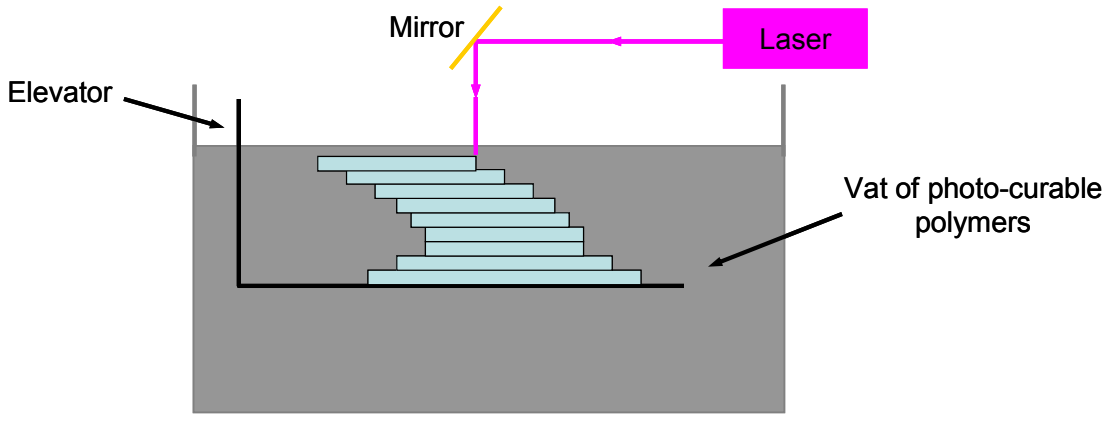

Figure 3.9 Illustration of the stereolithography process.

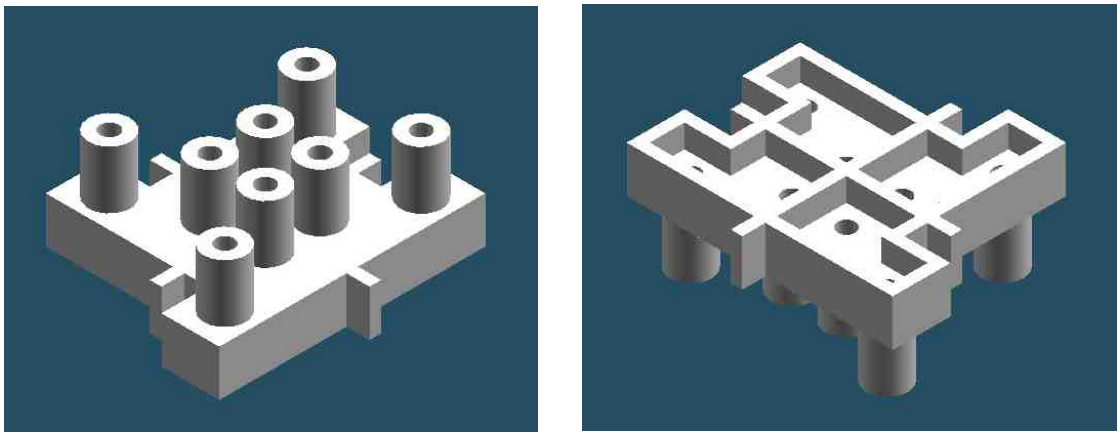

(a)

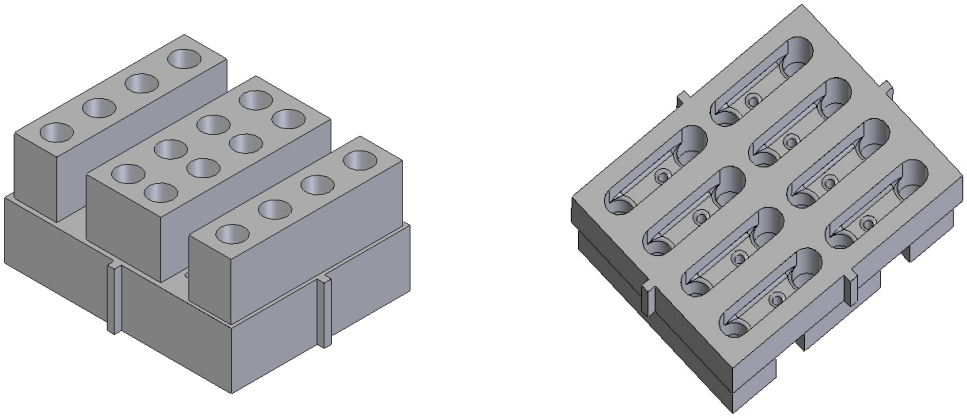

(b)

Figure 3.10 Design of the fluidic channel/interface part of (a) first generation that contains 4 fluidic chambers and (b) second generation that contains 8 fluidic channels.

width. The inlet/outlet ports are 1700 μm in diameter so that standard 1/16 inch outer diameter fluorinated ethylene propylene (FEP) tubing (Upchurch Scientific, Inc., USA) can be plugged into the ports and sealed using adhesives. These channels and ports are used to pull negative pressure through the via to position and capture a single cell. These channels are also used to control the intracellular fluid environment of the sealed region of the cell membrane.

Figure 3.11 shows the first two designs of the stereolithographically fabricated backside fluid channel/interface part including inlet and outlet ports. The first design as shown in Figure 3.11 (a) has four pairs of inlet and outlet ports each connected to a fluidic chamber. Each fluidic chamber covers four analysis sites when bonded to the silicon part so that up to four analysis sites can be used simultaneously. The second design as shown in Figure 3.11 (b) has eight pairs of inlet and outlet ports each connected to an 800 μm wide fluidic channel. The fluidic channel/interface part was aligned and bonded to the silicon part. Each channel covers two analysis sites, so that two analysis sites can be used simultaneously. Both fluidic channel/interface parts required the use of adhesive to prevent any leakage between the channel/interface part and the tubing. Due to the permanent nature of the bond between the tubing and the channel/interface part, connecting and disconnecting the system to a fluidic pumping/valving system was not convenient. To overcome this limitation, a third generation fluidic channel/interface part was designed so that tubing can be easily connected and disconnected without the need of adhesives.

The third fluidic channel/interface part design shown in Figure 3.12 still incorporated eight fluidic channels 800 μm wide but had barb-fitted inlet/outlet ports that

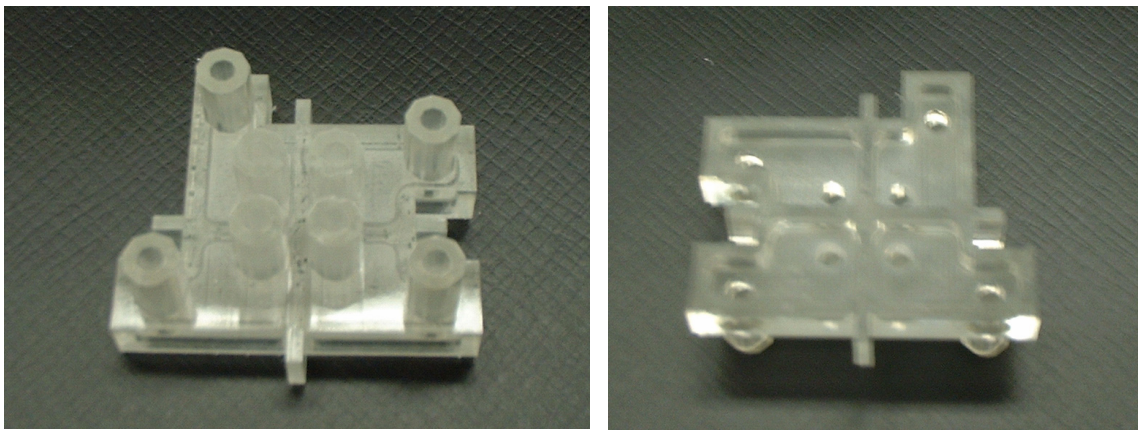

(a)

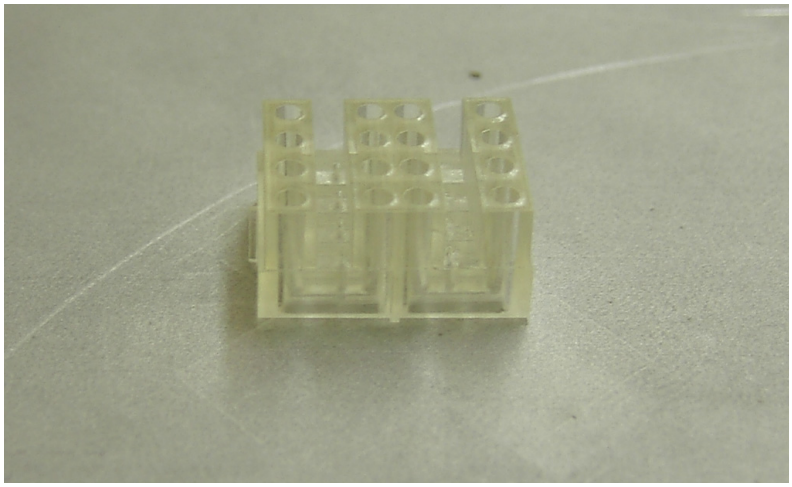

(b)

Figure 3.11 Picture of the stereolithographically fabricated fluidic channel/interface part. (a) The first design has 4 pairs of inlet/outlet ports into which tubing can be inserted. (b) The second design has 8 pairs of inlet and outlet ports connecting 8 channels.

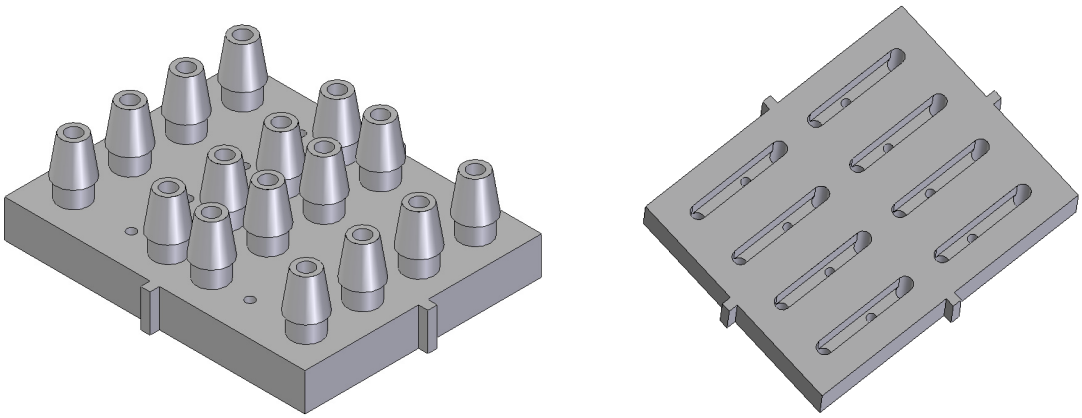

Figure 3.12 Design of the third generation fluidic channel/interface part.

were 800 μm in inner diameter. Each channel covers two analysis cavities. Flexible silicone tubing (Helix Medical, Inc., USA) with inner diameter of 1.02 mm can be plugged above the ports. The ports were created to a shape of barb-fitting so that the flexible silicon tubing can be simply plugged in and form a seal without the need of adhesive. These stereolithographically defined parts were aligned to the overlying silicon wafer and bonded using a two-part epoxy. Figure 3.13 shows the fabricated plastic channel/interface part. Using this design, cells can be trapped in two analysis cavities simultaneously and analyzed in parallel. Interfaces capable of trapping up to 16 cavities in parallel were also designed and fabricated.

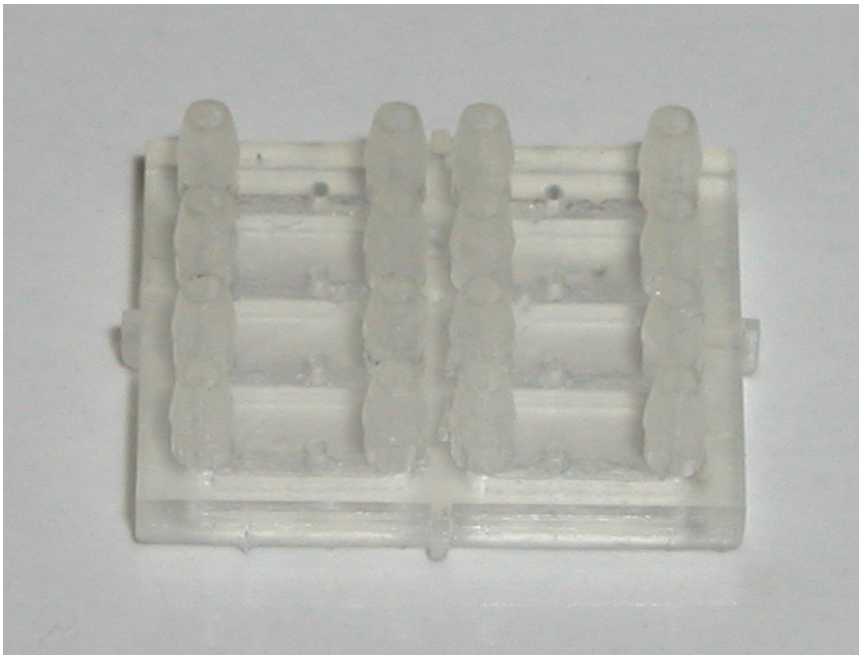

(a)

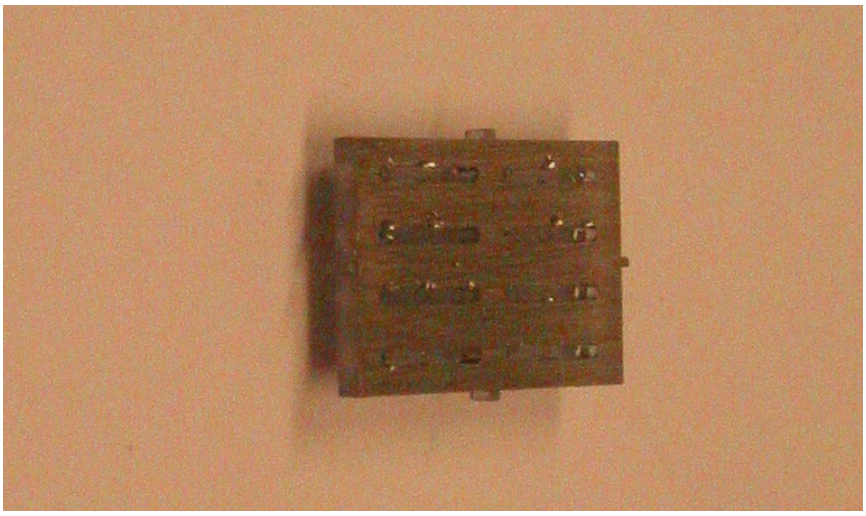

(b)

Figure 3.13 Picture of the stereolithographically fabricated fluidic channel/interface part showing the (a) barb-fitted interface onto which flexible silicone tubing can be directly connected and (b) the backside fluidic channels.

3.1.2.2 Frontside Fluidic Channel/Interface Part using Soft Lithography

The frontside fluidic channels were used to guide the cells toward the analysis sites and to control the extracellular fluidic environment. The channels were fabricated in poly(dimethylsiloxane) (PDMS) using soft lithography [99, 100]. The master mold was fabricated in SU-8 (MicroChem Corp., USA) to create an array of ridges with widths of 100 μm and heights of 25 μm on a 3-inch diameter silicon wafer. PDMS (Sylgard 184, Dow Corning Corp., USA) resin and curing agent was mixed in a 12:1 ratio and poured onto the master mold. The mixture was cured in a 70 ^{o}C oven for 1 hour to create a 500 μm thick PDMS channel layer. The PDMS layer was released and 350 μm diameter inlet/outlet holes were created using a CO_2 laser micromachining system (LS500, Gravograph New Hermes, Inc., USA). This PDMS layer was aligned and bonded thermally to the fabricated silicon part so that the fluidic channels are located on top of the analysis cavities. The bonding occurred in an 80 ^{o}C oven for 24 hours.

A second PDMS interface layer that can accommodate tubing from the side instead of from the top was fabricated using a mold created with stereolithography, as shown in Figure 3.14. The resulting PDMS layer, 2.0 mm thick, had side channels into which 1/16 inch outer diameter tubing was inserted from the side. These large channels are connected to smaller channels leading to the microchannel in the underlying PDMS layer. Connecting fluidic tubing from the side prevented the optical view-path being blocked by tubing sticking out vertically on the frontside of the system during testing. The second PDMS layer was aligned and bonded to the first PDMS channel layer in an

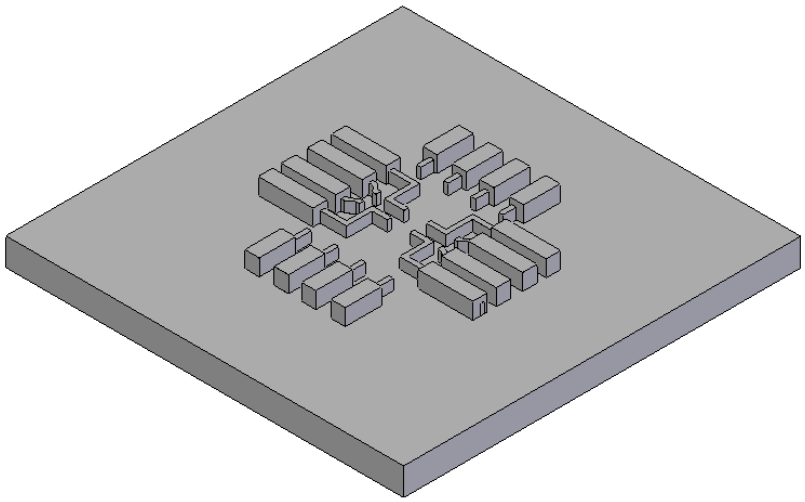

Figure 3.14 Mold design for soft lithography of the frontside PDMS interface.

80 ^{o}C oven for 24 hours. Figure 3.15 shows the fabrication process flow for the fluidic channel/interface part and its connecting scheme to the fluidic tubing.

The fabricated frontside PDMS channels/interface part is shown in Figure 3.16. Fluidic tubing connected to the PDMS part from the side can be observed. Two-part epoxy was used to provide mechanical support and to prevent any leakage. Although PDMS is relatively transparent, a thick layer can still create optical distortion to the image under a microscope. To improve the image quality, the top PDMS layer was fabricated so that the middle section containing analysis sites is not covered with the second PDMS layer. Better visualization of the analysis sites and cells under a microscope was possible through this design.

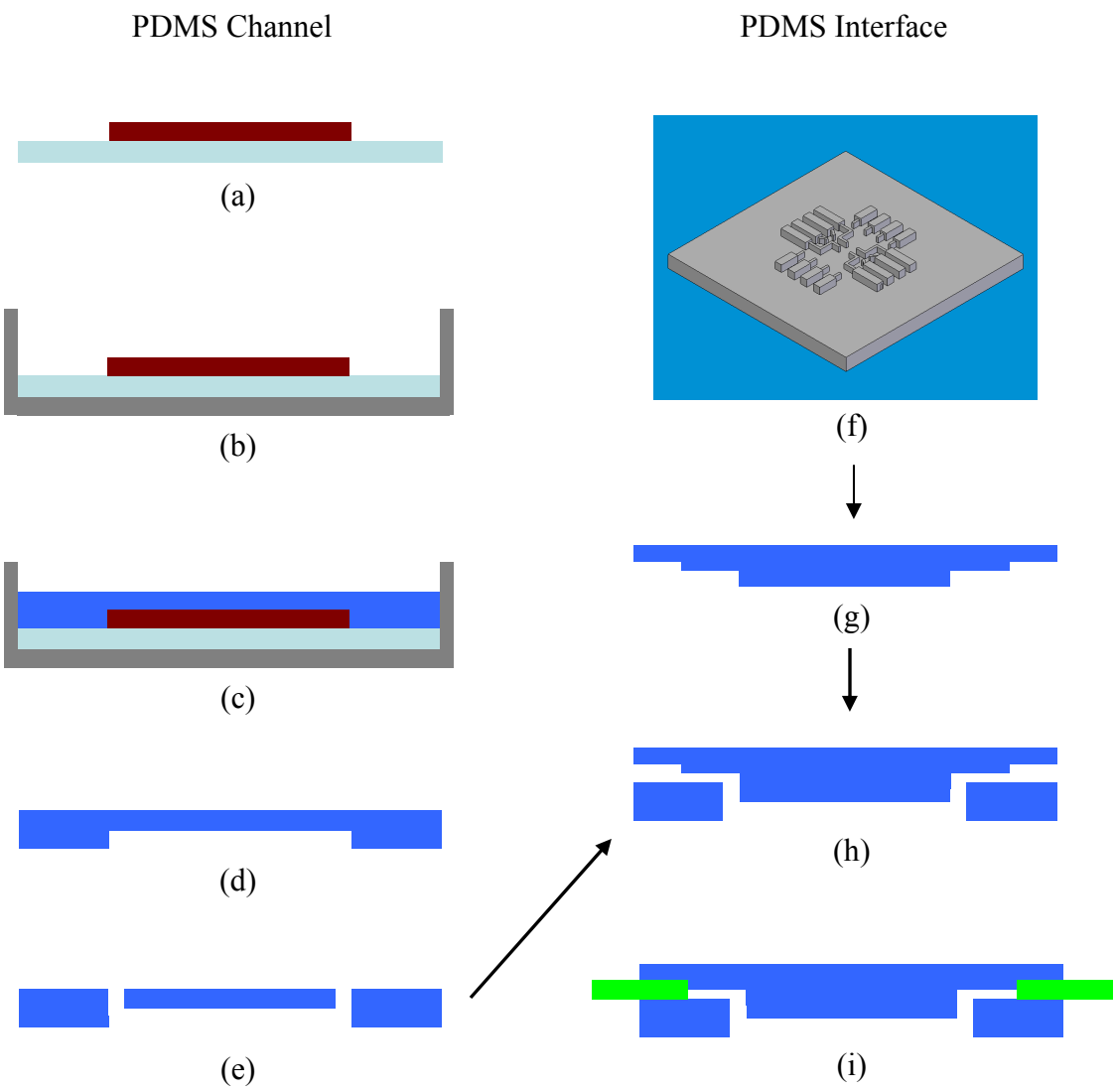

Figure 3.15 Processing flow for the two PDMS layers and the bonding/assembling scheme with tubing. (a) Silicon substrate patterning with channel structures, (b) Placing silicon master mold in a support structure, (c) Pouring PDMS followed by curing, (d) Releasing PDMS layer from silicon master mold, (e) Ablating inlet/outlet holes using laser micromachining, (f) Creating plastic mold for PDMS interface layer using stereolithography, (g) Repeating process (a) to (d) to create PDMS replica using the stereolithographically fabricated mold, (h) Bonding two PDMS layers from (e) and (g), (i) Inserting tubing.

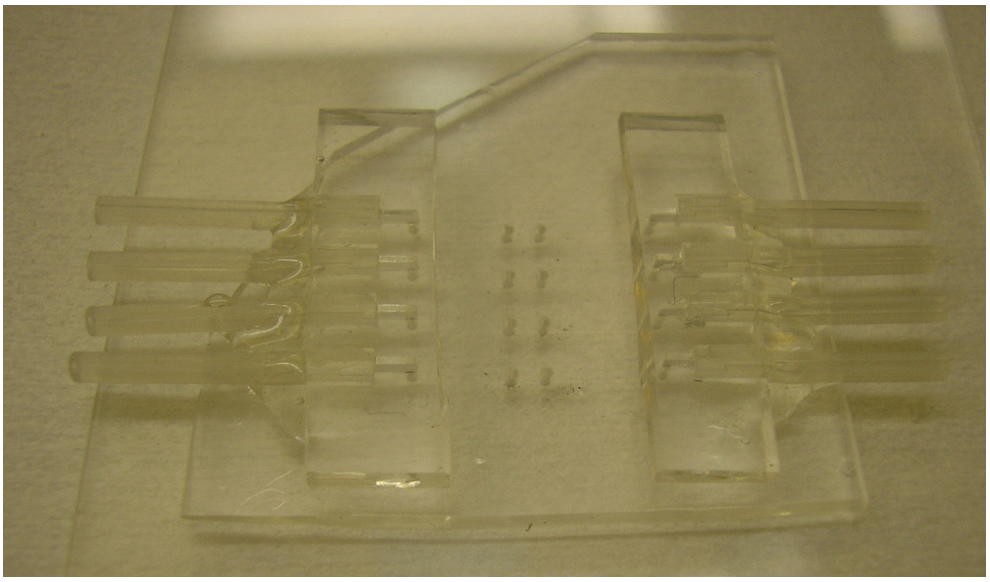

Figure 3.16 Picture of the fabricated PDMS channel/interface part. The bottom PDMS layer (0.5 mm thick) contains microchannels with inlet/outlet holes ablated using laser micromachining. The top PDMS interface layer (2.0 mm thick) contains channels that can accommodate fluidic tubing from the side so that fluid can run from tubing to the underlying microchannels.

To optimize the bonding between the PDMS layers and the PDMS layer to the silicon part, several bonding and curing conditions were tested. The PDMS curing conditions were tested with temperature between 50 ^{o}C and 100 ^{o}C and with curing times between 10 minutes and 24 hours. Mixing ratios of PDMS resin and curing agent were adjusted from 10:1 to 14:1. Bonding conditions were tested with temperatures between 50 ^{o}C and 100 ^{o}C and with curing times between one hour and 24 hours. The bond strength was tested by pealing off the PDMS layer from the side. Optimum bonding condition was achieved when the PDMS resin and curing agent was mixed at a 12:1 ratio and was cured to a minimum but still hard enough to be able to release it from the master

mold. Curing the mixed PDMS at 70 ^{o}C for 30 minutes and bonding it in a 70 ^{o}C oven for 24 hours provided maximum bond strength.

Figure 3.17 shows the assembled device consisting of the silicon part, backside fluidic channel/interface part, and topside PDMS channel/interface part.

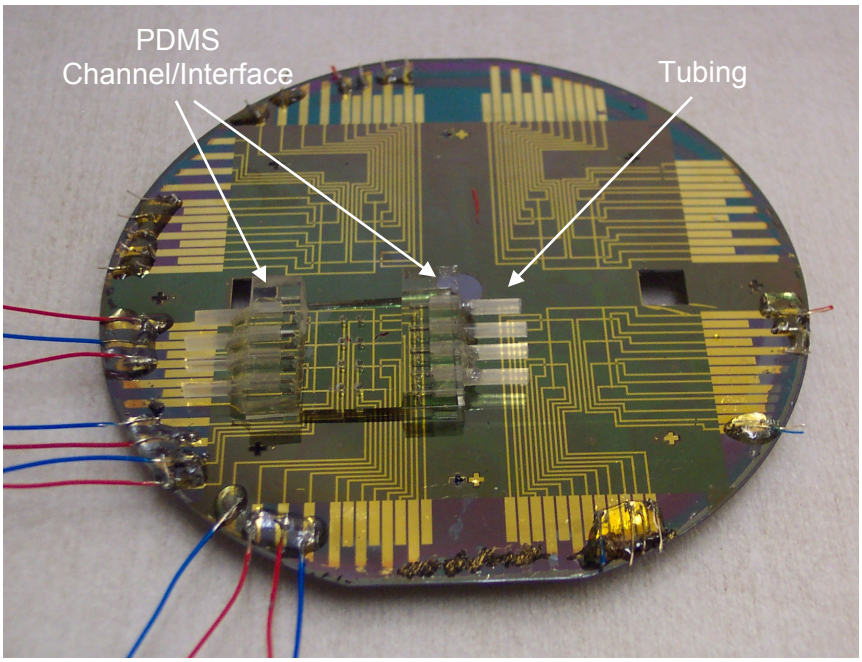

(a)

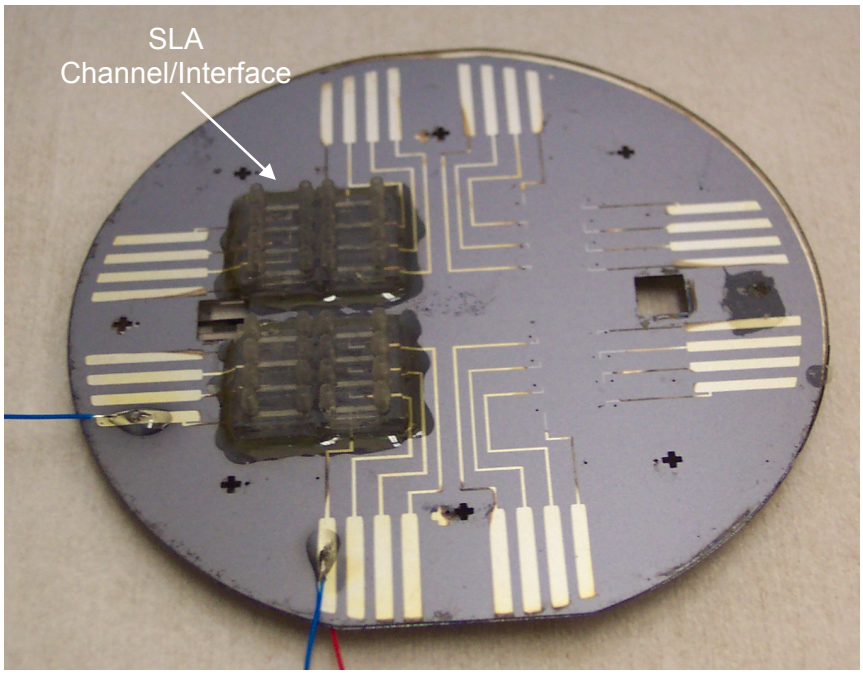

(b)

Figure 3.17 Picture of the assembled device showing (a) the silicon part with PDMS channel/interface part bonded on top of it and connected to tubing and wires and (b) backside fluidic channel/interface part bonded on the backside of the silicon part.

3.2 Device Preparation and Characterization

To prepare the device for testing, the 1.02 mm inner diameter silicone tubing (Helix Medical Inc., USA) was plugged into the backside fluid interface. Silicone tubing was chosen due to its flexibility compared to fluorinated ethylene propylene (FEP) tubing. The inlet tubing was connected to a syringe to deliver intracellular solutions or buffer solutions to the device and to apply negative pressure for positioning and capturing of cells. The outlet tubing was connected to a three-way valve to control the flow and pressure.

Two sample loading methods were used. Initially, samples were simply dropped on top of the cavities using a pipette. In the second method, the PDMS microchannel/fluidic interface described above was used. The second sample loading method enabled selecting a specific cell of interest under a microscope and trapping the cell inside an analysis cavity. The first method is suitable when arrays of analysis sites are used simultaneously for high throughput analysis and the second method is suitable when an operator wants to select a specific cell for analysis.

To connect tubing to the frontside PDMS microchannels, standard 1/16 inch outer diameter FEP tubing was attached from the side to the two-stack PDMS channel/fluidic interface structure using epoxy, as shown in Figure 3.16. Silicone tubing was then plugged over these FEP tubing and subsequently connected to a syringe. A 10 μl Gastight® syringe (1701, Hamilton Co., USA) was either used manually or used with a syringe pump (PHD 2000, Harvard Apparatus, Inc., USA) to manipulate the cells in

suspension and guide them toward the analysis cavity. Wires were connected to the frontside and the backside bonding pads on the device using soldering.

To test the fluidic functionality, the backside fluidic channel was filled with phosphate-buffered saline (Dulbecco's PBS, Invitrogen Corp., USA) and pushed through the via. Fluid pushed through the via toward the frontside could be observed under a microscope. No leakage was observed throughout the system. To test the system for single cell capturing, 10 μm diameter polystyrene beads (Bangs Laboratories, Inc., USA) were suspended in D-PBS and used as cell replicas. The beads were loaded into the system and manipulated using the syringe connected to the backside channel. The pushing and pulling motion of the syringe was transferred to the capturing and releasing motion of a single polystyrene bead.

CHAPTER 4

PATCH CLAMP RECORDING AND WHOLE CELL ELECTRICAL IMPEDANCE SPECTROSCOPY

In this chapter, the fabricated micro-electrophysiological analysis system (μ-EPAS) was used to perform patch clamp recording and whole cell electrical impedance spectroscopy (EIS) on single cells. Primary cultured bovine chromaffin cells were tested using patch clamping. The ion channel activities of this cell were also studied using whole cell EIS. Human breast cancer cells from different pathological stages were differentiated using EIS.

4.1 Chromaffin Cells

Ion channel activities of the primary cultured bovine chromaffin cells were characterized using patch clamping and whole cell EIS.

4.1.1 Cell Preparation

Bovine chromaffin cells were prepared in Dr. Engisch's lab at Emory University (Department of Physiology, Atlanta, GA) [101-103]. The primary cultured cells were maintained in a 37 ^{o}C, 95 % humidity, and 5 % CO_2 environment for up to five days. The primary cultured cells were transferred to a centrifuge tube and centrifuged for 15 minutes at 700 RPM (Fisher Scientific Centrifuge Model 225, Fisher Scientific Co., USA). After centrifugation, the culture media was disposed of and 3 ml of phosphate-buffered saline (Dulbecco's PBS, Invitrogen Corp., USA) or extracellular solution described below was added.

The extracellular solution was made by first making a 10X extracellular stock solution by adding 75.97 g NaCl, 1.49 g KCl, and 10 ml 1 M $MgCl_2$ to one liter of DI water. To make an extracellular solution with 5 mM calcium concentration, 900 ml of DI water was mixed with 101 ml of 10X extracellular stock solution, followed by adding 1.802 g dextrose (D16-500, Fisher Scientific, Inc., USA), 2.493 g N-(2-Hydroxyethyl)piperazine-N'-(2-ethanesulfonic acid) (HEPES, H7637, Sigma-Aldrich Co., USA), 0.735 g $CaCl_2(2H_2O)$ (20891, Calbiochem® EMD Biosciences, Inc., USA), and 0.976 g N-Methyl-D-Glucamine (M-2004, Sigma-Aldrich Co., USA). The pH was adjusted to 7.23 with HCl and the osmolality was adjusted to 295 with the 10X extracellular stock solution. The extracellular solution was filtered using a 0.2 μm syringe filter (Acrodisk®, Pall Corp., USA).

The intracellular solution was made by adding 1.066 g D-glutamic acid (G1001, Sigma-Aldrich Co., USA), 1 M CsOH (101328, ICN Biomedicals, Inc., USA), 0.014 g

BAPTA (B1214, Molecular Probes, USA), 0.1046 g 4-Morpholinepropanesulfonic acid (MOPS, M5162, Sigma-Aldrich Co., USA, USA), and 474 μl 1 M NaCl to 30 ml DI water. The pH was adjusted to 7.2 using CsOH with the total volume adjusted to 50 ml. The osmolality was adjusted to 308 using mannitol (Sigma-Aldrich Co., USA). The intracellular solution was filtered using a 0.2 μm syringe filter (Acrodisk®, Pall Corp., USA).

For perforated patch clamping, amphotericin B (Calbiochem® EMD Biosciences, Inc., USA) was prepared by adding 5 mg of amphotericin B to 40 μl dimethyl sulfoxide (DMSO, Sigma-Aldrich Co., USA), followed by sonication, vortexing, and centrifuging for 30, 15, and 10 seconds respectively twice. Seven microliters of this solution were added to 1.4 ml of intracellular solution and homogenized twice for five seconds.

Before using the cells for testing, the viability of the cells were confirmed by either using Trypan blue (Sigma-Aldrich Co., USA) or a fluorescent live/dead viability kit (L-3224, Molecular Probes, Inc., USA). Trypan blue is a blue acid dye that contains two azo chromophores, which will react with the cell when the membrane is damaged. Live (viable) cells do not take up the dye and dead (non-viable) cells do. The fluorescent live/dead viability kit contains calcein and ethidium homodimer-1. Calcein stains live cells emitting green fluorescence and ethidium homodimer-1 stains dead cells emitting bright red fluorescence.

4.1.2 Sample Loading Methods

To insure good control over a single cell, optimal sample loading methods were studied. Loading a drop of the cell-suspended sample onto the device using a pipette is the most common method used in most planar patch clamp systems. This method does not require additional structures to be created on the topside of the system for sample delivery. One of the major drawbacks of this method is that the cell selection process is random compared to that of a conventional patch clamping setup. In a conventional setup, a specific cell that an operator deems healthy can be selected visually under a microscope and patch clamp recording can be performed on that particular cell. In a planar patch clamp system, any cell or cell debris that is close enough to the via can be pulled toward the via and trapped inside a cavity. Due to this random selection process, this method is best suited for when highly uniform cell samples with minimum debris are available, such as cell lines.

Primary cultured cells are generally not as uniform as cell lines in terms of cell sizes and their health, and also contain a large amount of debris. Cell debris that is typically in the size range of 0.5-3 μm caused unwanted blockage of the via when trying to capture a cell for analysis. In the case of the primary cultured bovine chromaffin cells, they also tend to clump together, creating large clumps of cells that are hard to dissociate into individual cells. Figure 4.1 shows a micrograph of the primary cultured bovine chromaffin cells. A mixture of round healthy cells, irregularly shaped cells, cell clumps, and cell debris can be observed. Several methods such as centrifugation and filtering have been tried to remove or reduce debris from the cell sample. The cells and cell debris

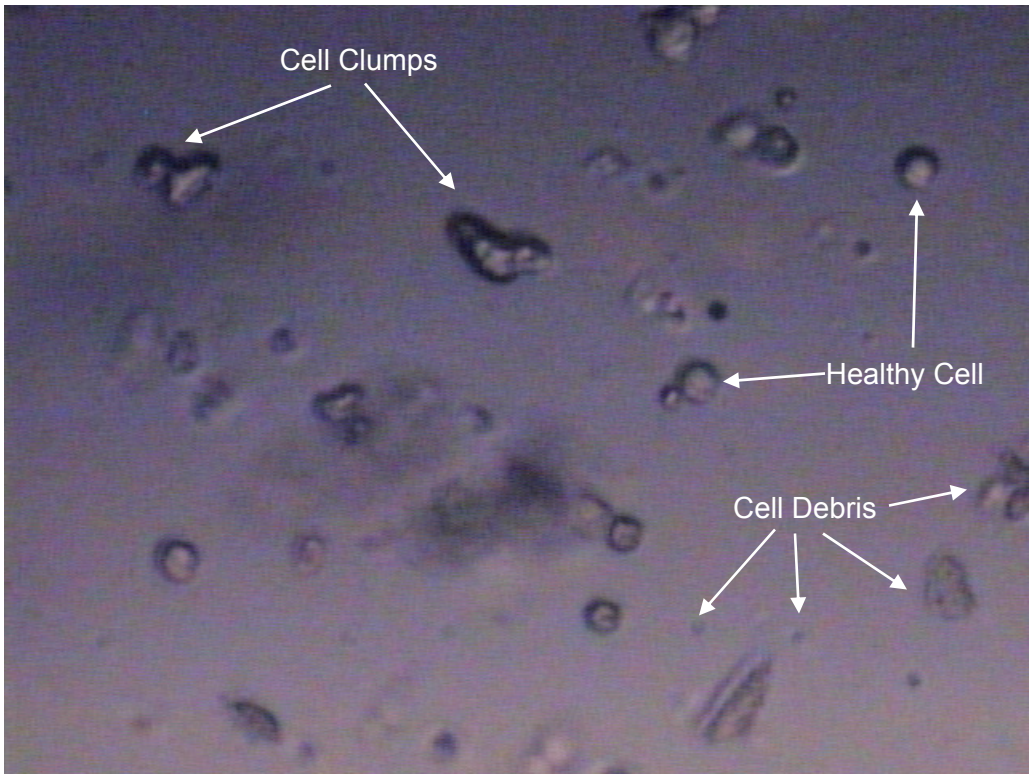

Figure 4.1 Micrograph of primary cultured bovine chromaffin cells. Mixture of round healthy cells, irregularly shaped cells, cell clumps, and cell debris can be observed.

were counted using a Hemacytometer (Hausser Scientific, USA) and a Coulter Counter (Multisizer™ 2 Coulter Counter®, Beckman Coulter, Inc., USA) before and after the centrifugation or filtering. Centrifugation for a short time, such as 700 RPM for five minutes was used to remove cell debris, utilizing the difference in weight between cells and cell debris. Although a lower amount of cell debris was observed, the differences in the number of cell debris were not statistically significant. To remove debris using filtration, a cellulose nitrate membrane filter with pore sizes of 5.0 μm (Whatman International Ltd., England) was used. This method helped remove a large amount of the cell debris but the loss of good cells during the filtration process limited this method in practice.

To dissociate cell clumps that can block both the fluidic channels and the via, enzymes known to help dissociate cells, such as Accumax™ and Accutase™ (Innovative Cell Technologies, Inc., USA) were used. Five ml of Accumax™ was added to 20 ml of sample containing cells and incubated for up to 10 minutes at 37 ^{o}C. Even with this enzyme treatment, dissociation of cells was limited. The next method tried was to remove cell clumps using a filter. A cell strainer with pore sizes of 40 μm (BD Biosciences Discovery Labware, USA) was used. This helped remove most of the large cell clumps from the sample but at a cost of losing a large number of cells.

Since most cell clumps form during culturing, it would be beneficial to prevent cells from clumping from the very beginning. During a typical cell culture on a plastic culture dish, some cells attach to the bottom of the dish and immobilize but a large number of cells can also float. These floating cells tend to move around and clump together when in contact with each other. To prevent individual cells from clumping into

a large colony of cells during culture, a collagen-coated culture dish was used. Rat-tail collagen prepared from Dr. Engisch's lab was coated evenly on the surface of the culture dish and dried in an ammonium hydroxide environment to evaporate the acetic acid inside the collagen solution. Collagen enhances the adhesion of cells to the culture dish, hence immobilizing the cells during culture. Also, since high density of cells during a typical culture cause a higher tendency for the cells to clump, cells were cultured at a lower density. The cell density during culture was reduced by a third from 0.6×10^5 cells/ml to 0.2×10^5 cells/ml.

To release chromaffin cells from the collagen-coated culture dish, culture media was pipetted out and 3 ml of Trypsin EDTA .05 % (Invitrogen Corp., USA) was added and kept at room temperature for 5-15 minutes. Once the cells were released from the dish, 15 ml of D-PBS was added and the cells were transferred to a centrifuge tube. The sample was centrifuged and after removing the remaining D-PBS, D-PBS or extracellular solution was added to a desired cell concentration. This method reduced the number of cell clumps dramatically compared to cells cultured on a dish with no collagen coating. Cell clumps consisting of several cells still existed but large colonies of cells (cell clumps consisting of more then several tens of cells) were not observed. This also helped reduce the amount of cell debris. Healthy cells tend to adhere better on the surface compared to dead cells or cell debris, causing cell debris or unhealthy cells to be removed when pipetting out the media to release the cells in Trypsin EDTA. This was confirmed by counting the cells using a Coulter Counter. The cell to cell debris ratio dropped from 1:13 to 1:3.5. In conclusion, the best method for having a relatively debris-free and

clump-free sample was to culture the cells on a collagen-coated surface at a low cell density.

Even though this method helped improve the chance of getting a healthy cell into an analysis cavity, the nature of this sample delivery method is still random and the outcome is hard to predict. It will be beneficial to have better control over the cell selection process.

A microfluidic channel passing above an analysis cavity and connected to a syringe was used to manipulate cells. By pushing and pulling the fluid using a syringe, cells suspended in the fluid were manipulated. The fabrication method of such a channel/interface and the resulting PDMS structure is described in the previous section. A sample containing cells was dispensed onto the inlet of the channel. A Gastight® syringe connected to the outlet of the channel was used to draw the sample through the channel. Once a good healthy cell passed above an analysis cavity, the syringe was held still and negative pressure was applied through the via inside the analysis cavity using a second syringe connected to the backside fluidic channel, hence drawing the cell into the cavity. The small syringe volume (10 μl) enabled good control over the manipulation of a single cell. The syringe could be either manually pushed and pulled or mounted on a syringe pump and controlled by a computer. In both cases, easy manipulation of a single cell was achieved. The overall sample delivery procedure was observed and controlled under a microscope. Since visual observation of individual cells is required, this method is not suitable for automatic analysis using multiple analysis sites simultaneously. This sample delivery method was used in most of the subsequent experiments.

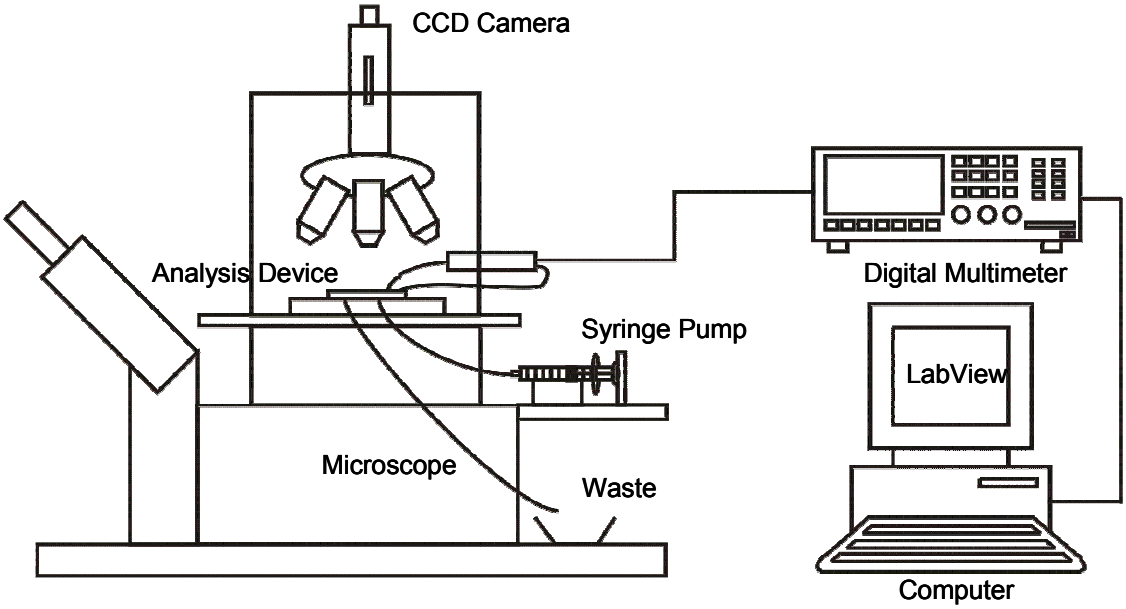

Figure 4.2 Illustration of the experimental setup for access resistance and seal resistance measurement in the patch clamping mode.

4.1.3 Patch Clamp Recording

The experimental setup for patch clamping is shown in Figure 4.2. The system was setup so that individual analysis sites were used one by one, but not simultaneously. To measure the seal resistance, the device was first placed under a microscope (Eclipse ME600, Nikon Corp., USA) and the frontside and backside electrode were connected to a digital multimeter (3458A, Agilent Technologies, Inc., USA). The digital multimeter was linked to a computer through a GPIB board (National Instruments, Inc., USA) and a continuous measurement was taken using LabView^{TM} software (National Instruments,

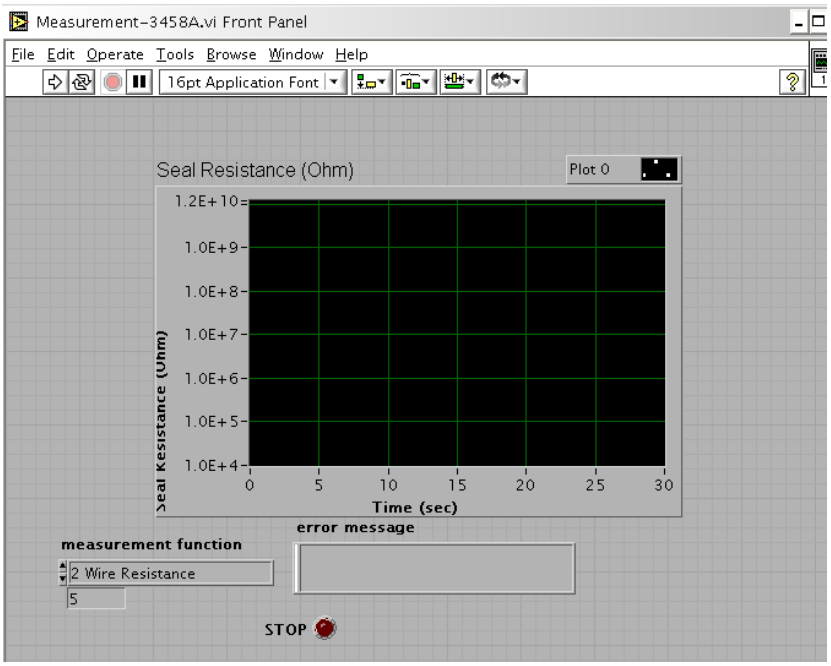

Figure 4.3 LabView™ interface for access resistance and seal resistance measurement through a digital multimeter.

Inc., USA). Figure 4.3 shows the LabView™ interface created for data acquisition from the digital multimeter.

The fluid channel on the backside of the device was filled with D-PBS and pushed through the via from the backside to remove any air trapped inside the system. Using the first sample loading method, a 5 µl drop of D-PBS was dispensed on top of the analysis cavity with a pipette and the resistance between the topside gold electrode and the backside silver/silver chloride electrode was measured. The measured resistance, termed access resistance, indicates the resistance between the topside fluid and backside fluid through the via. To characterize the seal formation capability of this system, a 5 µl drop

of cell-suspended sample was dispensed on top of the analysis cavity. Negative pressure was applied using a syringe connected to the backside fluidic channel to manipulate a single cell toward the analysis cavity through the via. Once a single cell was trapped, the valve connected to the outlet tubing of the backside fluidic channel was closed to maintain the cell in position. The resistance between the top and bottom electrodes was measured. When a cell is trapped inside the cavity and blocks the via, the measured resistance, termed seal resistance, should increase to a range of more than several hundred megaohms. The second sample loading method described above was also used to trap a single cell inside the analysis cavity.

With D-PBS present and without a cell trapped, the access resistance showed an average of 2.1 ± 0.04 MΩ (average ± standard deviation of approximately 10 analysis sites on a single system). The measured resistance shows the resistance of D-PBS through the 2.0 μm diameter via. Once the access resistance was measured, a 5 μl sample of bovine chromaffin cells suspended in D-PBS was used to measure the seal resistance. Once a single cell was trapped inside an analysis cavity and blocked the via, the measured resistance increased to as high as 1.2 GΩ, as shown in Figure 4.4. The maximum resistance measured was limited by the testing equipment used (digital multimeter, Agilent 3458A). The increase in seal resistance shows that the cell was effectively blocking the 2.0 μm diameter via and preventing D-PBS from flowing through the via. Trapping and releasing of a single cell can be observed. Average seal resistance obtained for the chromaffin cells was 0.69 ± 0.17 GΩ (average ± standard deviation of approximately 10 analysis sites on a single system). Approximately 10 cells were tested with seal resistance of each cell measured at least five times and averaged.

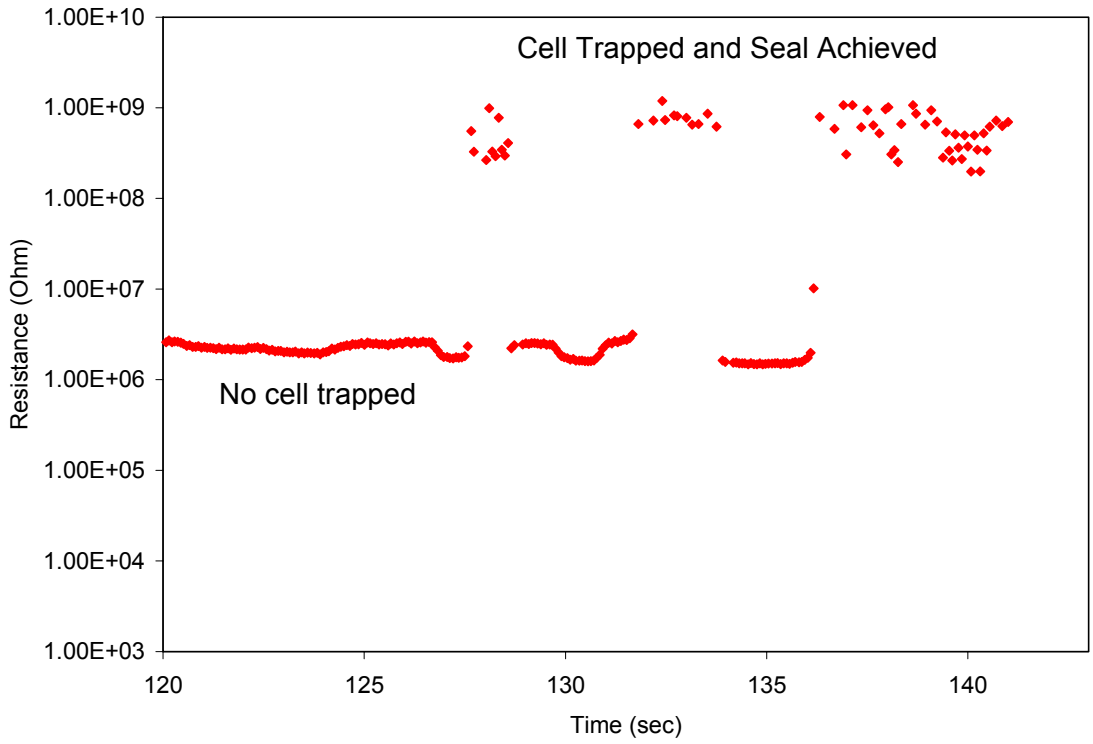

Figure 4.4 Graph of the measured seal resistance over time. When no cell was trapped, access resistance showed 2.1 MOhm. When a cell was trapped, maximum seal resistance showed 1.2 GOhm. Trapping and releasing of a single cell can be observed.

When measuring the ion channel current in a cell membrane using the patch clamping technique, a high seal resistance is important to measure only the ion channel current without the leakage current around the cell. Typically, a seal resistance higher then 200 MΩ is sufficient to measure the whole cell ion channel current. The average measured seal resistance of 0.69 GΩ in the presence of a trapped cell shows that the device can be used for patch clamping to study the ion channel activities of the chromaffin cells.

Although the seal resistance of this particular experiment showed high enough seal resistance for a successful ion channel current measurement, seal resistance can vary widely depending on the health of the cell obtained from week to week, pH and osmolality of the fluid, and the type of cells used. The surface onto which the cells adhere and form a seal is another big factor affecting the seal resistance. Several surface modification techniques were used to determine whether the seal resistance can be further improved.

The silicon dioxide surface of the system had a residue or a rough surface due to the numerous processing steps following the via formation, as described in Figure 3.8. To improve on this, oxygen plasma treatment, depositing PECVD SiO_2 to improve the surface roughness, and poly-L-Lysin coating was used. The fabricated three-inch diameter microsystem was divided into four quarters and the three processes mentioned above were applied to each quarter with one quarter being unmodified and used as a control.

Chromaffin cells showing average seal resistance of 380 ± 30 MΩ was used as a control. First, the surface was treated with oxygen plasma at a 10 sccm O_2, 75 mTorr,

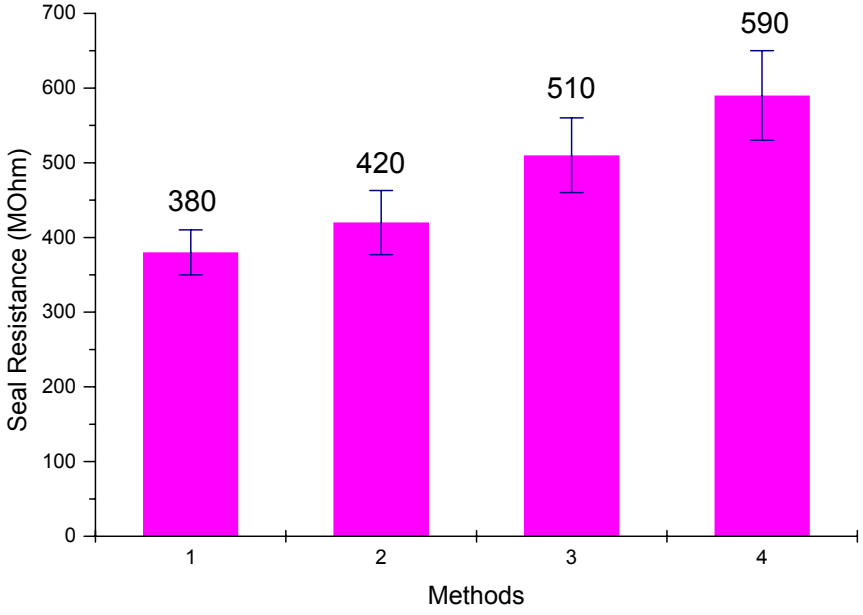

Figure 4.5 Seal resistance for 1: control, 2: oxygen plasma treatment, 3: PECVD SiO_2, and 4: Poly-L-Lysin coating.

and 150 W environment for two minutes. The measured seal resistance improved slightly to 420 ± 43 MΩ. Next, 2000 Å of SiO_2 was deposited using a plasma enhanced vapor deposition system (STS PECVD, Surface Technology Systems plc., UK). The measured seal resistance improved further to 510 ± 50 MΩ. Poly-L-Lysin (Sigma-Aldrich Co., USA) solution was coated on the surface to enhance the cell adhesion to the surface. The measured seal resistance was 590 ± 60 MΩ. This set of experiments demonstrated that depending on the methods and the applications, seal resistance can be improved up to 55 %. Figure 4.5 shows the comparison of the measured seal resistance for each method.

To apply voltage stimuli and record the ion channel current, the frontside and backside electrodes were connected to a patch clamp amplifier (EPC 10, HEKA

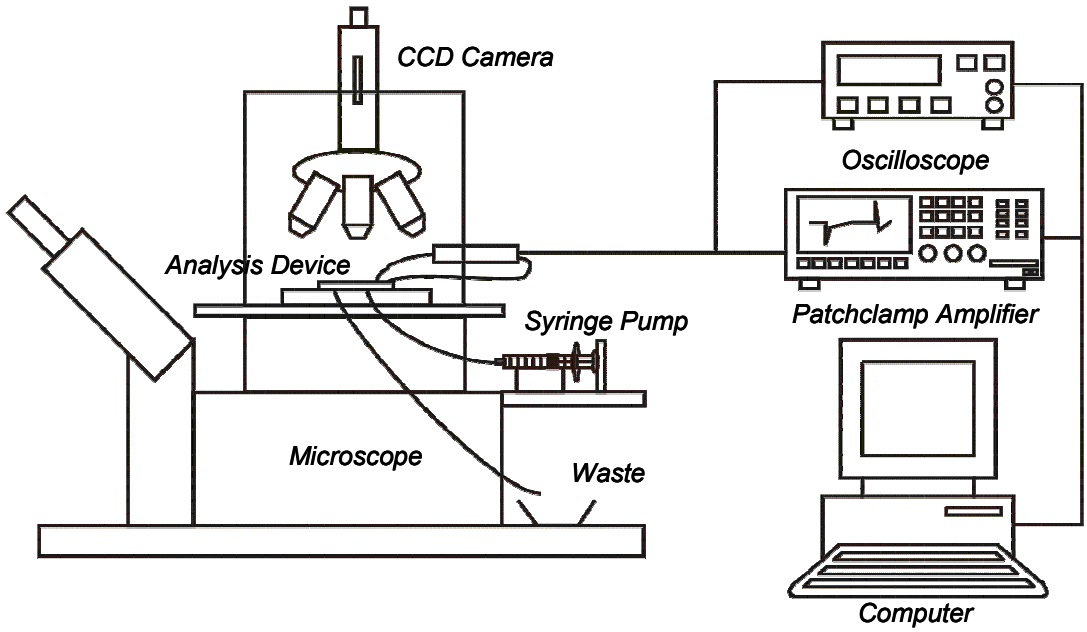

Figure 4.6 Illustration of the experimental setup for patch clamp recording.

Instruments, Inc., USA or Axopatch-1D, Axon Instruments, Inc., USA). Figure 4.6 shows the experimental setup. The amplifier had a computer interface through which stimuli could be applied and data could be recorded. The backside fluidic channel was filled with the intracellular solution. Cells were suspended in the extracellular solution. Before capturing a cell, a 10 mV, 200 ms oscillating square wave was applied and the current was measured to obtain the access resistance of the via. Figure 4.7 shows a typical shape of a resulting current when a square voltage pulse was applied. Capacitive transient current can be observed at the beginning and the end of the voltage pulse. Ideally, the resulting current would be a square wave when a square wave voltage stimulus is applied. Due to the capacitance of the system, the current cannot follow the

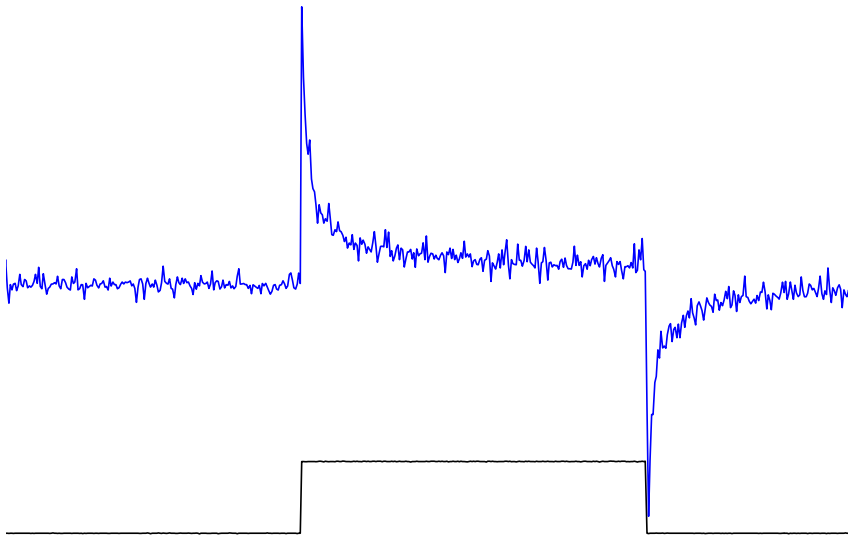

Figure 4.7 Typical shape of a current response (top graph) when a voltage pulse (bottom graph) of 10 mV, 200 ms was applied to the system with no cell captured.

voltage stimulus fast enough. Even with the built-in compensation circuit of the patch clamp amplifier, the capacitive transient current could not be fully compensated [2, 6].

To measure the whole cell current, electrical access to the cell interior has to be provided. A perforation or a physical break-in was used. For perforated patch clamping, 7 µl of amphotericin B stock solution was added to 1.4 ml of intracellular solution and delivered through the backside fluid channel. When using physical break-in, a hard pulse of suction using a syringe or a voltage pulse of up to 1 V was applied to physically break the cell membrane in the sealed region. Once the interior of the cell was accessed, a holding potential of negative 90 mV was applied to stabilize the influx and outflux of ions. Voltage pulses of different sizes and frequencies (e.g. 40 ms, 110 mV pulse

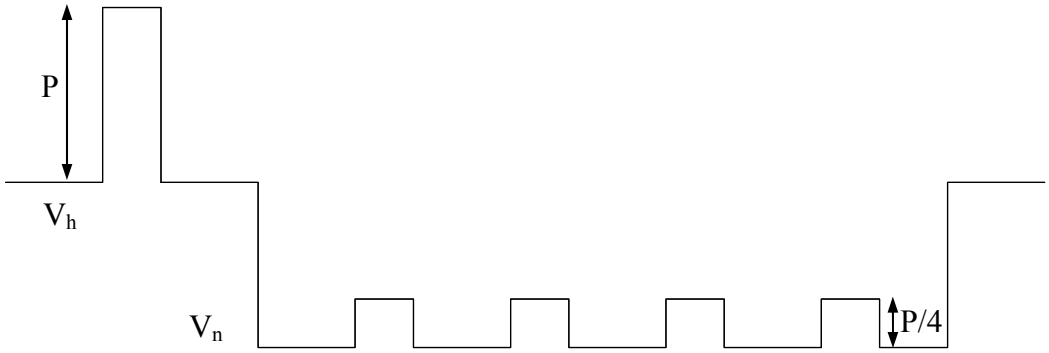

Figure 4.8 Pulse sequence for P/4 subtraction. V_h is the holding potential (-90mV) and V_n was -170 mV.

depolarizing from negative 90 mV to positive 20 mV) were applied and the resulting current was measured. By analyzing the current over time, the amount of ions going in and out of the cell in response to the applied stimulus could be calculated.

The capacitive transient current cannot always be compensated using the built-in compensation circuit in the patch clamp amplifier, as can be seen in Figure 4.7. To subtract the capacitive current from the recorded current, the P/4 leak subtraction method was used [104, 105]. A voltage pattern shown in Figure 4.8 was used. The currents resulting from four subtraction pulses of amplitude P/4 were subtracted from the current resulting from the test pulse (amplitude P). This procedure eliminated the capacitive transient current from the measured current. The resulting current is the ion channel associated current. Figure 4.9 (a) shows the measured current when a voltage pulse of 110 mV, 320 ms was applied to a perforated chromaffin cell. Capacitive current can be

still observed due to the device capacitance. Figure 4.9 (b) shows the current after P/4 leak subtraction. The shape of the current shows a typical current response from that of a chromaffin cell.

To validate and compare this result, conventional patch clamp recording was performed on bovine chromaffin cells. The recording was performed using a patch clamping system in Dr. Engisch's lab at Emory University (Department of Physiology, Atlanta, GA). The experimental setup is similar to that shown in Figure 1.3. A glass pipette was pulled using a glass pipette puller (PP-830, Narishige Co. LTD., Japan) and the tip was fire-polished using a forge (MF-830, Narishige Co. LTD., Japan). Sylgard 184 was applied toward the edge of the pipette to reduce the capacitive noise [6]. The backside of the glass pipette was also fire-polished. The pipette was then mounted on a precision micromanipulator (PCS-5300, EXFO Burleigh Products Group, Inc., USA). An Ag/AgCl wire was placed inside the glass pipette and connected to a patch clamp amplifier (Axopatch 200B, Axon Instruments, Inc., USA) and an oscilloscope (TDA 220, Tektronix Inc., USA). The sample was mounted on a microscope stage (Eclipse TE200, Nikon, Inc., USA). The microscope was on a vibration-free table and placed inside a faraday cage. A voltage pulse of 110 mV, 320 ms was applied and the resulting current was measured.

Figure 4.10 shows a current response using the conventional patch clamping setup compared to the response using the developed system when a 110 mV, 320 ms voltage pulse was applied to a perforated bovine chromaffin cell. It can be seen that the measured ion channel current from the developed μ-EPAS is similar to that from a

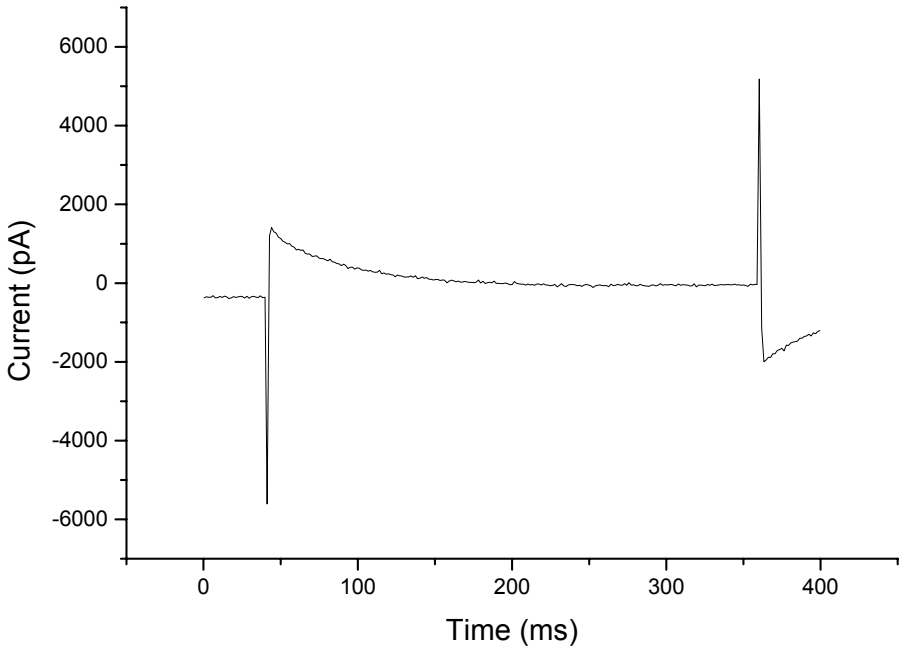

(a)

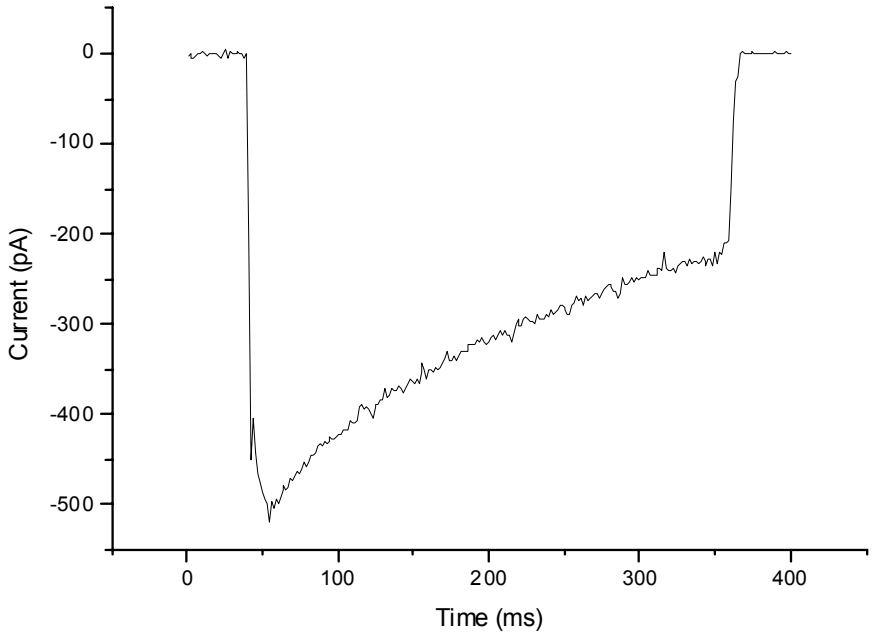

(b)

Figure 4.9 (a) Current measurement when a voltage pulse of 110 mV, 320 ms was applied to a perforated chromaffin cell. (b) Current after leak subtraction.

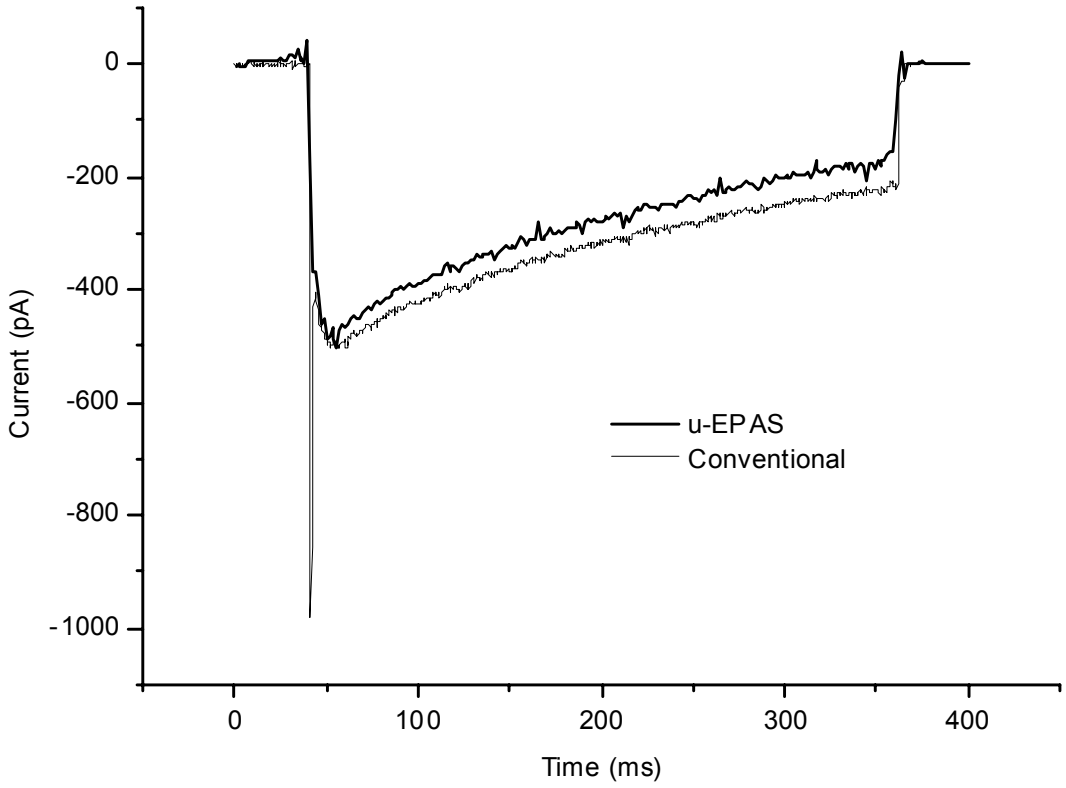

Figure 4.10 Ion channel current measurement using the developed system compared to the measurement using a conventional patch clamping setup when a voltage pulse was applied to a chromaffin cell.

conventional patch clamping system. The time associated with the overall recording process was reduced when the μ-EPAS was used to perform patch clamping. To perform a conventional patch clamp recording, the extracellular fluid level on the stage had to be optimized and the glass pipette had to be manipulated carefully toward the cell, which took several tens of minutes. Using the developed system, no fluid level adjustment was required and a single cell could be captured in less then 5 minutes. This demonstrated that the developed μ-EPAS can be used for patch clamp recording in an easier and more time-efficient way as compared to a conventional patch clamping system.

4.1.4 Whole Cell Electrical Impedance Spectroscopy

The ion channel activities of primary cultured bovine chromaffin cells were further studied using the μ-EPAS in the whole cell EIS mode. In this mode, two opposing electrodes positioned inside the analysis cavity were used to measure the impedance of a single trapped cell. The electrodes were connected to an impedance analyzer (4294A, Agilent Technologies Inc., USA), as shown in Figure 4.11. Bovine chromaffin cells were prepared using the same procedure as mentioned above. First, the impedance of air was measured at a frequency range of 100 Hz to 5.0 MHz as a reference. Next, the backside fluidic channel was filled with D-PBS and pushed through the via to remove any air trapped inside the system. D-PBS was either dropped on the analysis cavity or delivered through the frontside microfluidic channel and negative pressure was applied from the backside using a syringe to ensure that the fluid was in contact with the

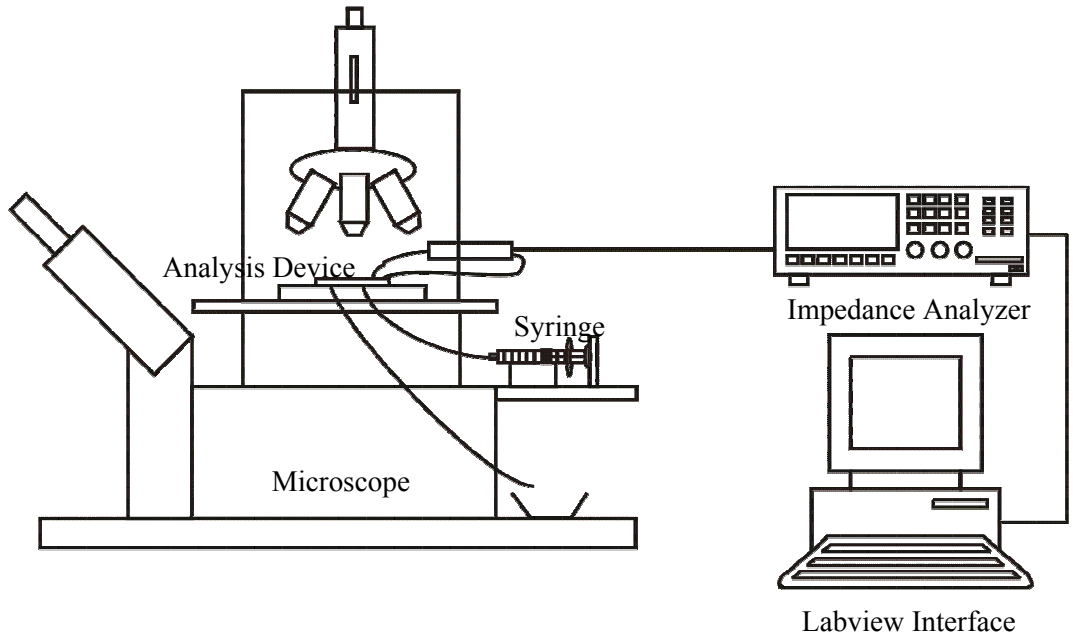

Figure 4.11 Experimental setup for whole cell electrical impedance spectroscopy.

electrodes. The chromaffin cells were introduced into the system and a single cell was captured into the analysis cavity. The electrodes inside the cavity were in direct contact or in proximity with the outer surface of the cell membrane with the cell snugly fit into the analysis cavity.

Impedance measurements for air and chromaffin cells over a frequency range of 100 Hz to 5.0 MHz were compared, as shown in Figure 4.12. For the chromaffin cells, more than 10 cells were measured and averaged. It can be seen that at low frequencies (below 130 Hz), the signal gets noisy, especially in the phase. The impedance magnitudes in both cases decreased as the frequencies increased. The phase components of the impedances decreased as the frequencies increased. Measurements from different

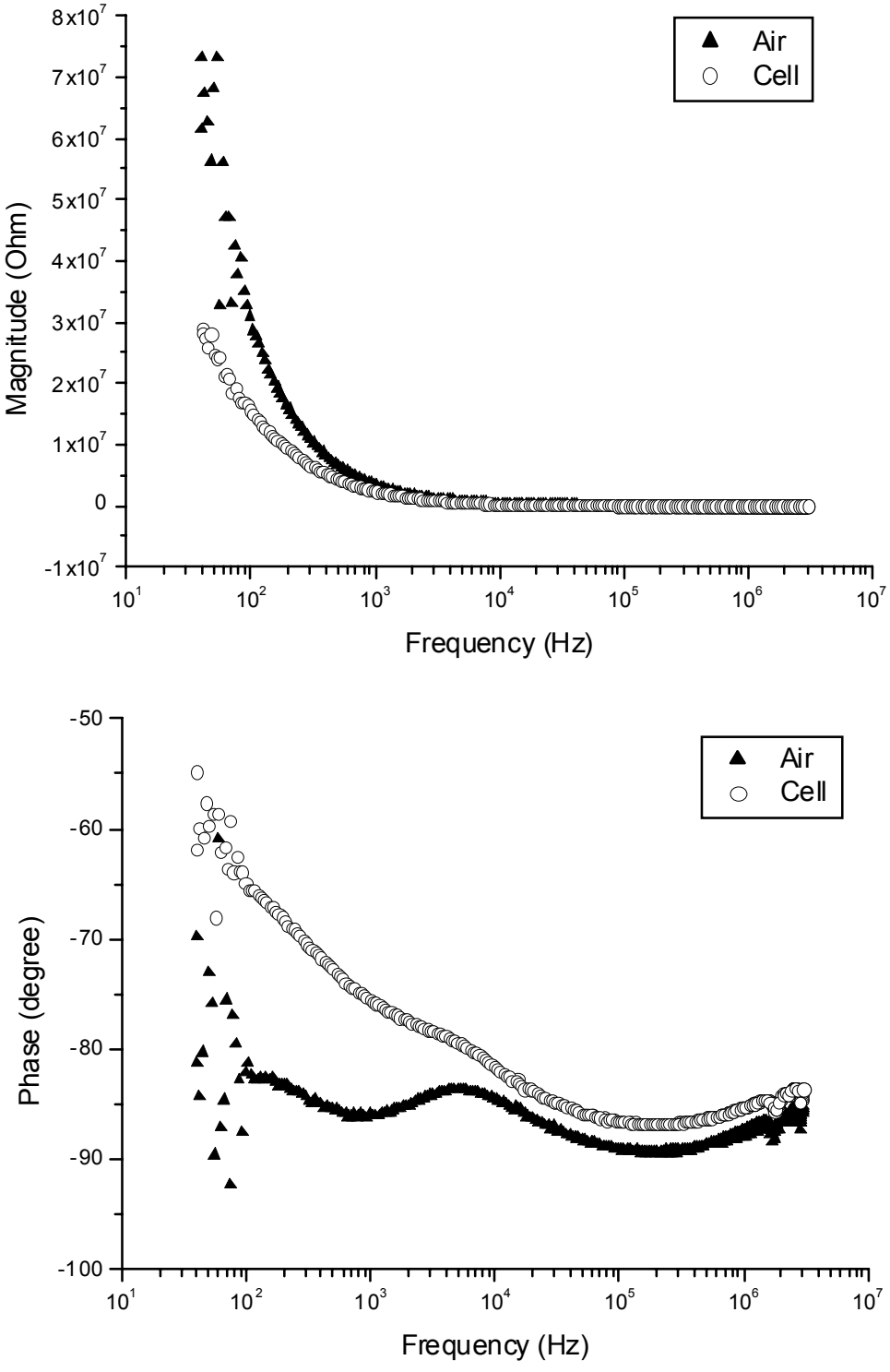

Figure 4.12 Impedance measurements of air and chromaffin cells at a frequency range of 100 Hz to 5.0 MHz.

analysis sites with identical dimension was also taken and compared. No noticeable difference could be observed from the measurements taken from different analysis sites. This further indicated that consistent results could be obtained using this system.

The membrane capacitance and resistance of the chromaffin cell was calculated based on the model shown in Figure 2.2. Because the measured impedance of a cell reflects both the cell impedance and the device impedance, the device impedance had to be subtracted from the measured cell impedance. To calculate the device impedance, the impedance measurement of air was used. A frequency of 100 kHz was chosen for this calculation. The measured impedance of air is composed of the device impedance Z_d parallel to the air impedance Z_a. The impedance of air can be modeled as a pure capacitor with no resistive component. Using equation 1, Z_a was calculated, where ε_a is the relative permittivity of air, ε_0 is the vacuum permittivity, A is the effective area of the electrodes, and d is the distance between the electrodes.

$$Z_a = \varepsilon_a \varepsilon_0 \frac{A}{d} \tag{1}$$

The device impedance can be shown in terms of the impedance measurement of air Z_2 and the calculated impedance of air Z_a, as shown in equation 2.

$$Z_d = \frac{Z_2 Z_a}{Z_a - Z_2} \tag{2}$$

To obtain the impedance of the cell Z_c, the device impedance Z_d was subtracted from the measured cell impedance Z_1. Z_1 is composed of the impedance of the cell Z_c and the device impedance Z_d in parallel. The calculated impedance of the cell Z_c was fit to the circuit diagram shown in Figure 2.3 to obtain the cell membrane capacitance and resistance. The capacitive component of the intracellular fluid C_c was ignored to simplify the calculation. The intracellular conductivity was assumed to be 0.5 S/m [54]. The calculated capacitance of chromaffin cells C_m at 100 kHz was 0.75 $\mu F/cm^2$ and the resistance R_m was 93.9 MOhm (equivalent to membrane conductivity of 270 μS/m). The calculated membrane capacitance is in line with the known cell capacitance of 1 $\mu F/cm^2$.

To study whether the ion channel activities of a single target cell can be measured using this system, chromaffin cells with certain ion channels blocked were compared to cells with no ion channels blocked. A high-enough concentration of toxins known to completely block certain ion channels were used. For K channels, 100 mM Tetraethylammonium chloride (TEACl, Sigma-Aldrich Co., USA) was used [106, 107]. For Ca channels, 200 μM CdCl (Sigma-Aldrich Co., USA) was used [101-103]. These toxins were added to the extracellular media in which cells were suspended and the impedances were measured at frequency ranges of 100 Hz to 5.0 MHz.

Figure 4.13 shows the impedance measurement of normal cells compared to that of cells with ion channels blocked using toxins. Each measurement shown is an average of 4-7 cells tested. When the K channels were blocked, the magnitude of the measured impedance increased and the phase decreased. This difference could be observed throughout the measured frequency range. For the cells with the Ca channels blocked, a similar difference could be observed for both magnitude and phase. Although the

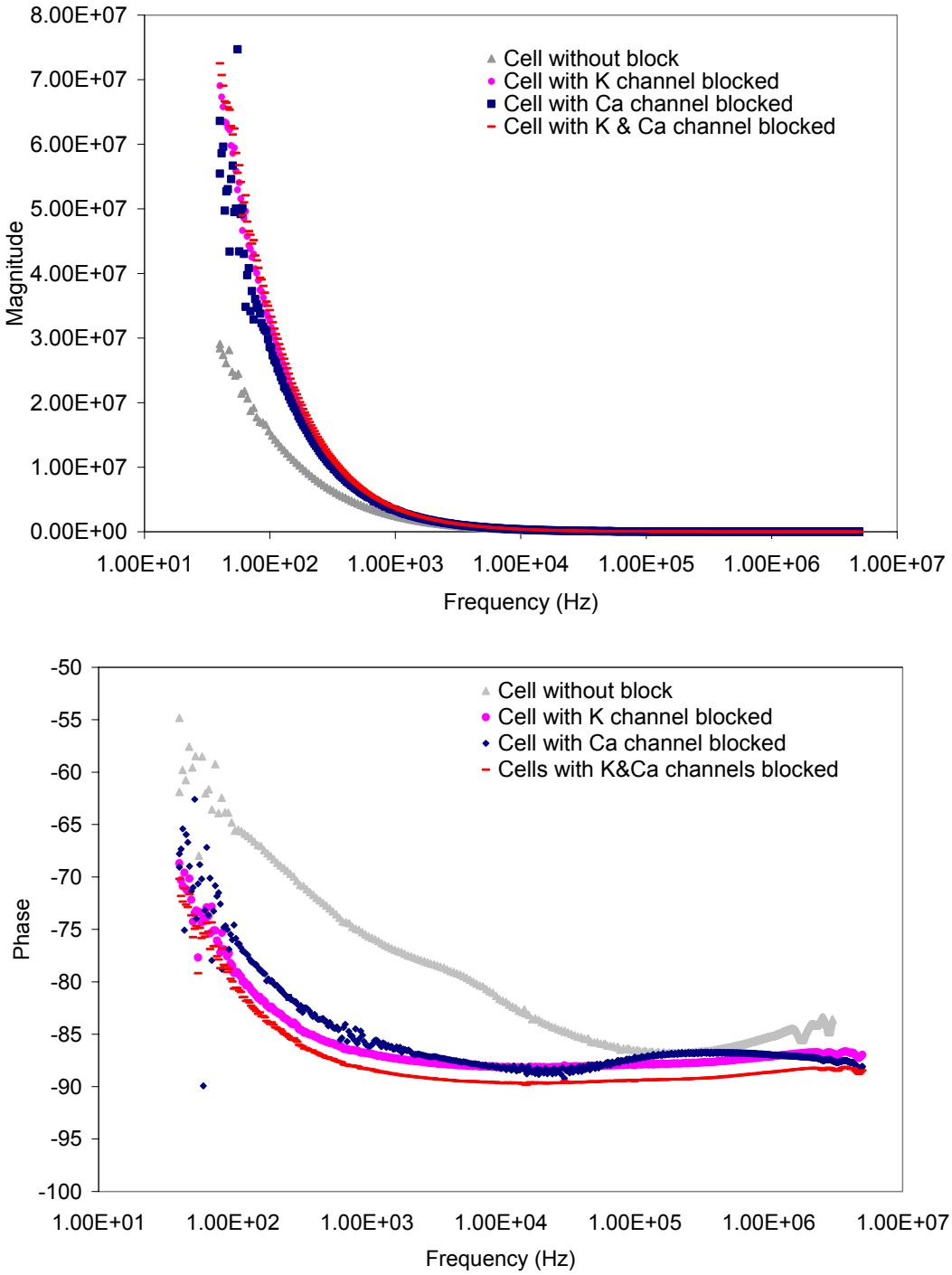

Figure 4.13 Impedance measurements of cells with no ion channels blocked compared to cells with K channels and Ca channels blocked.

differences in impedances were clear compared to that of normal cells, the difference between the impedances of cells with K channels blocked and Ca channels blocked was not very clear. When both the K and Ca channels were blocked simultaneously, the phase decreased further with a slight increase in magnitude. Figure 4.14 shows the change of impedances for all three cases at various frequencies of interest. Comparison was done at 100 Hz, 1 kHz, 10 kHz, 100 kHz, 500 kHz, 1 MHz, and 3 MHz. Overall, the percentage change decreased as the frequency increased. The magnitude changed up to 130 % and the phase changed up to 23 %.

The change in membrane capacitance and resistance at 100 kHz was calculated using the same method described above. When the K channels were blocked, the capacitance increased by 21 % to 0.91 $\mu F/cm^2$ compared to normal cells and the resistance was 80.7 MOhm (300 μS/m). When the Ca channels were blocked, the capacitance increased by 77 % to 1.33 $\mu F/cm^2$ compared to normal cells and the resistance was 85.5 MOhm (290 μS/m). When both channels were blocked, the capacitance increased by 163 % to 1.97 $\mu F/cm^2$ compared to normal cells and the resistance was 90.7 MOhm (276 μS/m). Only slight increase in resistance can be observed while the capacitance increased significantly. This change in capacitance is possibly due to the cell membrane becoming less permeable to ions due to the ion channel blockage. Further study is required to determine the cause of the membrane capacitance change.

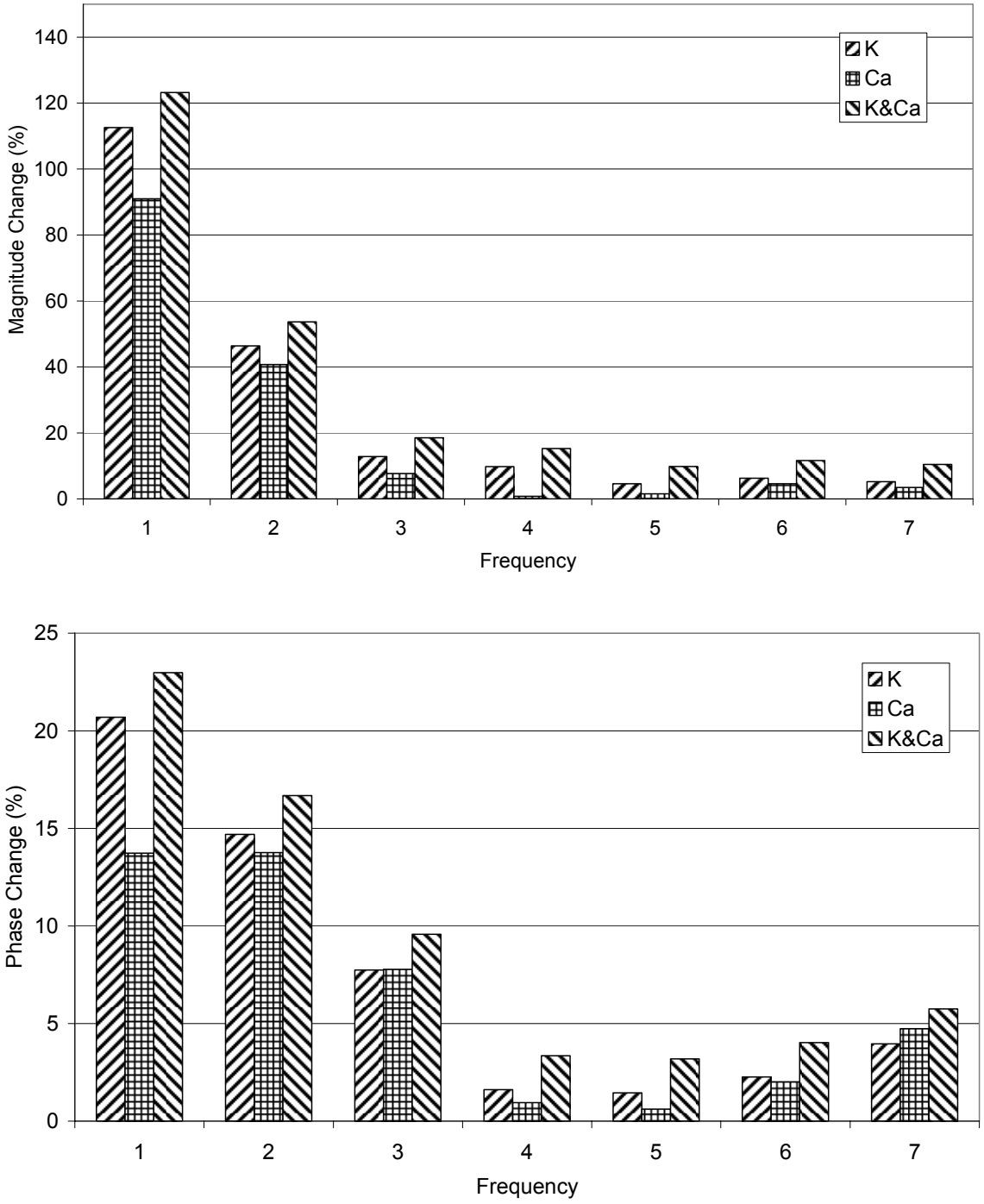

Figure 4.14 Change in impedances when the K channels are blocked (K), the Ca channels are blocked (Ca), and both the K and Ca channels blocked at various frequencies of interest (1: 100 Hz, 2: 1 kHz, 3: 10 kHz, 4: 100 kHz, 5: 500 kHz, 6: 1 MHz, 7: 3 MHz).

4.2 Human Breast Cancer Cells

4.2.1 Sample Preparation

To study cancer cells from different pathological status and to characterize the variance of dielectric properties, the impedance of human breast cancer cell lines from different pathological stages were compared to that of normal human breast tissue cells. Normal human breast tissue cell line MCF-10A, early stage breast cancer cell line MCF-7, invasive human breast cancer cell line MDA-MB-231, and metastasized human breast cancer cell line MDA-MB-435 were obtained from Dr. Yang's lab at the Department of Surgery, Emory University (Atlanta, GA). These cell lines were maintained in accordance with the American Type Culture Collection (ATCC) guidelines [110]. Cells were cultured in 37 °C, 5 % CO_2, and 95 % humidity environment in Dulbecco's modified Eagle medium (DMEM/F12, Invitrogen Corp., USA). MCF-7, MDA-MB-231, and MDA-MB-435 cell lines were supplemented with 10 % heat inactivated fetal bovine serum (FBS, Hyclone, USA). The MCF-7 line was also supplemented with 10 mg/ml bovine insulin (Invitrogen Corp., USA) and 100 mM sodium pyruvate (Sigma-Aldrich Co., USA). The MDA-MB-231 cell line and MDA-MB-435 cell line was supplemented by 2 mM L-glutamine (Invitrogen Corp, USA), 100 IU/ml penicillin and 100 μg/ml streptomycin (Invitrogen Corp., USA). The MCF-10A cell line was supplemented by 5 % heat inactivated FBS, 2 mM L-glutamine, 20 ng/ml epidermal growth factor (Invitrogen Corp., USA), 500 ng/ml hydrocortisone (Sigma-Aldrich Co., USA), 100

ng/ml cholera toxin (Calbiochem® EMD Biosciences, Inc., USA), and 10 μg/ml bovine insulin.

4.2.2 Whole Cell Electrical Impedance Spectroscopy

The impedance between two opposing electrodes in an analysis cavity was measured to obtain the impedance spectrums for D-PBS, human breast tissue cell line MCF-10A, and human breast cancer cell lines MCF-7, MDA-MB-231, and MDA-MB-435. The impedances were measured over a frequency range of 100 Hz to 3.0 MHz.

Figure 4.15 shows the measured impedances in magnitude and phase. Each measurement shown is an average of 7-10 cells tested with the error being approximately the size of each marker. In general, the magnitude decreased as the frequency increased. The phase decreased initially and increased sharply as the frequency increased. In both magnitude and phase, significant differences could be observed between the normal cells MCF-10A and the cancer cells. Also, when comparing cancer cells from different pathological statuses, impedances in both magnitude and phase could be easily distinguished. The magnitude decreased in the order of MCF-10A, MCF-7, MDA-MB-231, and MDA-MB-435 and the phase increased in the same order.

The membrane capacitance and resistance of each cell line at 100 kHz was calculated using the same method used for membrane capacitance and resistance calculation for bovine chromaffin cells. The calculated capacitance of MCF-10A, MCF-7, MDA-MB-231, and MDA-MB-435 was 1.94, 1.86, 1.63, and 1.57 $\mu F/cm^2$ respectively

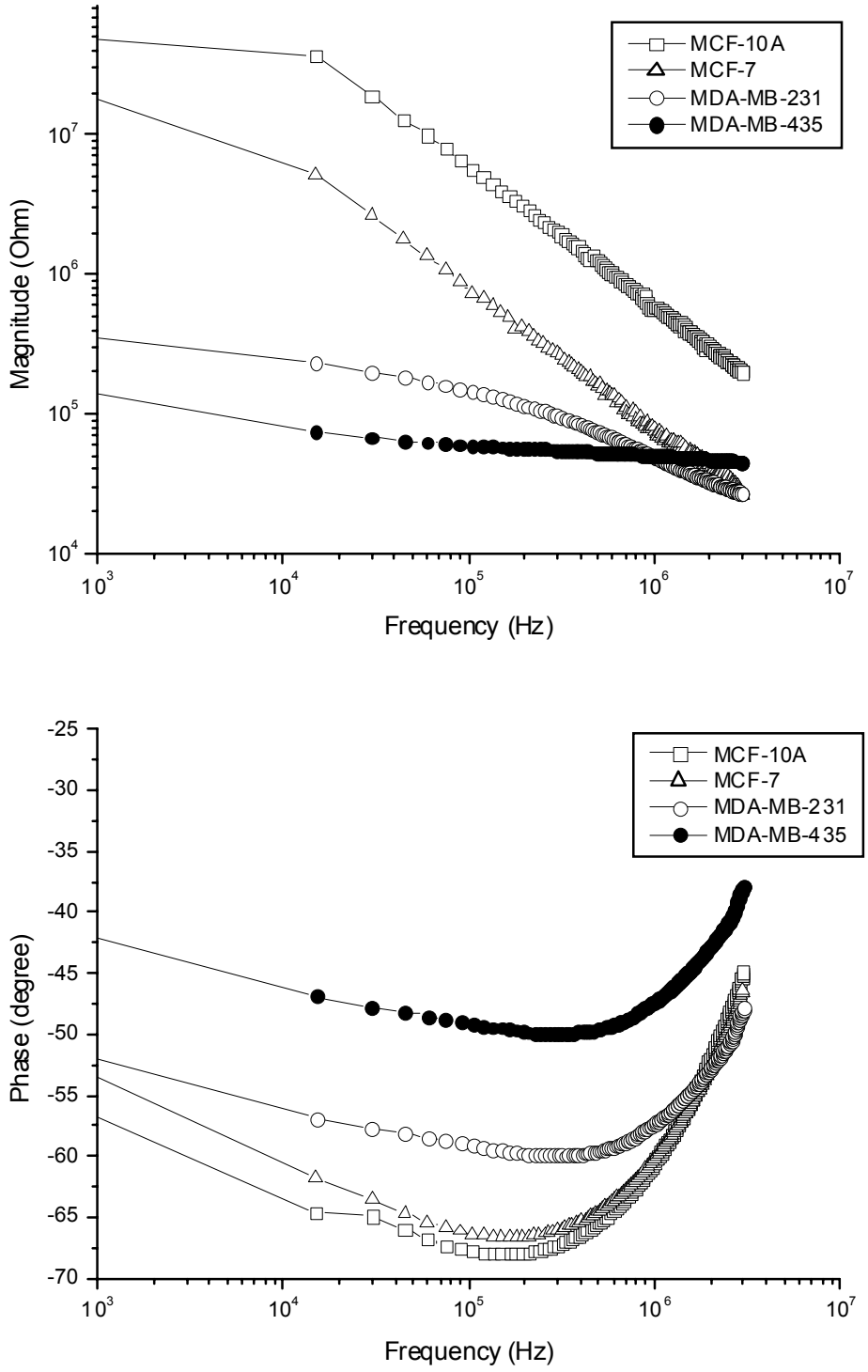

Figure 4.15 Impedance measurements of MCF-10A, MCF-7, MDA-MB-231, and MDA-MB-435 over a frequency range of 100 Hz to 3.0 MHz.

at 100 kHz. The calculated resistance of each cancer cell line at 100 kHz was 24.8 MOhm (1.00 mS/m), 24.8 MOhm (1.00 mS/m), 24.9 MOhm (1.00 mS/m), and 26.2 MOhm (0.95 mS/m) respectively. The decrease in capacitance of the cancer cell lines compared to the normal cell line MCF-10A was 4.1 %, 16.0 %, and 19.1 % respectively at 100 kHz. It can be seen that that the capacitance decreased for the more pathologically progressed cancer cell line. As the cancer progress, the cell membrane becomes more permeable, resulting in decreased capacitance. The change in the resistance was relatively small.

This result shows that the developed μ-EPAS can be used not only to distinguish cancer cells from normal cells, but also to distinguish cancer cells from different pathological stages. It is expected that this system can be used for detecting cancer cells for diagnostic purpose. The capability to determine at what pathological stage the cancer cells are could reduce the time and cost associated with advanced cancer diagnostics.

CHAPTER 5

CONCLUSIONS AND FUTURE WORK

A micro-electrophysiological analysis system (μ-EPAS) that can perform patch clamp recording and whole cell electrical impedance spectroscopy (EIS) was developed and characterized. The system was fabricated using combinations of conventional microfabrication techniques and plastic/polymer microfabrication techniques. For the silicon part, fabrication techniques such as lithography, silicon etching, metal patterning, and chemical vapor deposition of dielectric material were used. Microstenciling was used to create metal electrodes on the microfabricated substrate. To create the microfluidic channels and interfaces, 3D plastic microfabrication methods such as stereolithography were utilized. This enabled monolithic fabrication of microchannels and fluidic interfaces that warranted convenient interconnection between the system and outside macro-world. The microchannels on the frontside of the system were fabricated in transparent polymer using soft lithography technology. Two-layer approach was used where fluidic tubing was connected to the system from the side instead of from the top, enabling constant visual observation of the system during testing under a microscope.

The fabricated system was used to measure the ion channel activities of primary cultured bovine chromaffin cells. First, the system was characterized in the patch

clamping mode to study several sample delivery methods and test the sealing capability of the system. Using an integrated microchannel, better control over a single cell manipulation was possible. By culturing chromaffin cells on a collagen-coated surface, cells debris and cell clumping was minimized that improved the throughput of the single cell manipulation process. Good sealing capability was demonstrated and methods on improving seal resistance were studied. Patch clamp recording was performed on the chromaffin cells and the result was compared to that from a conventional patch clamping system. The resulting ion channel currents from both system were comparable.

Next, the chromaffin cells were tested in the whole cell EIS mode. The impedance of a single chromaffin cell was measured at a frequency range of 40 Hz to 5 MHz using two opposing electrodes. The measured impedance was used to obtain the chromaffin cell capacitance of 0.75 $\mu F/cm^2$ and membrane resistance of 93.6 MOhm (corresponding to conductivity of 270 $\mu S/m$) at 100 kHz. The ion channel activities were also studied in this mode. K and Ca channels of the bovine chromaffin cells were blocked and the impedances of those cells were measured and compared to that of normal cells. In both cases, cells with ion channels blocked showed different impedance, especially in phase, compared to normal cells. The membrane capacitance at 100 kHz for cells with no ion channels were blocked was 0.75 $\mu F/cm^2$ and increased by 21 % to 0.91 $\mu F/cm^2$ when the K channels were blocked, increased by 77 % to 1.33 $\mu F/cm^2$ when the Ca channels were blocked, and increased by 163 % to 1.97 $\mu F/cm^2$ when both K and Ca channels were blocked.

To study the capability of this system for cancer cell differentiation, the impedance of normal human breast tissue cell line (MCF-10A) was compared to that of

early stage human breast cancer cell line (MCF-7), invasive human breast cancer cell line MDA-MB-231, and metastasized human breast cancer cell line MDA-MB-435. In both the magnitude and phase of the measured impedances, each cell line clearly showed different characteristic impedance signature. The membrane capacitance of MCF-10A, MCF-7, MDA-MB-231, and MDA-MB-435 was 1.94, 1.86, 1.63, and 1.57 $\mu F/cm^2$ respectively at 100 kHz. The membrane resistance was 24.8 MOhm (1.00 mS/m), 24.8 MOhm (1.00 mS/m), 24.9 MOhm (1.00 mS/m), and 26.2 MOhm (0.95 mS/m) respectively at 100 kHz. The decrease in capacitance of the cancer cell lines compared to the normal cell line MCF-10A was 4.1 %, 16.0 %, and 19.1 % respectively at 100 kHz. This study showed that the developed system could be used for not only for differentiating cancer cells from normal cells but also for distinguishing cancer cells from different pathological statuses.

In conclusion, a micro-electrophysiological analysis system (μ-EPAS) was developed and tested in the patch clamping mode and the whole cell EIS mode. The system has the capability to perform both analyses simultaneously on a single cell. The automatic process and array-type system is expected to improve the throughput of this system in applications such as drug discovery and cancer diagnostic/staging.

Some of the future work is listed. Performing both patch clamp recording and impedance spectroscopy simultaneously on a single cell would provide further information about the capability of the whole cell EIS for ion channel activity studies. For cancer cell studies, comparing different types of cancer cells using EIS would be of great interest. Furthermore, testing the system with clinical sample would be a step further toward utilizing this system for cancer diagnostic.

APPENDIX A

MASK DESIGN

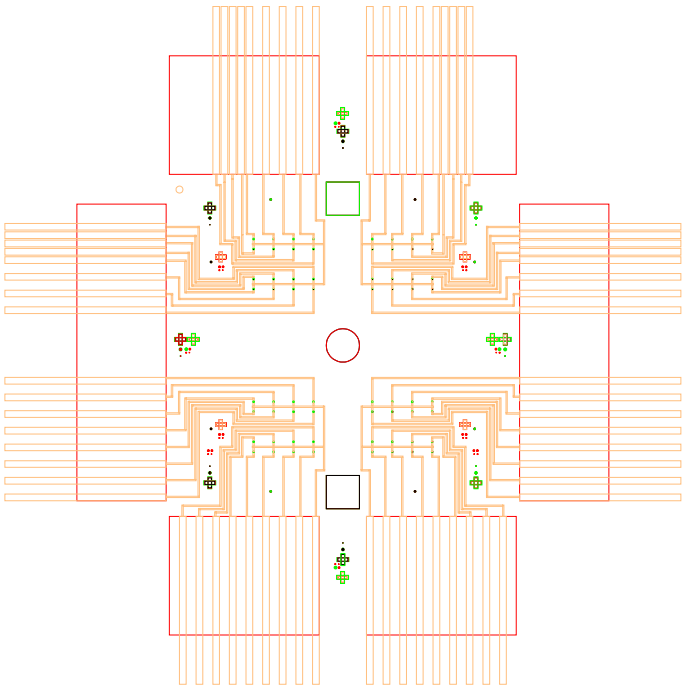

Figure A.1 Mask design of all the layers.

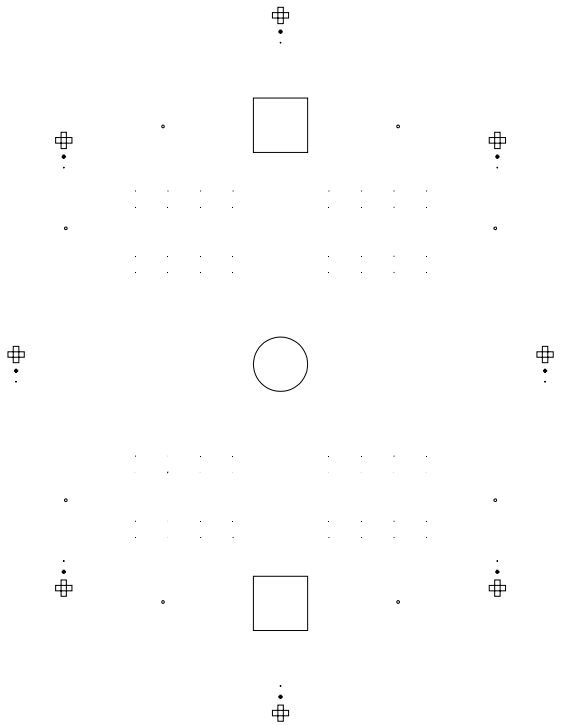

Figure A.2 Mask design of the via layer.

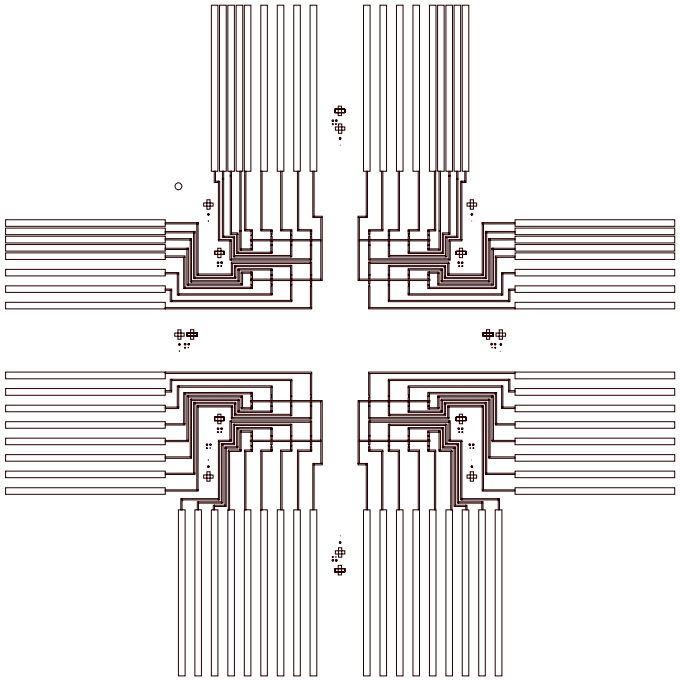

Figure A.3 Mask design of the electrode layer.

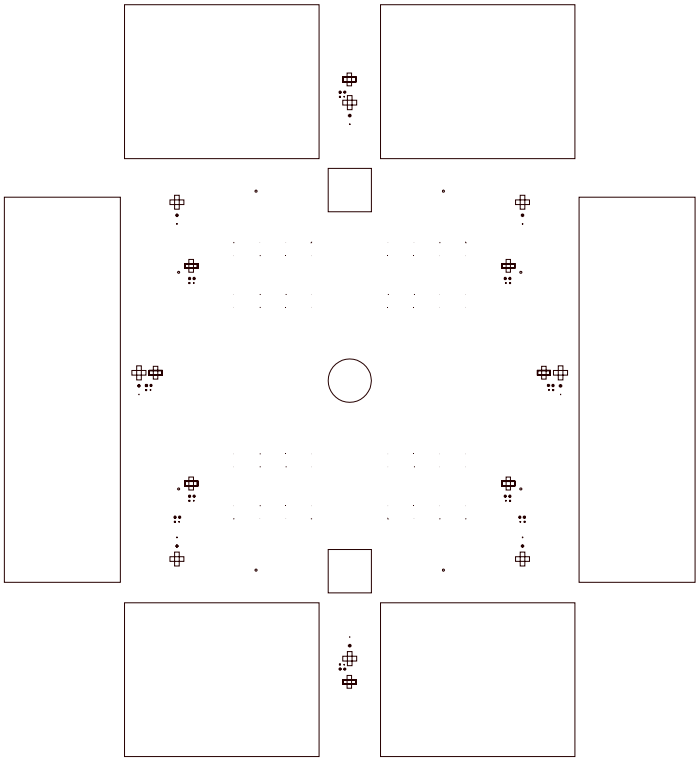

Figure A.4 Mask design of the cavity layer.

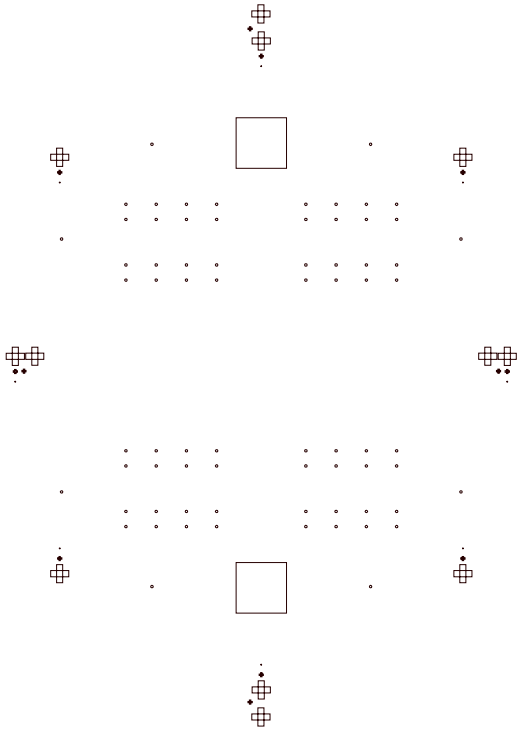

Figure A.5 Mask design of the ICP layer.

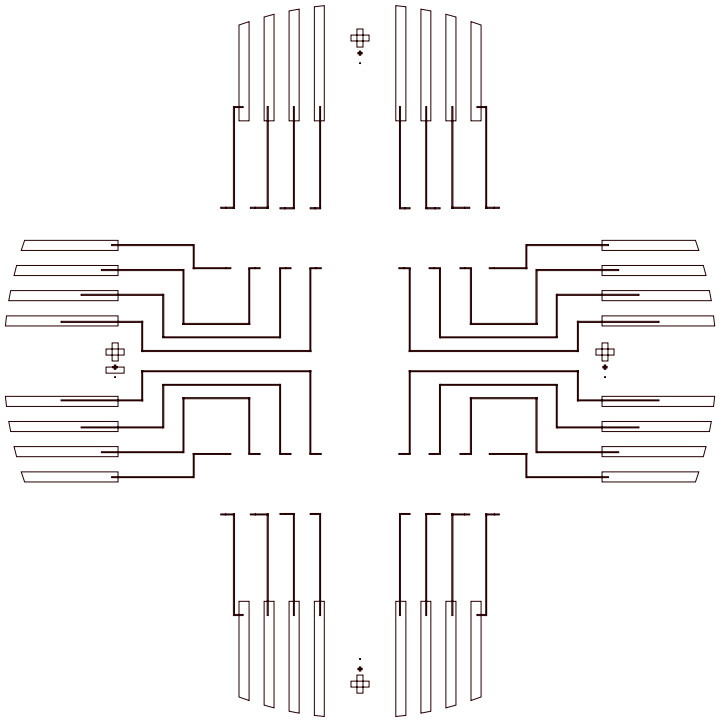

Figure A.6 Mask design of the backside electrode layer.

APPENDIX B

LABVIEW PROGRAM

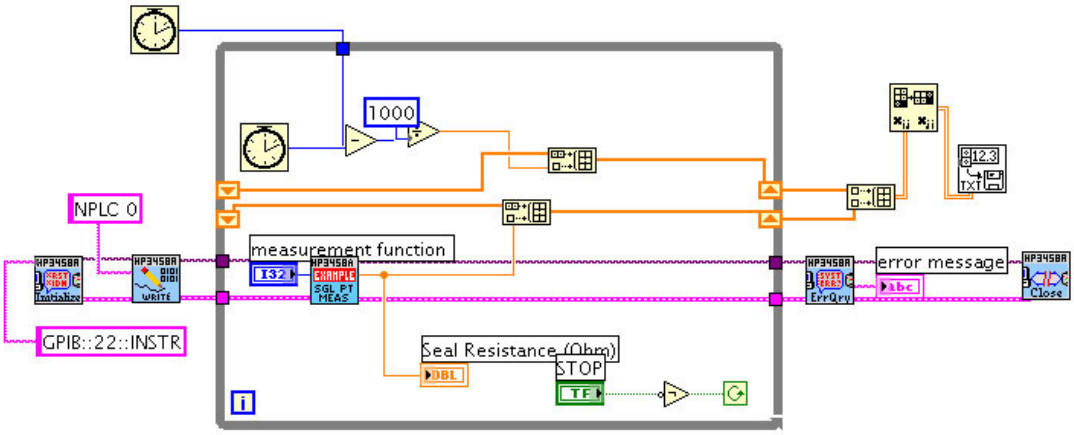

Figure B.1 Labview™ program for data acquisition from the HP 3458a digital multimeter.

REFERENCES

[1] E. Neher and B. Sakmann, "Single-channel Currents Recorded from Membrane of Denervated Frog Muscle Fibres," *Nature*, vol. 260, pp. 799-802, 1976.

[2] B. Sakmann and E. Neher, *Single-Channel Recording*. New York: Plenum Press, 1995.

[3] B. Hille, *Ion Channels of Excitable Membranes*. Sunderland: Sinauer Associates, 2001.

[4] D. J. Aidley and P. R. Stanfield, *Ion Channels: Molecules in Action*. Cambridge: Cambridge University Press, 1996.

[5] F. M. Ashcroft, *Ion channels and disease*: Academic Press, 2000.

[6] http://www.axon.com, "The Axon Guide for Electrophysiology & Biophysics Laboratory Techniques."

[7] J. Rae, K. Cooper, G. Gates, and M. Watsky, "Low Access Resistance Perforated Patch Recordings using Amphotericin B," *J. Neurosci. Methods*, vol. 37, pp. 15-26, 1991.

[8] J. Xu, X. Wang, B. ENsign, M. Li, L. Wu, A. Guia, and J. Xu, "Ion-Channel Assay Technologies: quo vadis?" *Drug Discovery Today*, vol. 6, pp. 1278-1287, 2001.

[9] C. Wood, C. Williams, and G. J. Waldron, "Patch Clamping by Numbers," *Drug Discovery Today*, vol. 9, pp. 434-441, 2004.

[10] B. P. Zambrowicz and A. T. Sands, "Knockouts Model the 100 Best-selling Drugs - Will they Model the Next 100?" *Nat. Rev. Drug Discov.*, vol. 2, pp. 38-51, 2003.

[11] M. E. Curran, I. Splawski, K. W. Timothy, G. M. Vincent, E. D. Green, and M. T. Keating, "A Molecular Basis for Cardiac Arrhythmia: *HERG* Mutations Cause Long QT Syndrome," *Cell*, vol. 80, pp. 795-803, 1995.

[12] B. Fermini and A. A. Fossa, "The Impact of Drug-induced QT Interval Prolongation on Drug Discovery and Development," *Nat. Rev. Drug Discov.*, vol. 2, pp. 439-447, 2003.

[13] L. C. Mattheakis and A. Savchenko, "Assay Technologies for Screening Ion Channel Targets," *Curr. Opin. Drug Discov. Devel.*, vol. 4, pp. 124-134, 2001.

[14] P. B. Bennett and H. R. Guthrie, "Trends in Ion Channel Drug Discovery: Advances in Screening Technologies," *Trends Biotechnol.*, vol. 21, pp. 563-569, 2003.

[15] N. Fertig, C. Meyer, R. H. Blick, C. Trautmann, and J. C. Behrends, "Microstructured Glass Chip for Ion-Channel Electrophysiology," *Physical Review E*, vol. 64, pp. 040901 (R), 2001.

[16] N. Fertig, R. H. Blick, and J. C. Behrends, "Whole Cell Patch Clamp Recording Performed on a Planar Glass Chip," *Biophysical Journal*, vol. 82, pp. 3056-3062, 2002.

[17] K. S. Schroeder and B. D. Neagle, "High-throughput Electrophysiological Measurement Apparatus," U. Patent 6488829, 2002.

[18] K. G. Klemic, J. F. Klemic, M. A. Reed, and F. J. Sigworth, "Micromolded PDMS Planar Electrode allows Patch Clamp Electrical Recordings from Cells," *Biosensors and Bioelectronics*, vol. 17, pp. 597-604, 2002.

[19] K. G. Klemic, J. F. Klemic, M. A. Reed, and F. J. Sigworth, "Planar Patch Clamp Electrodes," U. Patent 2002/0064841, 2002.

[20] Y. Osipchuk, A. Savtchenko, and A. A. Dromaretsky, "Polymeric Electrode for Electrophysiological Testing," US 2002/0195337, 2002.

[21] K. Cheung, T. Kubow, and L. P. Lee, "Individually Addressable Planar Patch Clamp Array," 2nd Annual International IEEE-EMBS Special Topic Conference on Microtechnologies in Medicine & Biology, Madison, Wisconsin, pp. 71-75 2002.

[22] A. Tixier-Mita, Y. Mita, K. Cozic, M. Frenea, B. L. Pioufle, and H. Fujita, "To Place Cells as an Array using Aspiration Technique," Micro Total Analysis Systems 2002 (uTAS 2002), pp. 888-890 2002.

[23] T. Lehnert, R. Netzer, U. Bischoff, and M. A. M. Gijs, "SiO2 Nozzle Array-Based Patch-Clamp Microsystem," Micro Total Analysis Systems 2002 (uTAS 2002), pp. 28-30 2002.

[24] T. Lehnert, M. A. M. Gijs, R. Netzer, and U. Bischoff, "Realization of Hollow SiO2 Micronozzles for Electrical Measurements on Living Cells," *Applied Physics Letters*, vol. 81, pp. 5063-5065, 2002.

[25] N. Ozaki, R. Ogawa, H. Sugihara, F. Emoto, M. Tanabe, S. Konishi, and H. Oka, "Electrophysiological High Throughput Drug Screening System," Micro Total Analysis Systems 2002 (uTAS 2002), pp. 856-858 2002.

[26] M. Tanabe, J. Makinodan, K. Suzuki, Y. Hosokawa, S. Konishi, N. Ozaki, and H. Oka, "Development of Micro Channel Array with Detecting Electrodes for Electrophysiological Biomedical Sensor," Sixteenth International Conference on Microelectromechanilcal Systems (IEEE MEMS 2003), Kyoto, Japan, pp. 2003.

[27] R. Vestergaard, J. Kutchinsky, S. Pedersen, R. Taboryski, C. Sorensen, R. Schroder, T. Ljungstrom, S. Friis, K. Krzywowski, M. Asmild, R. Jacobsen, N. Helix, M. Bech, J. Christensen, S. Dubeau, N. Willumsen, N. Hansen, D. Nielsen, and T. Freltoft, "Automation of the Patch Clamp Technique," 8th International Conference on Miniaturized System for Chemistry and Life Sciences, Malmo, Sweden, pp. 393-394 2004.

[28] C. Ionescu-Zanetti, J. Seo, and L. P. Lee, "Electrophysiology using a High-Density Microfluidic Array for High-Throughput Patch Clamp Measurements," 8th International Conference on Miniaturized Systems for Chemistry and Life Sciences, Malmo, Sweden, pp. 177-179 2004.

[29] T. Sordel, S. Garnier-Raveaud, F. Sauter, C. Pudda, N. Picollet-D'hahan, and F. Chatelain, "A Silicon-Based Multi-Patch Device: Application for Ionic Currents

Sensoring on Single Cells," 8th International Conference on Miniaturized Systems for Chemistry and Life Sciences, Malmo, Sweden, pp. 521-523 2004.

[30] J. Seo, C. Ionescu-Zanetti, J. Diamond, R. Lal, and L. P. Lee, "Integrated Multiple Patch-Clamp Array Chip via Lateral Cell Trapping Junctions," *Applied Physics Letters*, vol. 84, pp. 1973-1975, 2004.

[31] J. Morucci, M. E. Valentinuzzi, B. Rigaud, C. J. Felice, N. Chauveau, and P. Marsili, "Bioelectrical Impedance Techniques in Medicine Part I Bioimpedance Measurement," *Critical Reviews in Biomedical Engineering*, vol. 24, pp. 257-351, 1996.

[32] R. Pethig, *Dielectric and Electronic Properties of Biological Materials*: John Wiley & Sons, 1979.

[33] J. R. Macdonald, *Impedance Spectroscopy: Emphasizing Solid Materials and Systems*. New York: John Wiley & Sons, 1987.

[34] H. P. Schwan and K. R. Foster, "RF-Field Interactions with Biological Systems: Electrical Properties and Biophysical Mechanisms," *Proceedings of the IEEE*, vol. 68, pp. 104-113, 1980.

[35] K. R. Foster and H. P. Schwann, "Dielectric Properties of Tissues and Biological Materials: A Critical Review," *Critical Reviews in Biomedical Engineering*, vol. 17, pp. 25-104, 1989.

[36] R. Pethig and D. B. Kell, "The Passive Electrical Properties of Biological Systems: Their Significance in Physiology, Biophysics and Biotechnology," *Phys. Med. Biol.*, vol. 32, pp. 933-970, 1987.

[37] M. E. Valentinuzzi, J. Morucci, and C. J. Felice, "Bioelectrical Impedance Techniques in Medicine Part II Monitoring of Physiological Events by Impedance," *Critical Reviews in Biomedical Engineering*, vol. 24, pp. 353-466, 1996.

[38] K. R. Foster and J. L. Schepps, "Dielectric Properties of Tumor and Normal Tissues at Radio through Microwave Frequencies," *Journal of Microwave Power*, vol. 16, pp. 107-119, 1981.

[39] S. R. Smith, K. R. Foster, and G. L. Wolf, "Dielectric Properties of VX-2 Carcinoma Versus Normal Liver Tissue," *IEEE Transactions on Biomedical Engineering*, vol. BME-33, pp. 522-524, 1986.

[40] D. Haemmerich, S. T. Staelin, J. Z. Tsai, S. Tungjitkusolmun, D. M. Mahvi, and J. G. Webster, "In vivo Electrical Conductivity of Hepatic Tumours," *Physiol. Meas.*, vol. 24, pp. 251-260, 2003.

[41] B. Blad and B. Baldetorp, "Impedance Spectra of Tumour Tissue in Comparison with Normal Tissue; A Possible Clinical Application for Electrical Impedance Tomography," *Physiol. Meas.*, vol. 17, pp. A105-115, 1996.

[42] R. Pethig, "Dielectric Properties of Biological Materials: Biophysical and Medical Applications," *IEEE Transactions on Electrical Insulation*, vol. EI-19, pp. 453-474, 1984.

[43] A. M. Campbell and D. V. Land, "Dielectric Properties of Female Breast Tissue Measured in vitro at 3.2 GHz," *Phys. Med. Biol.*, vol. 37, pp. 193-210, 1992.

[44] A. Swarup, S. S. Stuchly, and A. Surowiec, "Dielectric Properties of Mouse MCA1 Fibrosarcoma at Different Stages of Development," *Bioelectromagnetics*, vol. 12, pp. 1-8, 1991.

[45] H. P. Schwan, "Electrical Properties of Tissue and Cell Suspensions," *Adv. Med. Biol. Phys.*, vol. 5, pp. 147-209, 1957.

[46] H. P. Schwan, *Determination of Biological Impedance*. New York: Academic, 1963.

[47] S. Takashima, K. Asami, and Y. Takahashi, "Frequency Domain Studies of Impedance Characteristics of Biological Cells using Micropipet Technique," *Biophysical Journal*, vol. 54, pp. 995-1000, 1988.

[48] K. Asami and K. S. Zhao, "Dielectric Measurement of a Single Sub-millimeter Size Microcapsule," *Colloid & Polymer Science*, vol. 272, pp. 64-71, 1994.

[49] K. Asami and A. Irimajiri, "Dielectric Dispersion of a Single Spherical Bilayer Membrane in Suspension," *Biochimica et Biophysica Acta*, vol. 769, pp. 370-376, 1984.

[50] P. V. Gerwen, W. Laureys, G. Huyberechts, M. O. D. Beeck, and K. Baert, "Nanoscaled Interdigitaed Electrode Arrays for Biochemical Sensors," The 9th International Conference on Solid-State Sensors and Actuators (Transducers 97), pp. 907-910 1997.

[51] G. R. Langereis, W. Olthuis, and P. Bergveld, "Measuring Conductivity, Temperature, and Hydrogen Peroxide Concentration using a Single Sensor Structure," The 9th International Conference on Solid-State Sensors and Actuators (Transducers 97), pp. 543-546 1997.

[52] R. Gomez, R. Bashir, A. Sarikaya, M. R. Ladisch, J. Sturgis, J. P. Robinson, T. Geng, A. K. Bhunia, H. L. Apple, and S. Wereley, "Microfluidic Biochip for Impedance Spectroscopy of Biological Species," *Biomedical Microdevices*, vol. 3, pp. 201-209, 2001.

[53] R. Gomez, M. R. Ladisch, A. K. Bhunia, and R. Bashir, "Microfabricated Device for Impedance-based Detection of Bacterial Metabolism," Mat. Res. Soc. Symp. Proc., pp. U461-U466 2002.

[54] S. Gawad, K. Cheung, U. Seger, A. Bertsch, and P. Renaud, "Dielectric Spectroscopy in a Micromachined Flow Cytometer: Theoretical and Practical Considerations," *Lab Chip*, vol. 4, pp. 241-251, 2004.

[55] S. Gawad, S. Metz, L. Schild, and P. Renaud, "Impedance Spectroscopy Cell Analysis in Microchannels," Micro Total Analysis Systems 2001, pp. 253-255 2001.

[56] S. Gawad, M. Wuthrich, L. Schild, O. Dubochet, and P. Renaud, "On-Chip Impedance-Spectroscopy for Flow-Cytometry using a Differential Electrode Sensor," The 11th International Conference on Solid-State Sensors and Actuators (Transducers 2001), Munich, Germany, pp. 1190-1193 2001.

[57] A. B. Frazier, R. D. Rabbitt, and H. E. Ayliffe, "Electrical Detector for Micro-Analysis Systems," USPTO 6169394, 2001.

[58] H. E. Ayliffe, A. B. Frazier, and R. D. Rabbitt, "Electric Impedance Spectroscopy using Microchannels with Integrated Metal Electrodes," *IEEE Journal of Microelectromechanical Systems*, vol. 8, pp. 50-57, 1999.

[59] S. K. Mohanty, S. K. Ravula, K. L. Engisch, and A. B. Frazier, "A Micro System using Dielectrophoresis and Electrical Impedance Spectroscopy for Cell Manipulation and Analysis," The 12th International Conference on Solid State Sensors, Actuators and Microsystems (Transducers 2003), Boston, MA, pp. 1055-1058 2003.

[60] Y. Huang, N. Chen, J. Borninski, and B. Rubinsky, "A Novel Microfluidic Cell-Chip for Single Cell Analysis and Manipulation," The 16th Annual International Conference on Microelectromechanical Systems (MEMS 2003), pp. 403-406 2003.

[61] P. D. Marley and B. G. Livett, "Neuropeptides in the Autonomic Nervous System," *CRC Critical Reviews in Clinical Neurobiology*, vol. 1, pp. 201-283, 1985.

[62] S. W. Carmichael and H. Winkler, "The Adrenal Chromaffin Cell," *Scientific American*, vol. 253, pp. 40-49, 1985.

[63] B. G. Livett, "Chromaffin Cells and Chromaffin Granules," *Encyclopedia of Neuroscience*, pp. 239-242, 1987.

[64] W. A. Catterall, "Neurotoxins that Act on Voltage-Sensitive Sodium Channels in Excitable Membranes," *Ann. Rev. Pharmacol. Toxicol.*, vol. 20, pp. 15-43, 1980.

[65] P. R. Stanfield, "Tetraethylammonium Ions and the Potassium Permeability of Excitable Cells," *Rev. Physiol. Biochem. Pharmacol.*, vol. 97, pp. 1-67, 1983.

[66] F. J. Sigworth, "The Variance of Sodium Current Fluctuations at the Node of Ranvier," *J. Physiol.*, vol. 307, pp. 97-129, 1980.

[67] J. L. Penzotti, H. A. Fozzard, G. M. Lipkind, and J. S. C. Dudley, "Differences in Saxitoxin and Tetrodotoxin Binding Revealed by Mutagenesis of the Na+ Channel Outer Vestibule," *Biophysical Journal*, vol. 75, pp. 2467-2657, 1998.

[68] S. E. Hochstetler and R. M. Wightman, "Detection of Secretion with Electrochemical Methods," *http://www.biophysics.org/education/techniques.htm*, 1997.

[69] M. Gillis and M. Anctil, "Monoamine Release by Neurons of a Primitive Nervous System: an Amperometric Study," *Journal of Neurochemistry*, vol. 76, pp. 1774-1784, 2001.

[70] E.R.Travis and R.M.Wightman, "Spatio-Temporal Resolution of Exocytosis from Individual Cells," *Annu. Rev. Biophys. Biomol. Struct.*, vol. 27, pp. 77-103, 1998.

[71] I. M. Robinson, M. Yamada, M. Carrion-Vazquez, V. A. Lennon, and J. M. Fernandez, "Specialized Release Zones in Chromaffin Cells Examined with Pulsed-Laser Imaging," *Cell Calcium*, vol. 20, pp. 181-201, 1996.

[72] R. M. Wightman, J. A. Jankowski, R. T. Kennedy, K. T. Kawagoe, T. J. Schroeder, D. J. Leszczyszyn, J. A. Near, E. J. Diliberto, and O. H. Viveros, "Temporally Resolved Catecholamine Spikes correspond to Single Vesicle Release from Individual Chromaffin Cells," *Proceedings of the National Academy of Sciences of the United States of America*, vol. 88, pp. 10754-10758, 1991.

[73] R. H. Chow, L. Ruden, and E. Neher, "Delay in Vesicle Fusion Revealed by Electrochemical Monitoring of Single Secretory Events in Adrenal Chromaffin Cells," *Nature*, vol. 356, pp. 60-63, 1992.

[74] S. Chan and C. Smith, "Physiological Stimuli evoke Two Forms of Endocytosis in Bovine Chromaffin Cells," *Journal of Physiology*, vol. 537, pp. 871-885, 2001.

[75] W. B. Coleman and G. J. Tsongalis, *The Molecular Basis of Human Cancer*. Totowa, NJ: Humana Press, 2002.

[76] E. Feuer, L. Wun, C. Boring, W. Flanders, M. Timmel, and T. Tong, "The Lifetime Risk of Developing Breast Cancer," *J. Natl. Cancer Inst.*, vol. 85, pp. 892-897, 1993.

[77] J. Kelsey and P. Horn-Ross, "Breast Cancer: Magnitude of the Problem and Descriptive Epidemiology," *Epidemiol. Rev.*, vol. 15, pp. 7-16, 1993.

[78] P. A. Wingo, R. Tong, and S. Bolden, "Cancer Statistics," *Ca: Cancer J. Clin.*, vol. 45, pp. 8-30, 1995.

[79] J. R. Harris, M. Morrow, and L. Norton, *Malignant Tumors of Breast*. Philadelphia: Lippincott-Raven, 1997.

[80] J. G. Elmore, M. B. Barton, V. M. Moceri, S. Polk, P. J. Arena, and S. W. Fletcher, "Ten-Year Risk of False Positive Screening Mammograms and Clinical Breast Examinations," *The New England Journal of Medicine*, vol. 338, pp. 1089-1096, 1998.

[81] J. Bosma, B. Weigelt, A. C. Lambrechts, O. J. H. M. Verhagen, R. Pruntel, A. A. M. Hart, S. Rodenhuis, and L. J. v. t. Veer, "Detection of Circulating Breast Tumor Cells by Differential Expression of Marker Genes," *Clinical Cancer Research*, vol. 8, pp. 1871-1877, 2002.

[82] B. Weigelt, J. Bosma, S. Rodenhuis, and L. J. V. t. Veer, "Marker Genes for Circulating Tumor Cells Predict Survival in Metastasized Breast Cancer Patients," *British J. of Cancer*, vol. 88, pp. 1091-1094, 2003.

[83] X. C. Hu, Y. Wang, D. R. Shi, T. Y. Loo, and L. W. Chow, "Immunomagnetic Tumor Cell Enrichment is Promising in Detecting Circulating Breast Cancer Cells," *Oncology*, vol. 64, pp. 160-165, 2003.

[84] P. D. Beitsch and E. Clifford, "Detection of Carcinoma Cells in the Blood of Breast Cancer Patients," *American Journal of Surgery*, vol. 180, pp. 446-449, 2000.

[85] L. W. Terstappen, C. Rao, S. Gross, and A. J. Weiss, "Peripheral Blood Tumor Cell Load reflects the Clinical Activity of the Disease in Patients with Carcinoma of the Breast," *Int. J. Oncol.*, vol. 17, pp. 573-578, 2000.

[86] J. J. Gaforio, M. J. Serrano, P. Sanchez-Rovira, A. Sirvent, M. Delgado-Rodriguez, M. Campos, N. D. L. Torre, I. Algarra, R. Duenas, and A. Lozano, "Detection of Breast Cancer Cells in the Peripheral Blood is Positively Correlated with Estrogen-Receptor Status and Predicts for Poor Prognosis," *Int. J. Cancer*, vol. 107, pp. 984-990, 2003.

[87] J. G. Moreno, C. M. Croce, R. Fischer, M. Monne, P. Vihko, S. G. Mulholland, and L. G. Gomella, "Detection of Hematogenous Micrometastasis in Patients with Prostate Cancer," *Cancer Research*, vol. 52, pp. 6110-6112, 1992.

[88] U. Guller, P. Zajac, A. Schnider, B. Bosch, S. Vorburger, M. Zuber, G. C. Spagnoli, D. Oertli, R. Maurer, U. Metzger, F. Harder, M. Heberer, and W. R. Marti, "Disseminated Single Tumor Cells as Detected by Real-Time Quantitative Polymerase Chain Reaction represent a Prognostic Factor in Patients undergoing Surgery for Colorectal Cancer," *Ann. Surg.*, vol. 236, pp. 768-775, 2002.

[89] E. Racila, D. Euhus, A. J. Weiss, C. Rao, J. McConnell, L. W. M. M. Terstappen, and J. W. Uhr, "Detection and Characterization of Carcinoma Cells in the Blood," *Proceedings of the National Academy of Sciences of the United States of America*, vol. 95, pp. 4589-4594, 1998.

[90] M. Cristofanilli and et.al, "Circulating Tumor Cells, Disease Progression, and Survival in Metastatic Breast Cancer," *New England Journal of Medicine*, vol. 351, pp. 781-7991, 2004.

[91] H. E. Ayliffe, R. D. Rabbitt, and A. B. Frazier, "Micro-Electric Impedance Spectroscopy of Electrophysiological Characterization of Cells," The 10th International Conference on Solid-State Sensors and Actuators (Transducers 1999), pp. 1999.

[92] S. Gawad, K. Cheung, and P. Renaud, "Impedance Spectroscopy Flow Cytometry: Model Validation," 8th International Conference on Miniaturized Systems for Chemistry and Life Sciences, Malmo, Sweden, pp. 58-60 2004.

[93] J. Gimsa and D. Wachner, "A Unified Resistor-Capacitor Model for Impedance, Dielectrophoresis, Electrorotation, and Induced Transmembrane Potential," *Biophysical Journal*, vol. 75, pp. 1107-1116, 1998.

[94] K. Asami, "Characterization of Biological Cells by Dielectric Spectroscopy," *Journal of Non-Crystalline Solids*, vol. 305, pp. 268-277, 2002.

[95] C. Lo, C. R. Keese, and I. Giaever, "Impedance Analysis of MDCK Cells Measured by Electric Cell-Substrate Impedance Sensing," *Biophysical Journal*, vol. 69, pp. 2800-2807, 1995.

[96] M. Graff, S. K. Mohanty, E. Moss, and A. B. Frazier, "Microstenciling: A Generic Technology for Microscale Patterning of Vapor Deposited Materials," *Journal of Microelectromechanical Systems*, vol. 13, pp. 956-962, 2004.

[97] A. Han, O. Wang, M. Graff, S. K. Mohanty, T. L. Edwards, K.-H. Han, and A. B. Frazier, "Multi-Layer Plastic/Glass Microfluidic Systems containing Electrical and Mechanical Functionality," *Lab Chip*, vol. 3, pp. 150-157, 2003.

[98] K. Ikuta, K. Hirowatari, and T. Ogata, "Three Dimensional Micro Integrated Fluid Systems (MIFS) Fabricated by Stereo Lithography," The 7th Annual International Conference on MicroElectroMechanical Systems (MEMS 94), pp. 1-6 1994.

[99] J. C. McDonald, D. C. Duffy, J. R. Anderson, D. T. Chiu, H. Wu, O. J. A. Schueller, and G. M. Whitesides, "Fabrication of Microfluidic Systems in Poly(dimethylsiloxane)," *Electrophoresis*, vol. 21, pp. 27-40, 2000.

[100] D. C. Duffy, J. C. McDonald, O. J. A. Schueller, and G. M. Whitesides, "Rapid Prototyping of Microfluidic Systems in Poly(dimethylsiloxane)," *Analytical Chemistry*, vol. 70, pp. 4974-4984, 1998.

[101] K. L. Engisch, M. M. Rich, N. Cook, and M. C. Nowycky, "Lambert-Eaton Antibodies Inhibit Ca^{2+} Currents but Paradoxically Increase Exocytosis during Stimulus Trains in Bovine Adrenal Chromaffin Cells," *The Journal of Neuroscience*, vol. 19, pp. 3384-3395, 1999.

[102] K. L. Engisch and M. C. Nowycky, "Compensatory and Excess Retrievla: Two Types of Endocytosis following Single Step Depolarizations in Bovine Adrenal Chromaffin Cells," *Journal of Physiology*, vol. 506, pp. 591-608, 1998.

[103] K. L. Engisch, N. I. Chernevskaya, and M. C. Nowycky, "Short-Term Changes in the Ca^{2+} - Exocytosis Relationship during Repetitive Pulse Protocols in Bovine Adrenal Chromaffin Cells," *The Journal of Neuroscience*, vol. 17, pp. 9010-9025, 1997.

[104] F. Bezanilla and C. M. Armstrong, "Inactivation of the Sodium Channel," *The Journal of General Physiology*, vol. 70, pp. 549-566, 1977.

[105] C. M. Armstrong and F. Bezanilla, "Charge Movement Associated with the Opening and Closing of the Activation Gates of the Na Channels," *The Journal of General Physiology*, vol. 63, pp. 533-552, 1974.

[106] A. Marty and E. Neher, "Potassium Channels in Cultured Bovine Adrenal Chromaffin Cells," *J. Physiol.*, vol. 367, pp. 117-141, 1985.

[107] C. R. Artalejo, M. K. Dahmer, R. L. Perlman, and A. P. Fox, "Two Types of Ca2+ Currents are Found in Bovine Chromaffin Cells: Facilitation is Due to the Recruitment of One Type," *Journal of PHysiology*, vol. 432, pp. 681-707, 1991.

[108] J. Klingauf and E. Neher, "Modeling Buffered Ca2+ Diffusion near the Membrane: Implications for Secretion in Neuroendocrine Cells," *Biophysical Journal*, vol. 72, pp. 674-690, 1997.

[109] E. M. Fenwick, A. Marty, and E. Neher, "Sodim and Calcium Channels in Bovine Chromaffin Cells," *J. Physiol.*, vol. 331, pp. 599-635, 1982.

[110] http://www.atcc.org.